Article

Cell

Dual RING E3 Architectures Regulate Multiubiquitination and Ubiquitin Chain Elongation by APC/C

Graphical Abstract

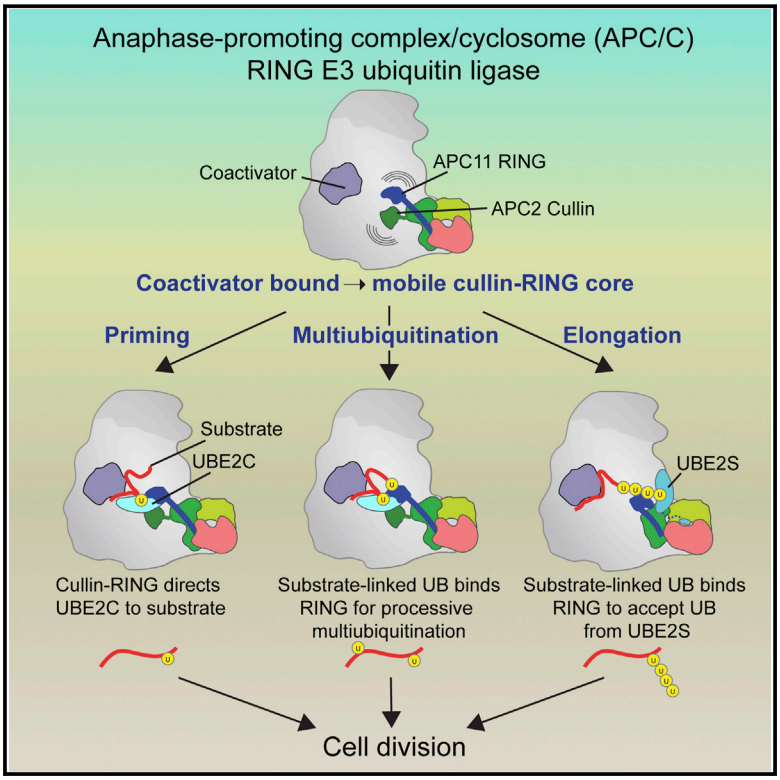

Highlights

- Cryo-EM shows mechanisms of polyubiquitination by cell-cycle regulator APC/C
- Distinct cullin-RING-E2 architectures for multiubiquitination and chain elongation
- RING activates UBE2C and binds substrate-linked ubiquitin to amplify processivity
- RING delivers ubiquitin for K11-linked chain elongation by UBE2S placed by cullin

Authors

Nicholas G. Brown, Ryan VanderLinden, Edmond R. Watson, ..., Jan-Michael Peters, Holger Stark, Brenda A. Schulman

Correspondence

jan-michael.peters@imp.ac.at (J.-M.P.), hstark1@gwdg.de (H.S.), brenda.schulman@stjude.org (B.A.S.)

In Brief

Alternate functions call for alternate architectures: proteins responsible for ubiquitination arrange themselves differently depending on the kind of ubiquitin modifications their substrate will receive.

Accession Numbers

5JG6

Brown et al., 2016, Cell *165*, 1440–1453
June 2, 2016
http://dx.doi.org/10.1016/j.cell.2016.05.037

CellPress

Cell

Article

Dual RING E3 Architectures Regulate Multiubiquitination and Ubiquitin Chain Elongation by APC/C

Nicholas G. Brown,[1,9] Ryan VanderLinden,[1,2,9] Edmond R. Watson,[1,9] Florian Weissmann,[3] Alban Ordureau,[4] Kuen-Phon Wu,[1] Wei Zhang,[5] Shanshan Yu,[1] Peter Y. Mercredi,[1] Joseph S. Harrison,[6] Iain F. Davidson,[3] Renping Qiao,[3] Ying Lu,[7] Prakash Dube,[8] Michael R. Brunner,[1] Christy R.R. Grace,[1] Darcie J. Miller,[1] David Haselbach,[8] Marc A. Jarvis,[3] Masaya Yamaguchi,[1] David Yanishevski,[1] Georg Petzold,[3] Sachdev S. Sidhu,[5] Brian Kuhlman,[6] Marc W. Kirschner,[7] J. Wade Harper,[4] Jan-Michael Peters,[3,*] Holger Stark,[8,*] and Brenda A. Schulman[1,2,*]

[1]Department of Structural Biology, St. Jude Children's Research Hospital, Memphis, TN 38105, USA
[2]Howard Hughes Medical Institute, Memphis, TN 38105, USA
[3]Research Institute of Molecular Pathology (IMP), Vienna Biocenter (VBC), 1030 Vienna, Austria
[4]Department of Cell Biology, Harvard Medical School, Boston, MA 02115, USA
[5]Donnelly Centre for Cellular and Biomolecular Research, University of Toronto, 160 College Street, Toronto, Ontario M5S3E1, Canada
[6]Department of Biochemistry and Biophysics and Lineberger Comprehensive Cancer Center, University of North Carolina, Chapel Hill, North Carolina 27599, USA
[7]Department of Systems Biology, Harvard Medical School, Boston, MA, 02115, USA
[8]Max Planck Institute for Biophysical Chemistry, 37077 Göttingen, Germany
[9]Co-first author
*Correspondence: jan-michael.peters@imp.ac.at (J.-M.P.), hstark1@gwdg.de (H.S.), brenda.schulman@stjude.org (B.A.S.)
http://dx.doi.org/10.1016/j.cell.2016.05.037

SUMMARY

Protein ubiquitination involves E1, E2, and E3 trienzyme cascades. E2 and RING E3 enzymes often collaborate to first prime a substrate with a single ubiquitin (UB) and then achieve different forms of polyubiquitination: multiubiquitination of several sites and elongation of linkage-specific UB chains. Here, cryo-EM and biochemistry show that the human E3 anaphase-promoting complex/cyclosome (APC/C) and its two partner E2s, UBE2C (aka UBCH10) and UBE2S, adopt specialized catalytic architectures for these two distinct forms of polyubiquitination. The APC/C RING constrains UBE2C proximal to a substrate and simultaneously binds a substrate-linked UB to drive processive multiubiquitination. Alternatively, during UB chain elongation, the RING does not bind UBE2S but rather lures an evolving substrate-linked UB to UBE2S positioned through a cullin interaction to generate a Lys11-linked chain. Our findings define mechanisms of APC/C regulation, and establish principles by which specialized E3–E2–substrate-UB architectures control different forms of polyubiquitination.

INTRODUCTION

Posttranslational modification by multiple ubiquitins (UBs) or UB chains is a predominant eukaryotic mechanism regulating protein half-life, location, interactions, or other functions. After an E1 enzyme links UB to the catalytic Cys of an E2 enzyme (~30 in humans), the thioester-bonded E2~UB intermediate is employed by an E3 enzyme (~600 in humans) (Deshaies and Joazeiro, 2009). Most E3s display a domain that recruits a substrate's degron motif and a hallmark RING domain thought to bind a cognate E2~UB intermediate that determines acceptor Lys properties (Metzger et al., 2014; Streich and Lima, 2014). Some E2s promiscuously modify lysines irrespective of context, while others generate linkage-specific UB chains (Christensen et al., 2007; Mattiroli and Sixma, 2014). Our current understanding is based on a limited number of landmark structures showing how RING domains align E2~UB active sites for nucleophilic attack, how a RING E3–E2 complex can target a preferred acceptor Lys, and how one RING forms homologous complexes with different E2~UB intermediates (Branigan et al., 2015; Dou et al., 2012; McGinty et al., 2014; Plechanovová et al., 2012; Pruneda et al., 2012; Reverter and Lima, 2005; Scott et al., 2014). However, structural models for dynamic polyubiquitination of substrates remain elusive.

Visualizing substrate polyubiquitination is challenging because proteins are modified on assorted sites, and UB chains are often elongated in a linkage-specific manner where each distal UB progressively added to a growing chain is successively presented to the catalytic center to accept another UB. The multiple ubiquitination sites are essentially moving targets for a catalytic RING–E2~UB assembly. Furthermore, E3 RING and degron-binding domains are often flexibly tethered, raising the question of how catalytic encounter could be achieved (Berndsen and Wolberger, 2014; Streich and Lima, 2014). Here, we addressed how mobile RING E3–E2 assemblies and UB-linked substrates are positioned for modification of multiple substrate lysines and evolving UBs by the essential human E3, the 1.2 MDa multisubunit

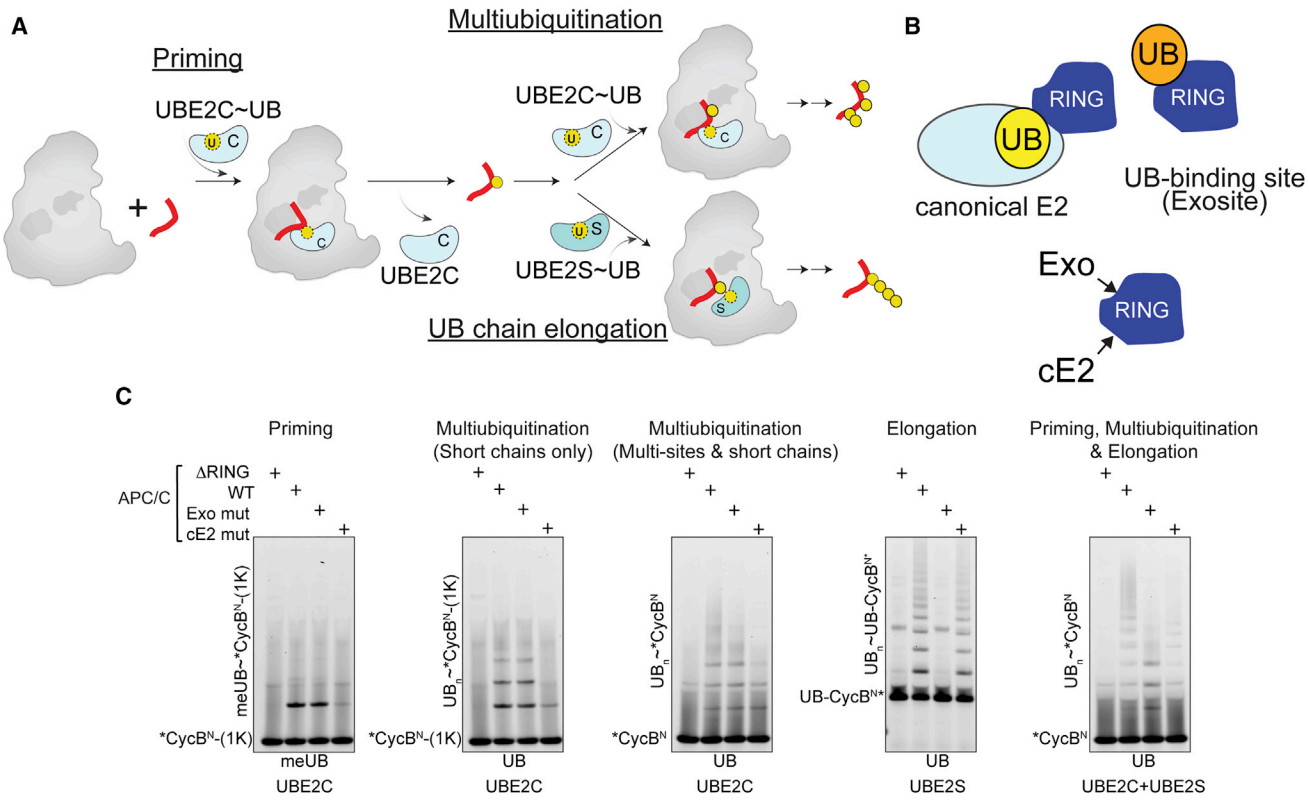

Figure 1. APC/C and Two E2 Partners Use Distinct Mechanisms for Polyubiquitination

(A) Distinct mechanisms of priming, multiubiquitination and UB chain elongation by APC/C, UBE2C, and UBE2S.

(B) Distinct APC11 RING surfaces involved in polyubiquitination: canonical E2 binding site - cE2; UB-binding exosite - Exo.

(C) APC11 RING mutants define distinctive priming, multiubiquitination, and UB chain elongation by APC/C^{CDH1} with UBE2C and/or UBE2S, using WT or methyl UB (meUB), during a single encounter of the indicated version of $CycB^N$ (1K = K67 only; UB- = UB-fusion).

anaphase-promoting complex/cyclosome (APC/C) (King et al., 1995; Sudakin et al., 1995).

APC/C catalyzes polyubiquitination of key cell cycle regulators to control the metaphase-to-anaphase transition, exit from mitosis, and maintenance of G1 (Primorac and Musacchio, 2013; Wieser and Pines, 2015). A seemingly simplistic code for substrate binding, with degrons such as KEN- or D-boxes recruited via a coactivator (CDC20 or CDH1) and APC10, is complemented by assorted catalytic mechanisms to achieve the variety and timing of polyubiquitination required to distinctly regulate vastly diverse substrates. Polyubiquitination is catalyzed with two E2s (Rodrigo-Brenni and Morgan, 2007), in humans UBE2C and UBE2S, in multiple steps (Figure 1A) (Aristarkhov et al., 1996; Garnett et al., 2009; Williamson et al., 2009; Wu et al., 2010; Yu et al., 1996). The priming reaction, where a substrate receives a single UB from UBE2C, was explained by prior structures that revealed how KEN- and D-box substrates bind APC/C^{CDH1} and how APC/C's cullin–RING catalytic core recruits and positions UBE2C adjacent to the preferred target lysine in a substrate (Brown et al., 2015; Buschhorn et al., 2011; Chao et al., 2012; da Fonseca et al., 2011; Tian et al., 2012). Furthermore, an atomic structure showed APC/C is blocked by the inhibitor EMI1 (Chang et al., 2015). However, the structures did not explain APC/C-catalyzed polyubiquitination.

After the priming reaction, APC/C catalyzes two forms of substrate polyubiquitination: multiubiquitination and chain elongation. During multiubiquitination, UBE2C adds more UBs either individually or as short chains with various linkages, while UBE2S catalyzes Lys11-linked chain elongation from a substrate-linked UB (Williamson et al., 2009; Wu et al., 2010; Yu et al., 1996). Ultimately, different forms of polyubiquitination—i.e., multiple monoUBs, multiple Lys11-linked chains, and branched chains—direct APC/C substrate degradation with different efficiencies (Dimova et al., 2012; Grice et al., 2015; Lu et al., 2015b; Meyer and Rape, 2014). Furthermore, processively polyubiquitinated substrates are degraded earlier in the cell cycle, whereas degradation occurs later for substrates receiving fewer UBs in a single encounter with APC/C. These latter substrates are subject to deubiquitination and competition with other substrates delaying their acquisition of a degradation signal (Kamenz et al., 2015; Lu et al., 2015a; Lu et al., 2014; Lu et al., 2015b; Rape et al., 2006). This is controlled in part by feed-forward *p*rocessive *a*ffinity *a*mplification (PAA), whereby relative to unmodified substrates, UB-linked substrates display higher affinity for APC/C, and are preferentially subjected to further rapid multiubiquitination by UBE2C followed by slower UB chain elongation by UBE2S (Lu et al., 2015c).

How does a single E3 produce such polyubiquitination variety? Although UBE2C is activated by the canonical E2-binding site on APC11's RING domain (Brown et al., 2014), mechanisms underlying PAA remain unknown (Lu et al., 2015c). And while UBE2S requires a distinct UB-binding site on the RING, hereafter referred to as "exosite" for simplicity, UBE2S lacks a standard E2 RING-binding signature sequence and instead its residues required for activity do not correspond to known RING E3 functions (Figure 1B) (Brown et al., 2014; Kelly et al., 2014; Williamson et al., 2009; Wu et al., 2010). Structural mechanisms explaining APC/C's massive enhancement of UBE2S's efficiency for generating Lys11-linked di-UB linkages remain elusive (Brown et al., 2014; Kelly et al., 2014).

Here, we describe structural studies that relied on protein engineering and crosslinking to overcome transient interactions to visualize APC/C complexes with their E2s representing different forms of polyubiquitination. The data reveal how a malleable E3 synergizes with different E2s and evolving ubiquitinated substrates to adopt distinct catalytic architectures that define assorted products of polyubiquitination reactions.

RESULTS

Distinct RING Roles in Priming, Multiubiquitination, and UB Chain Elongation

Using our recombinant APC/C^{CDH1} system (Weissmann et al., 2016), we discovered mechanistic differences between priming, multiubiquitination, and UB chain elongation in reactions with two different RING mutants. The "RING^{cE2}" mutant impairs *canonical E2∼UB* activation, while "RING^{exo}" bears Ala replacements for residues essential for recruiting the acceptor UB for chain elongation by UBE2S (Figure 1B) (Brown et al., 2014; Dou et al., 2012; Plechanovová et al., 2012; Pruneda et al., 2012). In reactions with either WT or methylated UB (meUB) that cannot form chains, we assayed modification of three variants of the canonical APC/C substrate cyclin B N terminus (CycB^{N}) during a single encounter with the different versions of APC/C (Figure 1C). Consistent with canonical RING activation of UBE2C, priming (monitored with a single Lys version of *CycB^{N} and meUB) and multiubiquitination (monitored with single Lys and WT versions of *CycB^{N} and WT UB) were impaired by the RING^{cE2} mutant. Also as expected, UBE2S-mediated UB chain elongation on a UB-fused CycB^{N}* substrate that bypasses the need for priming was eliminated by the APC/C RING^{exo} mutant. Unexpectedly, however, this mutant also subdued formation of high molecular weight conjugates by UBE2C, thereby uncovering that multiubiquitination by UBE2C is mechanistically distinct.

Anchoring the RING^{exo} Site, UBE2C, and UBE2S for Structural Studies of Polyubiquitination

Structural studies of E3–E2–substrate complexes have depended on artificial reinforcement because the interactions are fleeting (Brown et al., 2015; McGinty et al., 2014; Reverter and Lima, 2005; Scott et al., 2014). To visualize APC/C–E2–substrate architectures underlying polyubiquitination we used protein engineering to strengthen interactions with the RING exosite, and then crosslinking to stabilize UBE2C and UBE2S positioned for multiubiquitination and UB chain elongation, respectively.

First, a UB variant (UBv) with substantially increased affinity (1.6 μM K_D) for APC11's RING was selected by phage display (Figure 2A) (Ernst et al., 2013). After determining the crystal structure of the APC11 RING–UBv complex, NMR and enzyme assays demonstrated that the corresponding surfaces mediate APC11 RING domain binding to UBv and to UB and vice-versa, titrating free UBv impedes multiubiquitination and UB chain elongation by WT APC/C in a manner paralleling the APC/C RING^{exo} mutant, and the UBv is specific for APC/C and does not affect activities of a related RING or an unrelated UB-binding E3 (Figures 2A–2E, S1, Table S1). Furthermore, biological relevance was highlighted using a *Xenopus* egg extract system: the RING^{exo}-binding UBv, but not the negative control mutant, substantially slowed APC/C-dependent cyclin B degradation (Figure 2F). Although we cannot be certain that APC11-UBv and APC11-UB interactions are identical (a combination of mutations collaterally displace Lys11 so the UBv structure does not permit UBE2S-dependent chain elongation), the similarity between UBv and UB (0.37 Å RMSD), and the numerous experiments indicating that to a first approximation UBv binds the same surface as a substrate-linked UB suggested that UBv would be a useful tool for anchoring the dynamic APC/C^{CDH1} RING exosite.

As a prelude to structural studies, we performed crosslinking based on the notion that connecting several weak interactors would enable avidly capturing multiple sites in ubiquitination complexes. The 3-headed sulfhydryl-reactive crosslinker TMEA simultaneously joined a C-terminal Cys on UB representing the donor, the active site Cys on either UBE2C or UBE2S, and optimized sites to represent multiubiquitination or UB chain elongation in surrogates for UB-linked substrates where UBv was fused to fragments derived from the substrate Hsl1 (Figures 2G, 2H, and S2). Avid binding of the respective substrate and/or E2 portions of the crosslinked products was confirmed by the multiubiquitination trap inhibiting overall UBE2C activity, substrate-binding, and UBE2C activation, and the UB chain elongation trap inhibiting UBE2S activation at substantially lower concentrations than individual components (Figure S2).

Cryo-EM Reconstructions of APC/C–E2 Complexes Poised for Polyubiquitination

Each trap was purified with APC/C^{CDH1}, and cryo-EM was used to determine 3D reconstructions of the complex representing multiubiquitination with UBE2C at overall resolution of 6.4 Å and that representing UB chain elongation with UBE2S to 6 Å. The catalytic core, RING-UBv and E2 portions of maps displayed local resolutions of ∼6–10 Å, apparently limited by conformational heterogeneity consistent with the dynamic mechanisms of polyubiquitination. Initial models constructed by docking atomic structures were improved by molecular dynamics flexible fitting (Figure S3, Movies S1 and S2). The donor UB is not visible even at low contour in either complex, consistent with local variability of the "closed" E2∼UB conjugate in solution (Pruneda et al., 2012; Wickliffe et al., 2011). Overall, the EM data, together with structure-guided biochemical

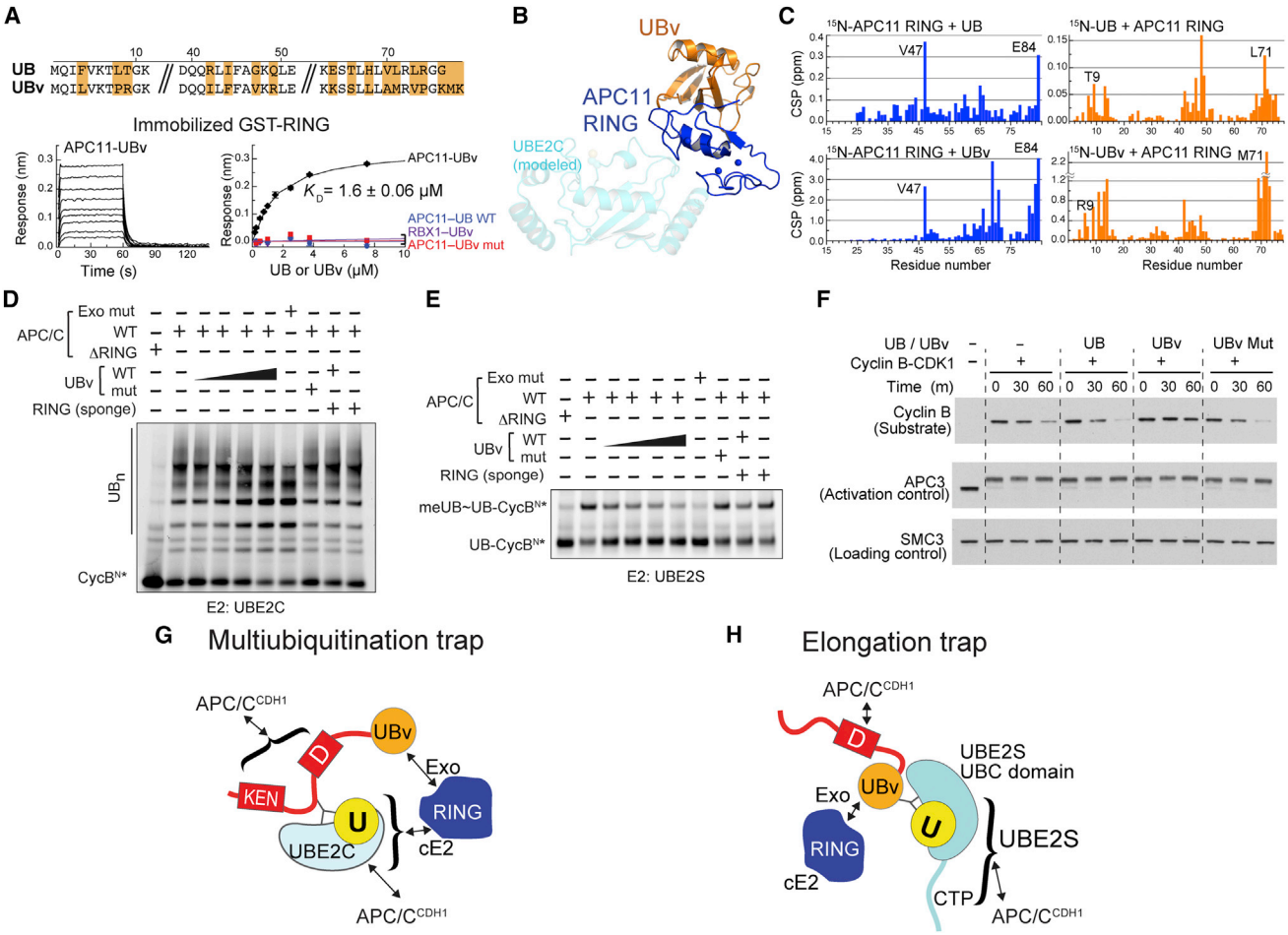

Figure 2. Anchoring the RING^{exo} Site, UBE2C, and UBE2S for Structural Studies of Polyubiquitination

(A) Phage display selected UB variant (UBv) binds APC11 RING with high affinity and selectivity, measured by BLI.

(B) Crystal structure UBv (orange)–APC11 (navy) confirms binding to exosite, opposite canonical E2 site (modeled, cyan).

(C) UB and UBv bind similar APC11 RING surface and vice-versa, based on NMR chemical shift perturbations (CSPs).

(D) Similar effects on UBE2C-dependent multiubiquitination for blocking RING exosite with either UBv or APC11 mutations. Sponge = excess APC11 RING sequestering UBv.

(E) Similar effects on UBE2S-dependent UB chain elongation for blocking RING exosite with either UBv or APC11 mutations.

(F) UBv inhibits APC/C-dependent degradation of cyclin B in mitotic *X. laevis* egg extracts, examined by indicated westerns.

(G) Scheme of 3-way crosslinked complex used to trap APC/C^{CDH1}–UBE2C architecture representing multiubiquitination.

(H) Scheme of 3-way crosslinked complex used to trap APC/C^{CDH1}–UBE2S architecture representing UB chain elongation.

analyses, reveal molecular mechanisms of multiubiquitination and UB chain elongation.

Structural "Snapshots" of APC/C–E2 Architectures Representing Steps in Polyubiquitination

To visualize steps in polyubiquitination, we compared the new EM reconstructions with prior data to provide "snapshots" along the process. EM maps were aligned representing substrate-bound APC/C^{CDH1} alone (Figure 3A) (Chang et al., 2014) and with UBE2C representing the priming reaction (Figure 3B) (Brown et al., 2015), alongside the maps representing multiubiquitination (Figure 3C) and UB chain elongation (Figure 3D). Side-by-side comparisons show the remarkable ways the dynamic APC2–APC11 cullin-RING catalytic core, evolving ubiquitinated substrates and E2s synergize to adopt distinct catalytic architectures specifying each reaction, illustrated beneath the EM reconstructions in Figure 3.

Prior structural data showed how a substrate degron is anchored on one side of APC/C, with the D-box corecruited by CDH1 and APC10 (Figure 3A). However, without interacting partners APC/C's cullin-RING catalytic core is mobile and not well resolved (Chang et al., 2014). How the mobile cullin-RING delivers the UBE2C~intermediate to substrate was revealed in a cryo-EM reconstruction representing "priming," which showed UBE2C's active site juxtaposed with the preferred target site, stabilized by crosslinking (Figure 3B) (Brown et al., 2015). UBE2C~UB is positioned by both the APC11 RING and APC2 WHB domains, which emanate from the intermolecular

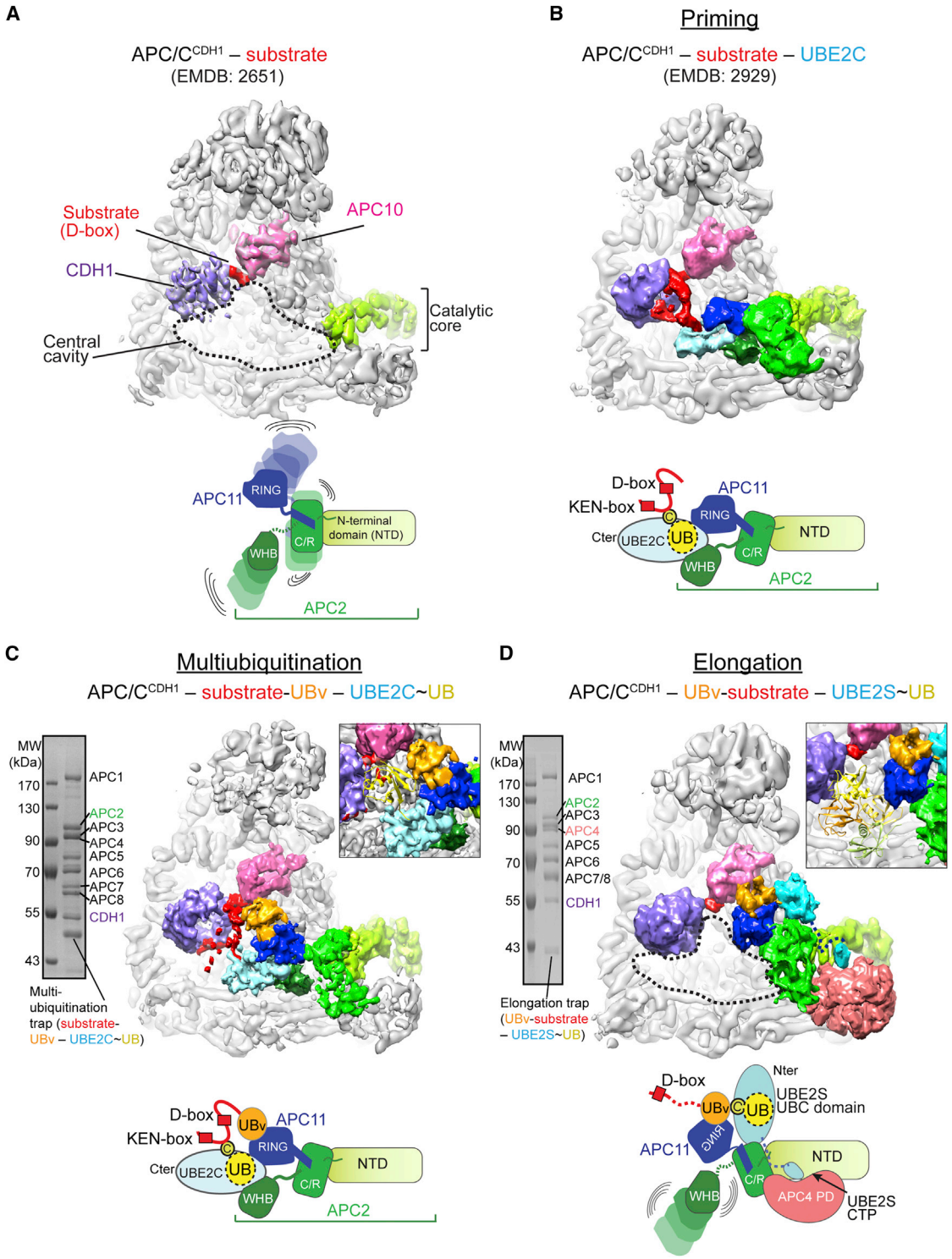

Figure 3. "Snapshots" of Distinct APC/C–E2 Architectures for Polyubiquitination

(A) Prior APC/C^{CDH1}–substrate complex (Chang et al., 2014). CDH1-purple, APC10-pink, APC2 NTD-light green, substrate-red.

(B) Prior structural data for complex representing priming (Brown et al., 2015), with UBE2C in light blue, APC2–APC11 intermolecular cullin–RING (C/R) domain green, and APC2 WHB domain in forest.

(C) Cryo-EM reconstruction representing multiubiquitination. UBv - orange. Inset, one UB (1UBQ, yellow) is shown fitting between substrate and active site.

(D) Cryo-EM reconstruction representing UB chain elongation. UBE2S - teal. Inset, distance between substrate binding and active sites accommodates polyUB, shown by tetraUB (2XEW, cartoon).

APC2–APC11 cullin-RING interaction domain (C/R) (Figure 3B). UBE2C∼UB is activated by binding the canonical E2 site on the RING, although primary recruitment occurs through APC2's WHB domain engaging the backside of UBE2C (Brown et al., 2015).

The cryo-EM reconstruction representing multiubiquitination provides insights into subsequent additional ubiquitination of a UB-linked substrate by APC/C^{CDH1}–UBE2C (Figure 3C). UBE2C is placed in the same manner for multiubiquitination as for priming (Figure 3B, C). This positioning of UBE2C, through co-binding the APC11 RING and the APC2 WHB domains, condenses the search radius for multiple fluctuating lysines emanating from a tethered substrate. Reinspection of this geometry to understand multiubiquitination shows the active site of UBE2C located ∼20 Å from the D-box. Importantly, this distance would allow numerous substrate lysines to access UBE2C and is large enough to accommodate a substrate-linked UB but small enough to constrain the catalytic geometry for generation of short chains (Figure 3C inset). UBv as a proxy for substrate-linked UB is bound to the RING exosite, providing a model for how this interaction would increase affinity and enhance processivity.

Finally, the new cryo-EM data reveal a completely different catalytic arrangement underlying APC/C-UBE2S-mediated UB chain elongation (Figure 3D). The "substrate" is recruited via a multisite mechanism, with the D-box binding CDH1 and APC10 on one side of APC/C, and the linked UBv localized by interactions with the RING exosite. This could place a homologous UB's K11 adjacent to UBE2S's active site. In agreement with prior mutational data (Brown et al., 2014; Kelly et al., 2014; Williamson et al., 2009), UBE2S is not recruited to the RING (Figure 3D). Furthermore, whereas RING domains typically bind the N-terminal portion of an E2 catalytic UBC domain, an APC2/APC4 groove binds UBE2S's unique *C-t*erminal *p*eptide (CTP), and APC2 interacts with the C-terminal portion of UBE2S's UBC domain (Figure 3D). The density for the N-terminal portion of the UBE2S UBC domain disappears at higher resolution, presumably due to the combination of a lack of direct contacts and greater relative motion furthest from the APC/C^{CDH1}-binding site (Figure S3B). Another difference from the priming and multiubiquitination catalytic architectures is that in the complex with UBE2S, APC2's WHB domain is not visible (Figure 3D), consistent with dispensability for UB chain extension (Brown et al., 2015).

Different positions of the E2s in the complexes representing multiubiquitination and UB chain elongation would explain differences in products of these distinct polyubiquitination reactions. During multiubiquitination, UBE2C is placed in the central cavity, with its active site facing inside APC/C and proximal to substrate. This confines the space available for a modified substrate and would account for the limited number of UBs typically linked to substrates in reactions with UBE2C. By contrast, UBE2S is placed at the edge of APC/C (Figure 3D). This open architecture would allow growth of a polyUB chain either entirely outside APC/C altogether, or inside the central cavity (Figure 3D, inset). Further experiments examining how multiubiquitination is amplified by a substrate-linked UB binding the RING exosite and how UB chain elongation is determined are described in separate sections below.

RING Exosite Binding to Substrate-Linked UB Influences Processivity of Multiubiquitination

The structure representing multiubiquitination suggested that a substrate-linked UB binding to the RING exosite could provide a secondary interaction (Figure 3C). This may underlie findings from a recent single-molecule study, which showed that ubiquitinated substrates have a relatively higher propensity to bind APC/C, which drives their further multiubiquitination (Lu et al., 2015c). We used the single molecule assay to confirm the role for the RING exosite. Indeed, during multiubiquitination reactions with UBE2C where the UB linkages to substrate are evolving, the RING exosite mutant showed relatively decreased binding as probed by the number of APC/C^{CDH1} complexes detected in a field-of-view with saturating substrate (Securin) molecules, $\sim 2 \times 10^5$, on the surface of a chip (Figure 4A).

This led to several predictions regarding mechanisms of multiubiquitination (Figures 4B and 4C). Enhanced lifetime of a ubiquitinated substrate on APC/C would increase processivity, thereby increasing the extent of modification while concomitantly decreasing catalytic turnover of substrate. Thus, mutating the RING exosite would be predicted to both decrease the extent of modification, and to correspondingly increase the fraction of substrate modified during the reaction. The notable exception would be during a single substrate encounter with APC/C^{CDH1}, if a particular substrate-linked UB could not access the RING, then blocking the exosite would not impact the extent of ubiquitination. CycB^{N*} could be a suitable substrate for these experiments, because the EM data predict that only one of its 16 potential ubiquitination sites (Lys51) could not access UBE2C, and a short UB chain linked to all the sites could access the RING exosite. We confirmed the predictions for ubiquitination site usage using a proteolytic strategy that isolates most sites and subsequent semiquantitative mass spectrometry analysis of the resultant peptides (Figures S4A–S4C). Mutating the RING exosite only subtly perturbed the site usage.

The predicted roles of the RING exosite on the *extent* of multiubiquitination were tested with several assays. First, we quantified UB chain formation using UB-AQUA, which showed a ∼20 percent reduction in UB chains formed upon mutating the RING exosite without apparent discrimination toward a specific chain linkage (Figures 4D, S4B, and S3C). Second, we assayed various forms of multiubiquitination for a suite of CycB^{N*} mutants with different numbers and locations of lysines. All acquired fewer UBs with the APC/C^{CDH1} RING^{exo} mutant, except the one mutant predicted to have limited potential for PAA due to few target lysines: the RING^{exo} mutant does not substantially affect modification of the single Lys substrate in a single encounter with APC/C (Figures 1C, 4E, S4D–S4J).

The role of the RING exosite on the *fraction* of substrate turned over was monitored during multibiquitination timecourses. As predicted (Figure 4C), free substrate was more rapidly depleted in reactions with the RING exosite mutant (Figures 4E–4G, S4B, S4D–S4J). Quantifying the effects showed that a higher proportion of the CycB^{N*} was modified by at least one UB in reactions with the RING exosite mutant (Figures 4F and 4G). However, a higher proportion of the ubiquitinated CycB^{N*} substrate received four or more UBs from UBE2C with wild-type APC/C^{CDH1}. The effects were magnified for the

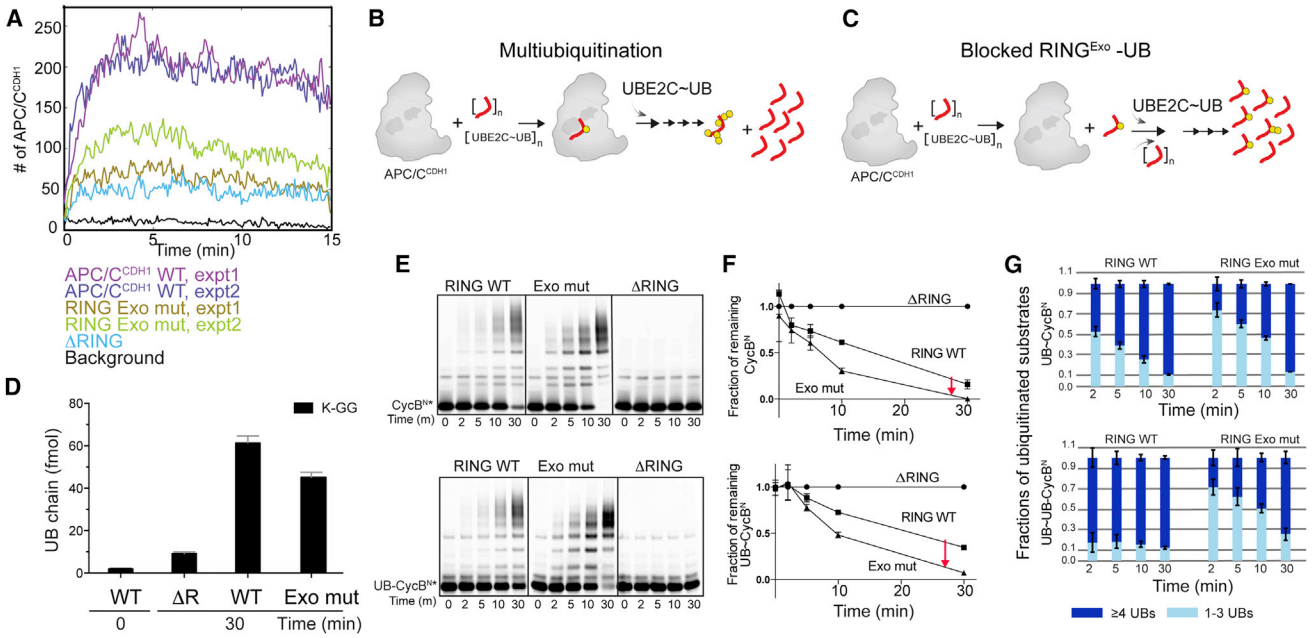

Figure 4. Substrate-Linked UB Binding to RING Exosite Contributes to Processive Affinity Amplification for Multiubiquitination

(A) Single-molecule time traces for binding to evolving ubiquitinated immobilized Securin molecules during multiubiquitination by UBE2C and APC/C^{CDH1} or indicated RING mutants.

(B) In processive multiubiquitination by APC/C and UBE2C, multiple UBs are added to substrate in a single binding event.

(C) Model if blocking substrate-linked UB binding to the RING exosite reduces processivity and shifts to distributive mode of multiubiquitination. A larger fraction of substrate would be modified, but with fewer UBs.

(D) RING exosite contributes to quantity of UB chains formed during CycB^{N*} multiubiquitination by APC/C^{CDH1} and UBE2C, measured by AQUA mass spectrometry.

(E) Role of UB-binding RING exosite on processivity, monitored by formation of high molecular weight conjugates and fraction of substrate modified during multiple turnover UBE2C-catalyzed multiubiquitination of CycB^{N*} (top) or UB-CycB^{N*} (bottom).

(F) Role of RING exosite on fraction of substrate modified over time, in assays as in (E), quantifying depletion of unmodified CycB^{N*} (top) or UB-CycB^{N*} (bottom). Error bars: SEM, N = 3.

(G) Role of RING exosite on extent of substrate modification during multiubiquitination with UBE2C. Ubiquitinated products generated as in (E) were divided into 2 categories, with $\geq$ 4 UBs (navy) or 1-3 UBs (blue) as resolved by SDS-PAGE to examine extent of generation of highly multiubiquitinated products. Error bars: SD, N = 3.

UB-fused CycB^{N*} substrate, further implicating a role for substrate-linked UB binding to the RING exosite (Figures 4E–4G). Taken together, the results suggested that UB-binding to the APC11 RING exosite supports processive affinity amplification during multiubiquitination.

Unique UBE2S Tethering

UB chain extension is achieved by an entirely distinct mechanism. Our EM data reveal how APC/C uses a unique E3 architecture that (1) anchors UBE2S via a tether, (2) positions the active site, and (3) delivers the acceptor UB to UBE2S. Although the structural data agree with prior scanning mutagenesis data for the acceptor UB, UBE2S, and APC11's RING domain (Brown et al., 2014; Kelly et al., 2014; Wickliffe et al., 2011), we performed mutational studies of APC/C to both confirm the structure and define how the novel APC/C catalytic architecture establishes UB chain elongation.

We identified key APC/C residues recruiting UBE2S based on interactions with the basic/hydrophobic tip of UBE2S's unique, flexible 66-residue C-terminal peptide (CTP) that is both necessary and sufficient for binding to APC/C (Williamson et al., 2009; Wu et al., 2010). The EM reconstruction shows this nestled in a complementary acidic and hydrophobic groove at the interface between APC2's N-terminal domain (NTD), C/R domain, and APC4's β-propeller (Figures 5A and 5B). Although the homologous sequence from the inhibitor EMI1 was assigned to comparable density in a prior EM structure, individual sidechains have yet to be resolved for this region for either UBE2S or EMI1, and roles of the APC2/APC4 groove have not been tested (Chang et al., 2015). Our molecular model shows the APC2/APC4 groove including APC2's Asp350 and Asp353, and APC4's Asp33 and the loop spanning from Asp747 through Glu751, and their mutation specifically impairs APC/C^{CDH1}-UBE2S-catalyed UB chain elongation without affecting multiubiquitination with UBE2C (Figure 5B, S5A–S5E). These APC2/APC4 groove mutations and the corresponding mutation from UBE2S's CTP (L222A) caused parallel defects, ~10- to 30-fold increases in apparent K_m (K_m^{app}) with little effect on apparent V_{max} (V_{max}^{app}) in reactions monitoring polyubiquitination of a UB-fused substrate while titrating UBE2S (Figure 5C). Thus,

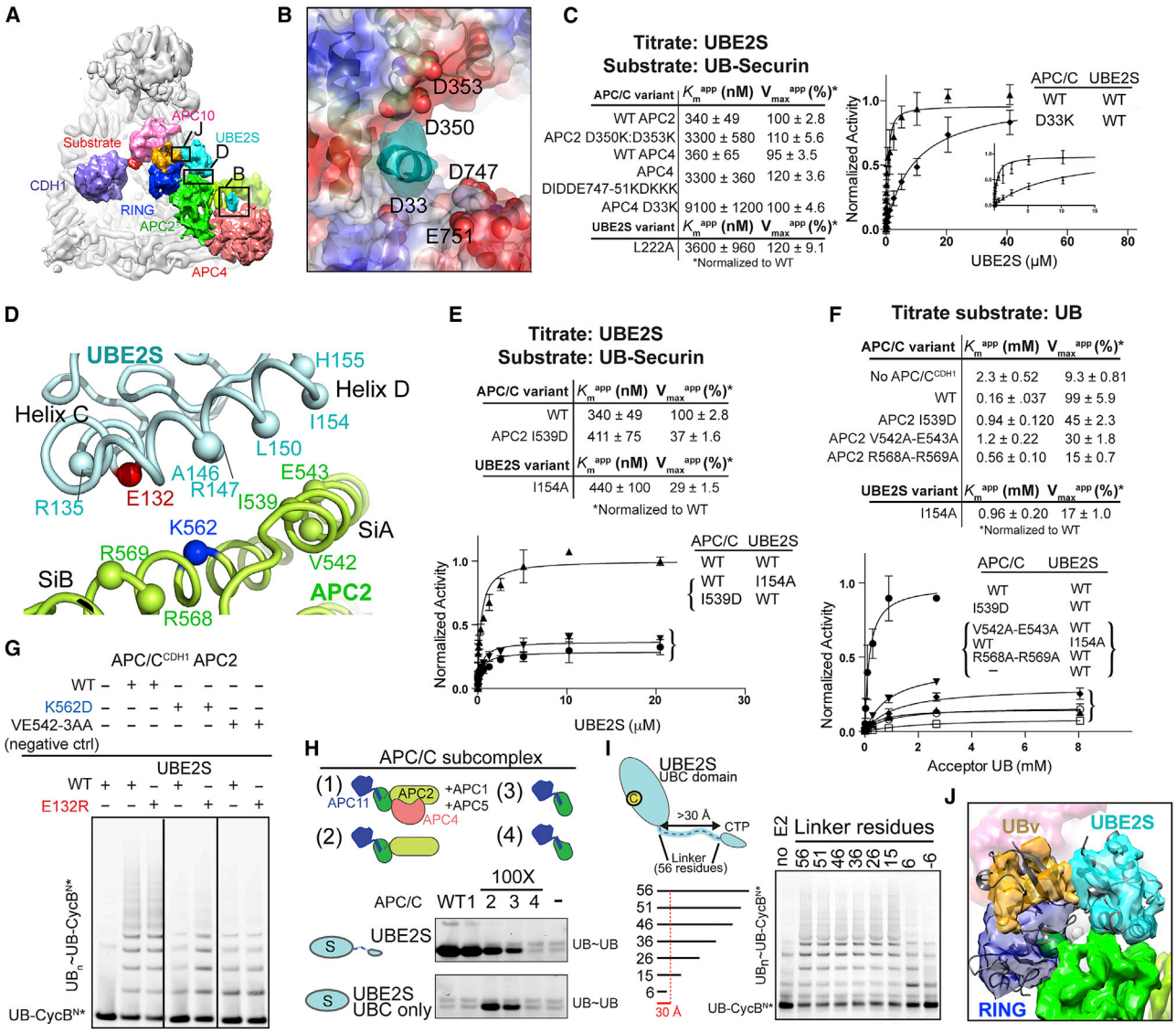

Figure 5. Distinctive Multisite Interactions Establish Unique Catalytic Architecture Specifying UB Chain Elongation by APC/C and UBE2S

(A) Cryo-EM reconstruction of APC/C-CDH1 complex with UBE2S representing UB chain elongation as in Figure 3D, indicating regions with close-ups in panels (B), (D), and (J).

(B) Model for APC2/APC4 groove interactions with UBE2S CTP, based on docking APC/C structure (Chang et al., 2015) in cryo-EM reconstruction. APC2/APC4 groove is shown as a surface colored by electrostatic potential, with selected side-chains lining the groove in spheres. EM density for UBE2S CTP - cyan.

(C) Role of APC2/APC4 groove in recruiting UBE2S CTP, as determined from kinetic parameters for the indicated mutants during polyubiquitination of a UB-Securin substrate while titrating UBE2S. SEM, n ≥ 3.

(D) Placement of UBE2S C- and D-helices (cyan) by APC2 Si helices modeled based on (Chang et al., 2015) (green).

(E) Role of APC2 placement of UBE2S UBC domain in substrate polyubiquitination, from kinetic parameters for mutants during polyubiquitination of a UB-Securin substrate while titrating UBE2S. SEM, n ≥ 3.

(F) Role of APC2 placement of UBE2S UBC domain in activating UB chain synthesis, from kinetic parameters for mutants upon titrating acceptor UB during APC/C^{CDH1}-UBE2S-mediated di-UB synthesis. SEM, n ≥ 3.

(G) APC2 placement of UBE2S UBC domain tested by charge-swap rescue assaying UBE2S E132R restoring UB chain elongation specifically to APC/C^{CDH1} with APC2 K562D mutant.

(H) Importance of placing UBE2S's UBC domain, or recruiting the CTP, determined from minimal APC/C subcomplexes (schematics on top) required to stimulate di-UB synthesis by WT UBE2S or isolated UBC domain lacking the CTP (bottom). Reactions with APC/C WT and subcomplexes 1–3 with WT UBE2S are controls based on (Brown et al., 2014).

(I) Importance of placing both UBE2S's UBC domain and CTP for APC/C activation of UB chain elongation. UBE2S deletion mutants with progressively shorter linkers between the two domains were assayed for APC/C^{CDH1}-dependent polyubiquitination of UB-CycB^{N}*. Reactions with WT UBE2S and linker deletions to 26 are controls based on (Brown et al., 2014).

(J) Model for acceptor UB (orange, UBv as proxy) in active site of UBE2S (cyan).

the interaction between UBE2S's CTP and the APC2/APC4 groove plays the predominant role in recruiting UBE2S, but other elements are crucial to activate UBE2S-mediated UB chain elongation.

Unique E2 and Acceptor Placement Promote Chain Elongation

UB chain elongation requires juxtaposition of an E2 active site with an acceptor UB. The EM density showed an unprecedented cullin-RING mechanism, whereby the cullin, not the RING, positions UBE2S. This provides a rationale for deleterious effects of mutating UBE2S's "C" and "D" helices (Brown et al., 2014; Kelly et al., 2014), which straddle a pair of APC2 C/R domain helices that we term SiA and SiB, for UBE2*S*-*i*nteracting *A* and *B*-helices (Figure 5A and 5D, Movie S2). UBE2S binding to APC2's SiA and SiB-helices orients the active site toward the APC/C central cavity and APC11's tethered RING domain, and places the machinery catalyzing UB chain elongation at the extreme edge of APC/C's central cavity. This cullin function of APC2 may be specialized for APC/C, as the corresponding region in canonical cullins is not known to play a catalytic role.

Several assays validated that APC2 placement of UBE2S's UBC domain is important to activate UB chain elongation. Parallel effects are observed for mutations in the APC2 Si-helices and the corresponding interacting C- and D-helices in UBE2S. Monitoring APC/C^{CDH1}-dependent chain elongation on a UB-primed substrate while titrating UBE2S showed that mutations disrupting the APC2–UBE2S UBC domain interface decreased V_{max}^{app}, without substantially impacting the K_m^{app} value for UBE2S (Figures 5E and S5F). In assays monitoring fluorescent UB transfer from UBE2S while titrating free UB as acceptor, the mutations caused increased K_m^{app} for the acceptor UB (3.5- to 7.5-fold) and decreased V_{max}^{app} (2- to 6-fold) (Figures 5F and S5G). Some mutations almost eliminated UB chain formation. Further support for APC2 placement of UBE2S's catalytic UBC domain comes from a compensatory charge-swap experiment, as defective UB chain elongation caused by the deleterious APC2 SiB-helix K562D mutation was specifically rescued by the structurally complementary E132R mutation from UBE2S's helix C (Figure 5G).

Subunit and domain deletion mutagenesis experiments confirmed that an APC2–APC11 subcomplex containing the Si helices and RING domain is minimally required to activate di-UB chain synthesis by UBE2S's isolated catalytic domain, albeit at 100-fold higher E3 concentrations due to lack of CTP-recruitment (Figures 5H and S5H). In agreement with the structural data, robust CTP-dependent activation required preserving the APC2/APC4 groove (Figure 5H). Importantly, even in the minimized systems, structure-based point mutations in APC2's Si helices thwarted activation of UBE2S-mediated di-UB synthesis (Figures S5I–S5K). NMR experiments further confirmed the distinctive interaction between APC/C's C/R and UBE2S's UBC domains: extreme line-broadening for resonances corresponding to ^{15}N-UBE2S's folded UBC domain occurred upon adding an APC2–APC11 subcomplex. This depended on intact Si helices but not the RING (Figures S6A–S6E).

To test if UB chain elongation involves APC/C^{CDH1} simultaneously engaging UBE2S's UBC and CTP domains as in the structure, we assayed a series of mutants with progressively shorter linkers connecting the domains. Indeed, only UBE2S variants with linkers that could span the 30 Å distance separating the CTP and UBC domains retained full activity (Figure 5I). Overall, the EM data suggest that it is essential to place UBE2S adjacent to the acceptor UB delivered by the RING exosite, as visualized by modeling UB in place of UBv in the EM reconstruction (Figure 5J).

UBE2S-Specific Assembly Elements Cannot Support UBE2C

Despite differences in catalytic architecture and the specific domains mediating interactions, there are some common principles underlying multiubiquitination and UB chain elongation (Figure 6A). First, APC/C recruits each E2 via auxiliary interactions: APC2's WHB binds UBE2C's backside while the APC2/APC4 groove recruits UBE2S's CTP. Second, the cullin-RING catalytic core positions both E2s proximal to their distinctive acceptors, albeit by APC2's WHB and APC11's RING domains co-positioning UBE2C and by APC2's Si-helices guiding UBE2S. To test if each E2 depends on its own interactions with APC/C, we wished to assay effects of transplanting their unique elements. Although we were unable to relocalize UBE2S to the site occupied by UBE2C, we were able to test if UBE2S-specific features could support APC/C^{CDH1} activity with UBE2C as follows.

First, we asked if UBE2S's CTP could substitute for APC2's WHB in recruiting UBE2C. We assayed a chimeric E2 harboring UBE2S's CTP grafted onto UBE2C (Chang et al., 2015). Control reactions showed that appending UBE2S's CTP does not hinder multiubiquitination with wild-type APC/C^{CDH1} (Figure 6B), and deleting the APC2 WHB domain does not impact UBE2S-catalyzed chain synthesis (Brown et al., 2015). However, >30-fold more of the UBE2C-UBE2S^{CTP} chimera was required to multiubiquitinate CycB^{N*} with the APC/C^{CDH1} mutant lacking APC2's WHB domain (Figure 6B). Thus, UBE2C requires its distinctive APC/C binding mechanism.

Next, we asked if specific RING positioning is important using the elongation trap to shackle the RING away from the UBE2C-specific architecture (Figures 2H and 3D). The elongation trap blocked APC/C^{CDH1}-dependent hydrolysis of an oxyester-linked UBE2C∼UB complex, which requires RING-mediated activation independent of substrate (Figure 6C). Inhibition depended on redirecting the RING, because mutating the exosite to prevent UBv tethering of the RING restored activation in the presence of the elongation trap, and neither UBv nor substrate alone impaired activity.

Finally, we noted that the two catalytic architectures display different relative orientations for APC2's NTD and C/R domains. The helix at the hinge comprising residues 500–506 is largely buried in the EM reconstructions with UBE2C, but is partially exposed in complex with UBE2S. Accordingly, there is little effect of mutating hinge-helix isoleucines (501 and 502) to aspartates on UBE2S-dependent polyubiquitination of a UB-fused substrate, whereas this substantially impairs multiubiquitination with UBE2C (Figure 6D). Thus, the distinctive cullin conformation is required for multiubiquitination.

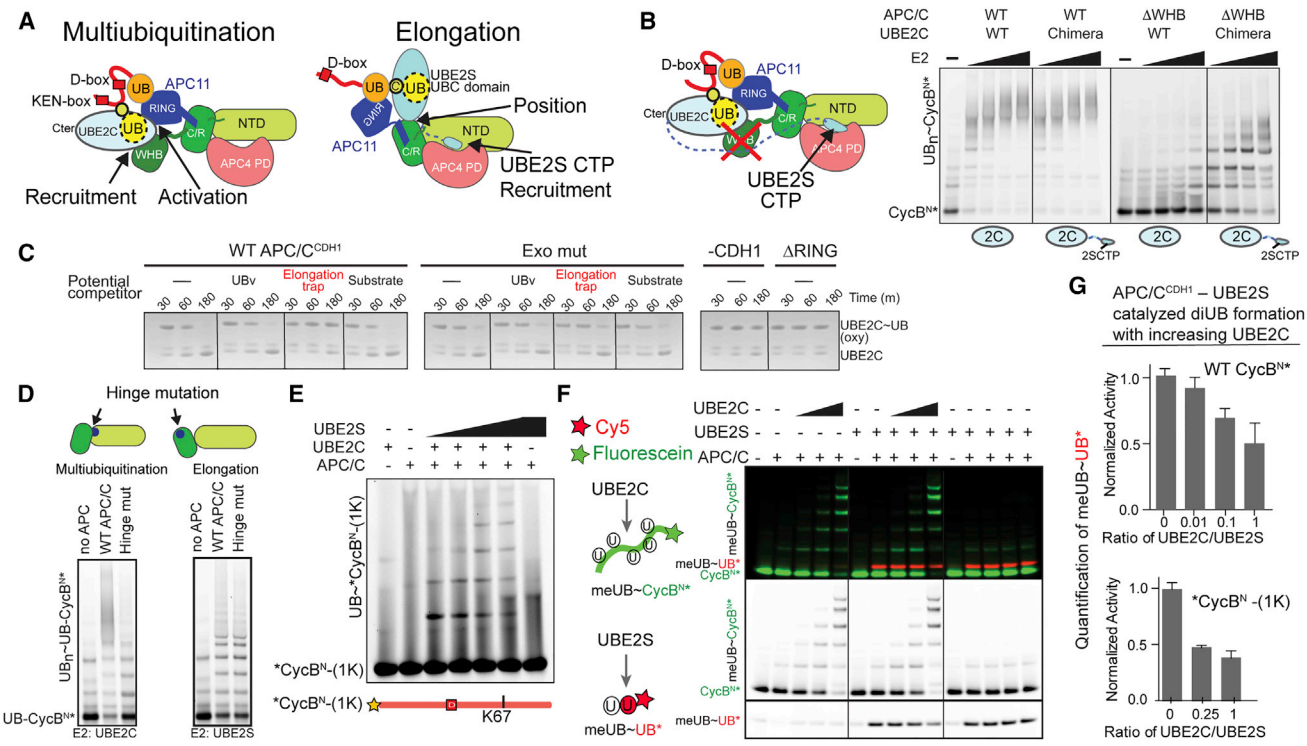

Figure 6. Functional Specialization of Each Polyubiquitination Architecture

(A) Distinct APC/C mechanisms recruiting, positioning, and/or activating UBE2C or UBE2S for multiubiquitination and UB chain elongation, respectively.

(B) UBE2S CTP is a poor substitute for APC2 WHB in supporting UBE2C-dependent substrate multiubiquitination, as shown from assays with WT UBE2C or a chimera with appended UBE2S's CTP, and WT APC/C^{CDH1} or a deletion mutant lacking APC2 WHB domain.

(C) Shackling the RING away from the multiubiquitination architecture by the elongation trap inhibits APC/C activation of intrinsic UBE2C activity, monitored by inhibition of APC/C^{CDH1}-stimulated hydrolysis of oxyester-linked UBE2C~UB.

(D) Specific APC2 cullin conformation is required for multiubiquitination. Top – schematic of distinctive APC2 NTD-C/R domain orientations showing burial or exposure of hinge. Distinct defects with hinge mutant (APC2 I501D, I502D) for multiubiquitination or UB chain elongation of UB-CycB^{N}*.

(E) UBE2C and UBE2S build a UB chain on *CycB^{N}-(1K) during the substrate's single encounter with APC/C^{CDH1}.

(F) Competition between APC/C^{CDH1} activities with UBE2C and UBE2S probed simultaneously with 2 colors. MeUB can only be donor and not acceptor. Only fluorescein-CycB^{N}* (green) accepts meUB from UBE2C. Only Cy5-UB* (red) with blocked C terminus accepts meUB from UBE2S.

(G) Bar graphs showing reduced APC/C^{CDH1}-UBE2S-catalyzed meUB~UB* formation in (F) and S6G in the presence of UBE2C activity. SD, n $\geq$ 2.

Weak RING Interactions May Limit Competition between Multiubiquitination and Chain Elongation

Previous studies raised the question if multiubiquitination and UB chain elongation can occur simultaneously (Williamson et al., 2009; Wu et al., 2010). Indeed, priming, multiubiquitination, and UB chain elongation can occur independently (Figure 1C), and both E2s can function during a substrate's single encounter with APC/C^{CDH1} (Wang and Kirschner, 2013), including on a substrate with a single Lys (Figure 6E). Nonetheless, there has been no evidence of synergy. Instead, single molecule kinetic experiments indicated that UBE2S can act after UBE2C in a second gradual phase of polyubiquitination (Lu et al., 2015c).

To further explore the extent to which UBE2C and UBE2S could compete or catalyze their respective reactions simultaneously, we monitored activities of both E2s independently of each other but in the same tube using a donor meUB that cannot serve as acceptor, Cy5-labeled C-terminally blocked UB that only accepts meUB from UBE2S, and fluorescein-CycB^{N}* or the single Lys version that only accept meUB from UBE2C. Increasing UBE2C to concentrations ~2-fold above K_m slightly but reproducibly reduced di-UB synthesis by UBE2S (Figure 6F, 6G, S6F, and S6G), although no further inhibition was observed by adding more UBE2C. Such minor inhibition could be explained by competition between a UB-modified substrate and UBE2S acceptor UB for the RING exosite. Or RING positions for the two reactions could be mutually exclusive as observed in the EM reconstructions for the UBv-trapped structures (Figures 3C and 3D). Alternatively, it is also possible that WT UB binds the RING differently and could allow simultaneous engagement of UBE2C at the cE2 site and UBE2S's acceptor UB at the exosite. Irrespective of the mechanism, competition would be limited if RING interactions with different partners were fleeting. Indeed, UB-binding to the RING exosite is weak (Figure 2A) (Brown et al., 2014) and NMR chemical shift perturbation experiments did not detect interaction between 100 μM ^{15}N-labeled APC11 RING domain and 400 μM UBE2C or a disulfide-linked proxy for a UBE2C~UB intermediate (Figures S6H–S6J). Overall, it seems that the RING interactions

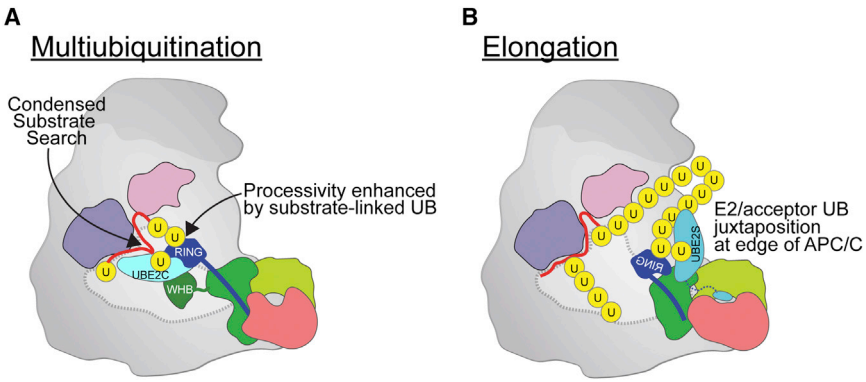

Figure 7. Specialized APC/C–E2 Architectures for Multiubiquitination and UB Chain Elongation

(A) Processive multiubiquitination occurs by APC/C's APC2 cullin (green)-APC11 RING (blue) positioning UBE2C proximal to substrate (red), reducing the search volume for catalytic encounter while substrate-linked UB (yellow) binds the RING exosite to increase the evolving ubiquitinated substrate's lifetime on APC/C and enhance processivity. Each UB transfer cycle is accompanied by catalytic core dynamics releasing the used UBE2C for replacement by a charged UBE2C∼UB to donate the next UB for ligation.

(B) Specialized architecture for UB chain elongation. APC2/APC4 recruits UBE2S's CTP, APC2 (cullin) places UBE2S's catalytic UBC domain, and APC11's RING guides the acceptor UB's Lys11 to the active site. Location of UBE2S at the edge of APC/C would accommodate growth of long UB chains.

visualized by trapping occur transiently in the context of multisite binding during APC/C^{CDH1}-mediated polyubiquitination (Figure 3).

DISCUSSION

A major challenge in understanding RING E3 catalyzed polyubiquitination has been to explain how dynamically tethered substrates and mobile RING-E2 assemblies collide. We were able to address this through cryo-EM and biochemical analyses, which revealed distinct APC/C–E2–UB-linked substrate architectures specialized for distinct geometric challenges of multiubiquitination and UB chain elongation.

Multiubiquitination is specified by multisite interactions between APC/C's cullin-RING core, UBE2C, and a tethered UB-linked substrate that (1) secure UBE2C∼UB to condense the search volume for catalytic encounter with the fluctuating substrate; (2) localize the active site proximal to substrate yet in a position that also accommodates a substrate-linked UB for further modification; and (3) additionally bind a primed substrate's linked UB to increase lifetime on APC/C and enhance processivity (Figure 7A). Constraining the proximity of substrate and UBE2C may contribute to preferential addition of individual UBs or short chains.

Topological requirements for linkage-specific UB chain elongation are satisfied by specialized placement of UBE2S, which (1) employs an extraordinary cullin-RING mechanism—where the cullin binds E2 and RING binds the substrate-linked UB—to juxtapose UBE2S's active site and the acceptor UB and (2) localizes the catalytic center at the edge of APC/C, spatially allowing growth of long UB chains (Figure 7B). Because elements of the catalytic complex are flexible relative to each other, catalytic engagement of APC2–APC11, UBE2S, and the acceptor UB may occur dynamically, as in the various orientations observed for 3D classes in negative stain EM (Movie S2). Although future studies will be required to determine if and how UB binding to the RING and UBE2S binding to APC2 synergize for catalysis, a rationale for APC/C tracking substrate-linked UBs for chain elongation (Kelly et al., 2014) comes from the RING–UBv structure: interactions with a homologous acceptor UB would include the β1/β2-loop harboring Lys11, which after linkage to another UB would disengage from the catalytic assembly, thereby promoting further chain elongation.

Each architecture is optimal for its own form of polyubiquitination but suboptimal for the other activity. For example, the constrained assembly for multiubiquitination would hinder growth of long UB chains due to limited space between a substrate degron and E2 active site (Figure 7A). Meanwhile, the placement of UBE2S would be suboptimal for priming or multiubiquitination because the long distance between a tethered substrate's D-box and the active site would limit opportunities for catalytic encounter with substrate lysines (Figure 7B).

It seems that the RING acting as a hub depends on individual interactions being weak, with multiple contacts converging to avidly support polyubiquitination architectures. While RING-UBE2C binding is undetectable in isolation, multisite interactions promote catalytic encounter (Figure 3C and S6H–S6J), after which the used UBE2C must dissociate from APC2–APC11 to be replaced by a charged UBE2C∼UB for another UB to be ligated (Brown et al., 2015). On the opposite side of the RING, evolving substrate-linked UBs apparently transiently sample the exosite either to promote PAA during UBE2C-catalyzed multiubiquitination or for chain elongation by UBE2S without jamming the system. Although future studies and new tools will be required determine the precise structure of UB bound to APC11's RING during these reactions, UB binding may be "fuzzy" due to dynamic hydrophobic interactions, or may involve specific contacts dynamically presenting UB from various formats akin to UB chain binding to the proteasome. We speculate that APC/C, like the proteasome (Shi et al., 2016), has multiple weak UB binding site(s) awaiting discovery as either promotiong PAA, UB chain elongation, or regulation.

APC/C's diverse catalytic architectures could comprise a combinatorial system for decorating substrates with various UB conjugate topologies. Although the rules determining whether a ubiquitinated substrate is preferentially modified by UBE2C and/or UBE2S remain to be determined, we envision that numerous input signals, for example D- and KEN-box affinities for CDH1, relative substrate lysine positions, and propensity for further polyubiquitination by UBE2C or UBE2S establish a "mix-and-match" system for differentially modifying substrates to regulate their proteasomal degradation (Dimova et al., 2012;

Grice et al., 2015; Kirkpatrick et al., 2006; Lu et al., 2015b; Meyer and Rape, 2014).

The different catalytic architectures are likely to be distinctly regulated. Some APC/C inhibitors, perhaps Mitotic Checkpoint Complex, could inhibit activity with UBE2C but still allow binding of UBE2S (Herzog et al., 2009; Kelly et al., 2014). Also, APC/C's assembly with the E2s is differentially regulated, for example by phosphorylation and protein interactions (Craney et al., 2016). Furthermore, UBE2C and UBE2S themselves undergo APC/C-dependent ubiquitin-mediated proteolysis through poorly characterized mechanisms (Garnett et al., 2009; Rape and Kirschner, 2004; Williamson et al., 2009; Wu et al., 2010). It is tempting to speculate that the two architectures enable the E2s to regulate each other. It seems likely that future studies will reveal how, when, and where the two catalytic architectures contribute to distinct APC/C functions and cell division.

Principles derived from the APC/C–E2 structures may apply to polyubiquitination by many RING E3s (Figure 7). Indeed, key features have parallels in other systems, including RING E3 collaboration with multiple E2s, multisite E3–E2 interactions, polyubiquitinating E2s forming an active conformation even without RING-binding, and UB-binding exosites in other E3s or E2s (Figure S7) (Metzger et al., 2014; Streich and Lima, 2014). APC/C presents fascinating re-use of a UB-binding exosite for different functions in distinct polyubiquitination architectures (Figure 7). The stage is now set for future studies aimed at understanding how other multidomain RING E3s dynamically respond in their own specialized ways to the distinctive features of multiple assorted E2∼UB and ubiquitinated substrate partners to establish the enormous conjugate variety associated with cellular polyubiquitination.

EXPERIMENTAL PROCEDURES

Protein Purification

Proteins described are human, except sequences derived from Hsl1, the tight-binding APC/C^{CDH1} substrate from *S. cerevisiae*. Baculoviruses expressing APC/C and subcomplexes were generated using biGBac (Weissmann et al., 2016). APC/C, subcomplexes, and UBA1 were expressed insect cells, and all other proteins in bacteria, and purified as described (Brown et al., 2015; Brown et al., 2014). The multiubiquitination and elongation traps were generated in a manner similar to that described for the priming trap (Brown et al., 2015) but with modifications. For multiubiquitination, the "substrate" was a fusion between a KEN- and D-box containing fragment of Hsl1 and C-terminal UBv, with a single Cys in place of Hsl1 K788, and the E2 was a catalytic Cys only version of UBE2C (C102A) that is active in multiubiquitination. For elongation, the "substrate" was a fusion between UBv at the N terminus and a D-box containing fragment of Hsl1 with a single Cys in place of UBv K11, and the E2 was a catalytic Cys only version of UBE2S (C118F, linker 15, see Figures S2G–S2L). 3-way crosslinking and trap purification were performed largely as described (Brown et al., 2015), except using the trifunctional sulfhydryl crosslinker TMEA (Pierce). For generation of samples for cryo-EM, APC/C^{CDH1} was first affinity purified based on tags on APC/C, the traps were added, and complexes were enriched by anti-Flag purification based on tags on the traps.

Structural Studies

NMR, X-ray crystallography, and cryo-EM were performed largely as described previously (Brown et al., 2015).

Assays

Ubiquitination assays were performed largely as described (Brown et al., 2014), with some differences. APC/C, CDH1, substrate, E1, and E2 were mixed on ice prior to initiating reactions, which were performed at room temperature in buffer used for purification (20 mM HEPES pH 8.0, 200 mM NaCl, 1 mM DTT) supplemented with 5 mM $MgCl_2$, 5 mM ATP, and 0.25 mg/mL BSA. For kinetic analyses, product bands were quantitated based on a fluorescein label on *UB, UB-CycB^{N}*, or UB-Securin* (* denotes location of fluorescein, N- or C terminus) using a Typhoon FLA 9500 PhosphorImager. For APC/C-dependent substrate ubiquitination reactions, APC/C-independent products were subtracted as background. Details of assays in each figure are in Supplemental Experimental Procedures.

ACCESSION NUMBERS

The accession numbers reported in this paper include: cryo-EM reconstructions representing multiubiquitination and elongation, EMDB: EMD-3432 and EMD-3433, respectively; crystal structure of APC11-UBv, PDB: 5JG6; and NMR assignments related to the APC11-UBv interaction, BMRB: 26783, 26784, and 26785.

SUPPLEMENTAL INFORMATION

Supplemental Information includes Supplemental Experimental Procedures, seven figures, one table, and two movies and can be found with this article online at http://dx.doi.org/10.1016/j.cell.2016.05.037.

AUTHOR CONTRIBUTIONS

N.G.B., R.V., E.R.W., A.O., W.Z., Y.L., J.-M.P., H.S., B.A.S. designed research supervised by N.G.B., S.S.S., B.K., M.W.K., J.W.H., B.A.S., J.M.P., B.A.S.; N.G.B., R.V., E.R.W., F.W., A.O., K.-P.W., W.Z., S.Y., J.S.H., R.Q., I.F.D., Y.L., P.D., M.R.B., C.R.R.G., D.J.M., D.H., D.Y., M.A.J., M.Y., P.Y.M., and G.P. performed research and/or contributed new reagents; N.G.B., R.V., E.R.W., A.O., W.Z., Y.L., J.S.H., C.R.R.G., J.-M.P., H.S., and B.A.S. analyzed data; and N.G.B., R.V., E.R.W., K.-P.W., J.W.H. and B.A.S. wrote the paper.

ACKNOWLEDGMENTS

We thank J. Bollinger, J. Rogers, J.R. Michael, D.W. Miller, K. Kavdia, J. Peng, S. Frase. Funding: Jane Coffin Childs, Leukemia & Lymphoma Society (N.G.B.); Edward R. & Anne G. Lefler Center (A.O.); CIHR and Mitacs Elevate (W.Z.); FWF–Hertha Firnberg Program (R.Q.); Damon Runyon, Lallage Feazel Wall Fund (Y.L.); Japan Society for the Promotion of Science (M.Y.); CIHR MOP#111149 and 136956 (S.S.S.); NIH R01GM073960 (B.K.), R01GM026875 (M.W.K.), R01AG011085 (J.W.H.), R37GM065930 and P30CA021765 (B.A.S.), P41GM103403 (NECAT); Boehringer Ingelheim, the Austrian Science Fund (SFB-F34 and Wittgenstein award), the Austrian Research Promotion Agency (Headquarter grants FFG-832936 and FFG-852936, Laura Bassi Centre for Optimized Structural Studies grant FFG-840283), and the European Community (FP7/2007-2013, grant 241548, MitoSys) (J.-M.P.); DFG Sonderforschungsbereich 860 (H.S.); ALSAC, HHMI (B.A.S.). NECAT and APS - NIH P41GM103403, DOE DE-AC02-06CH11357. J.W.H. consults for Millennium: the Takeda Oncology Company and Biogen.

Received: January 22, 2016
Revised: April 16, 2016
Accepted: May 9, 2016
Published: June 2, 2016

REFERENCES

Aristarkhov, A., Eytan, E., Moghe, A., Admon, A., Hershko, A., and Ruderman, J.V. (1996). E2-C, a cyclin-selective ubiquitin carrier protein required for the destruction of mitotic cyclins. Proc. Natl. Acad. Sci. USA *93*, 4294–4299.

Berndsen, C.E., and Wolberger, C. (2014). New insights into ubiquitin E3 ligase mechanism. Nat. Struct. Mol. Biol. *21*, 301–307.

Branigan, E., Plechanovová, A., Jaffray, E.G., Naismith, J.H., and Hay, R.T. (2015). Structural basis for the RING-catalyzed synthesis of K63-linked ubiquitin chains. Nat. Struct. Mol. Biol. *22*, 597–602.

Brown, N.G., Watson, E.R., Weissmann, F., Jarvis, M.A., VanderLinden, R., Grace, C.R., Frye, J.J., Qiao, R., Dube, P., Petzold, G., et al. (2014). Mechanism of polyubiquitination by human anaphase-promoting complex: RING repurposing for ubiquitin chain assembly. Mol. Cell *56*, 246–260.

Brown, N.G., VanderLinden, R., Watson, E.R., Qiao, R., Grace, C.R., Yamaguchi, M., Weissmann, F., Frye, J.J., Dube, P., Ei Cho, S., et al. (2015). RING E3 mechanism for ubiquitin ligation to a disordered substrate visualized for human anaphase-promoting complex. Proc. Natl. Acad. Sci. USA *112*, 5272–5279.

Buschhorn, B.A., Petzold, G., Galova, M., Dube, P., Kraft, C., Herzog, F., Stark, H., and Peters, J.M. (2011). Substrate binding on the APC/C occurs between the coactivator Cdh1 and the processivity factor Doc1. Nat. Struct. Mol. Biol. *18*, 6–13.

Chang, L., Zhang, Z., Yang, J., McLaughlin, S.H., and Barford, D. (2014). Molecular architecture and mechanism of the anaphase-promoting complex. Nature *513*, 388–393.

Chang, L., Zhang, Z., Yang, J., McLaughlin, S.H., and Barford, D. (2015). Atomic structure of the APC/C and its mechanism of protein ubiquitination. Nature *522*, 450–454.

Chao, W.C., Kulkarni, K., Zhang, Z., Kong, E.H., and Barford, D. (2012). Structure of the mitotic checkpoint complex. Nature *484*, 208–213.

Christensen, D.E., Brzovic, P.S., and Klevit, R.E. (2007). E2-BRCA1 RING interactions dictate synthesis of mono- or specific polyubiquitin chain linkages. Nat. Struct. Mol. Biol. *14*, 941–948.

Craney, A., Kelly, A., Jia, L., Fedrigo, I., Yu, H., and Rape, M. (2016). Control of APC/C-dependent ubiquitin chain elongation by reversible phosphorylation. Proc. Natl. Acad. Sci. USA *113*, 1540–1545.

da Fonseca, P.C., Kong, E.H., Zhang, Z., Schreiber, A., Williams, M.A., Morris, E.P., and Barford, D. (2011). Structures of APC/C(Cdh1) with substrates identify Cdh1 and Apc10 as the D-box co-receptor. Nature *470*, 274–278.

Deshaies, R.J., and Joazeiro, C.A. (2009). RING domain E3 ubiquitin ligases. Annu. Rev. Biochem. *78*, 399–434.

Dimova, N.V., Hathaway, N.A., Lee, B.H., Kirkpatrick, D.S., Berkowitz, M.L., Gygi, S.P., Finley, D., and King, R.W. (2012). APC/C-mediated multiple monoubiquitylation provides an alternative degradation signal for cyclin B1. Nat. Cell Biol. *14*, 168–176.

Dou, H., Buetow, L., Sibbet, G.J., Cameron, K., and Huang, D.T. (2012). BIRC7-E2 ubiquitin conjugate structure reveals the mechanism of ubiquitin transfer by a RING dimer. Nat. Struct. Mol. Biol. *19*, 876–883.

Ernst, A., Avvakumov, G., Tong, J., Fan, Y., Zhao, Y., Alberts, P., Persaud, A., Walker, J.R., Neculai, A.M., Neculai, D., et al. (2013). A strategy for modulation of enzymes in the ubiquitin system. Science *339*, 590–595.

Garnett, M.J., Mansfeld, J., Godwin, C., Matsusaka, T., Wu, J., Russell, P., Pines, J., and Venkitaraman, A.R. (2009). UBE2S elongates ubiquitin chains on APC/C substrates to promote mitotic exit. Nat. Cell Biol. *11*, 1363–1369.

Grice, G.L., Lobb, I.T., Weekes, M.P., Gygi, S.P., Antrobus, R., and Nathan, J.A. (2015). The Proteasome Distinguishes between Heterotypic and Homotypic Lysine-11-Linked Polyubiquitin Chains. Cell Rep. *12*, 545–553.

Herzog, F., Primorac, I., Dube, P., Lenart, P., Sander, B., Mechtler, K., Stark, H., and Peters, J.M. (2009). Structure of the anaphase-promoting complex/cyclosome interacting with a mitotic checkpoint complex. Science *323*, 1477–1481.

Kamenz, J., Mihaljev, T., Kubis, A., Legewie, S., and Hauf, S. (2015). Robust Ordering of C Events by Adaptive Thresholds and Competing Degradation Pathways. Mol. Cell *60*, 446–459.

Kelly, A., Wickliffe, K.E., Song, L., Fedrigo, I., and Rape, M. (2014). Ubiquitin chain elongation requires E3-dependent tracking of the emerging conjugate. Mol. Cell *56*, 232–245.

King, R.W., Peters, J.M., Tugendreich, S., Rolfe, M., Hieter, P., and Kirschner, M.W. (1995). A 20S complex containing CDC27 and CDC16 catalyzes the mitosis-specific conjugation of ubiquitin to cyclin B. Cell *81*, 279–288.

Kirkpatrick, D.S., Hathaway, N.A., Hanna, J., Elsasser, S., Rush, J., Finley, D., King, R.W., and Gygi, S.P. (2006). Quantitative analysis of in vitro ubiquitinated cyclin B1 reveals complex chain topology. Nat. Cell Biol. *8*, 700–710.

Lu, D., Hsiao, J.Y., Davey, N.E., Van Voorhis, V.A., Foster, S.A., Tang, C., and Morgan, D.O. (2014). Multiple mechanisms determine the order of APC/C substrate degradation in mitosis. J. Cell Biol. *207*, 23–39.

Lu, D., Girard, J.R., Li, W., Mizrak, A., and Morgan, D.O. (2015a). Quantitative framework for ordered degradation of APC/C substrates. BMC Biol. *13*, 96.

Lu, Y., Lee, B.H., King, R.W., Finley, D., and Kirschner, M.W. (2015b). Substrate degradation by the proteasome: a single-molecule kinetic analysis. Science *348*, 1250834.

Lu, Y., Wang, W., and Kirschner, M.W. (2015c). Specificity of the anaphase-promoting complex: a single-molecule study. Science *348*, 1248737.

Mattiroli, F., and Sixma, T.K. (2014). Lysine-targeting specificity in ubiquitin and ubiquitin-like modification pathways. Nat. Struct. Mol. Biol. *21*, 308–316.

McGinty, R.K., Henrici, R.C., and Tan, S. (2014). Crystal structure of the PRC1 ubiquitylation module bound to the nucleosome. Nature *514*, 591–596.

Metzger, M.B., Pruneda, J.N., Klevit, R.E., and Weissman, A.M. (2014). RING-type E3 ligases: master manipulators of E2 ubiquitin-conjugating enzymes and ubiquitination. Biochim. Biophys. Acta *1843*, 47–60.

Meyer, H.J., and Rape, M. (2014). Enhanced protein degradation by branched ubiquitin chains. Cell *157*, 910–921.

Plechanovová, A., Jaffray, E.G., Tatham, M.H., Naismith, J.H., and Hay, R.T. (2012). Structure of a RING E3 ligase and ubiquitin-loaded E2 primed for catalysis. Nature *489*, 115–120.

Primorac, I., and Musacchio, A. (2013). Panta rhei: the APC/C at steady state. J. Cell Biol. *201*, 177–189.

Pruneda, J.N., Littlefield, P.J., Soss, S.E., Nordquist, K.A., Chazin, W.J., Brzovic, P.S., and Klevit, R.E. (2012). Structure of an E3:E2~Ub complex reveals an allosteric mechanism shared among RING/U-box ligases. Mol. Cell *47*, 933–942.

Rape, M., and Kirschner, M.W. (2004). Autonomous regulation of the anaphase-promoting complex couples mitosis to S-phase entry. Nature *432*, 588–595.

Rape, M., Reddy, S.K., and Kirschner, M.W. (2006). The processivity of multiubiquitination by the APC determines the order of substrate degradation. Cell *124*, 89–103.

Reverter, D., and Lima, C.D. (2005). Insights into E3 ligase activity revealed by a SUMO-RanGAP1-Ubc9-Nup358 complex. Nature *435*, 687–692.

Rodrigo-Brenni, M.C., and Morgan, D.O. (2007). Sequential E2s drive polyubiquitin chain assembly on APC targets. Cell *130*, 127–139.

Scott, D.C., Sviderskiy, V.O., Monda, J.K., Lydeard, J.R., Cho, S.E., Harper, J.W., and Schulman, B.A. (2014). Structure of a RING E3 trapped in action reveals ligation mechanism for the ubiquitin-like protein NEDD8. Cell *157*, 1671–1684.

Shi, Y., Chen, X., Elsasser, S., Stocks, B.B., Tian, G., Lee, B.H., Shi, Y., Zhang, N., de Poot, S.A., Tuebing, F., et al. (2016). Rpn1 provides adjacent receptor sites for substrate binding and deubiquitination by the proteasome. Science *351*, 831.

Streich, F.C., Jr., and Lima, C.D. (2014). Structural and functional insights to ubiquitin-like protein conjugation. Annu. Rev. Biophys. *43*, 357–379.

Sudakin, V., Ganoth, D., Dahan, A., Heller, H., Hershko, J., Luca, F.C., Ruderman, J.V., and Hershko, A. (1995). The cyclosome, a large complex containing cyclin-selective ubiquitin ligase activity, targets cyclins for destruction at the end of mitosis. Mol. Biol. Cell *6*, 185–197.

Tian, W., Li, B., Warrington, R., Tomchick, D.R., Yu, H., and Luo, X. (2012). Structural analysis of human Cdc20 supports multisite degron recognition by APC/C. Proc. Natl. Acad. Sci. USA *109*, 18419–18424.

Wang, W., and Kirschner, M.W. (2013). Emi1 preferentially inhibits ubiquitin chain elongation by the anaphase-promoting complex. Nat. Cell Biol. *15*, 797–806.

Weissmann, F., Petzold, G., VanderLinden, R., Huis in 't Veld, P.J., Brown, N.G., Lampert, F., Westermann, S., Stark, H., Schulman, B.A., and Peters, J.M. (2016). biGBac enables rapid gene assembly for the expression of large multisubunit protein complexes. Proc. Natl. Acad. Sci. USA *113*, E2564–E2569.

Wickliffe, K.E., Lorenz, S., Wemmer, D.E., Kuriyan, J., and Rape, M. (2011). The mechanism of linkage-specific ubiquitin chain elongation by a single-subunit E2. Cell *144*, 769–781.

Wieser, S., and Pines, J. (2015). The biochemistry of mitosis. Cold Spring Harb. Perspect. Biol. *7*, a015776.

Williamson, A., Wickliffe, K.E., Mellone, B.G., Song, L., Karpen, G.H., and Rape, M. (2009). Identification of a physiological E2 module for the human anaphase-promoting complex. Proc. Natl. Acad. Sci. USA *106*, 18213–18218.

Wu, T., Merbl, Y., Huo, Y., Gallop, J.L., Tzur, A., and Kirschner, M.W. (2010). UBE2S drives elongation of K11-linked ubiquitin chains by the anaphase-promoting complex. Proc. Natl. Acad. Sci. USA *107*, 1355–1360.

Yu, H., King, R.W., Peters, J.M., and Kirschner, M.W. (1996). Identification of a novel ubiquitin-conjugating enzyme involved in mitotic cyclin degradation. Curr. Biol. *6*, 455–466.

Cell

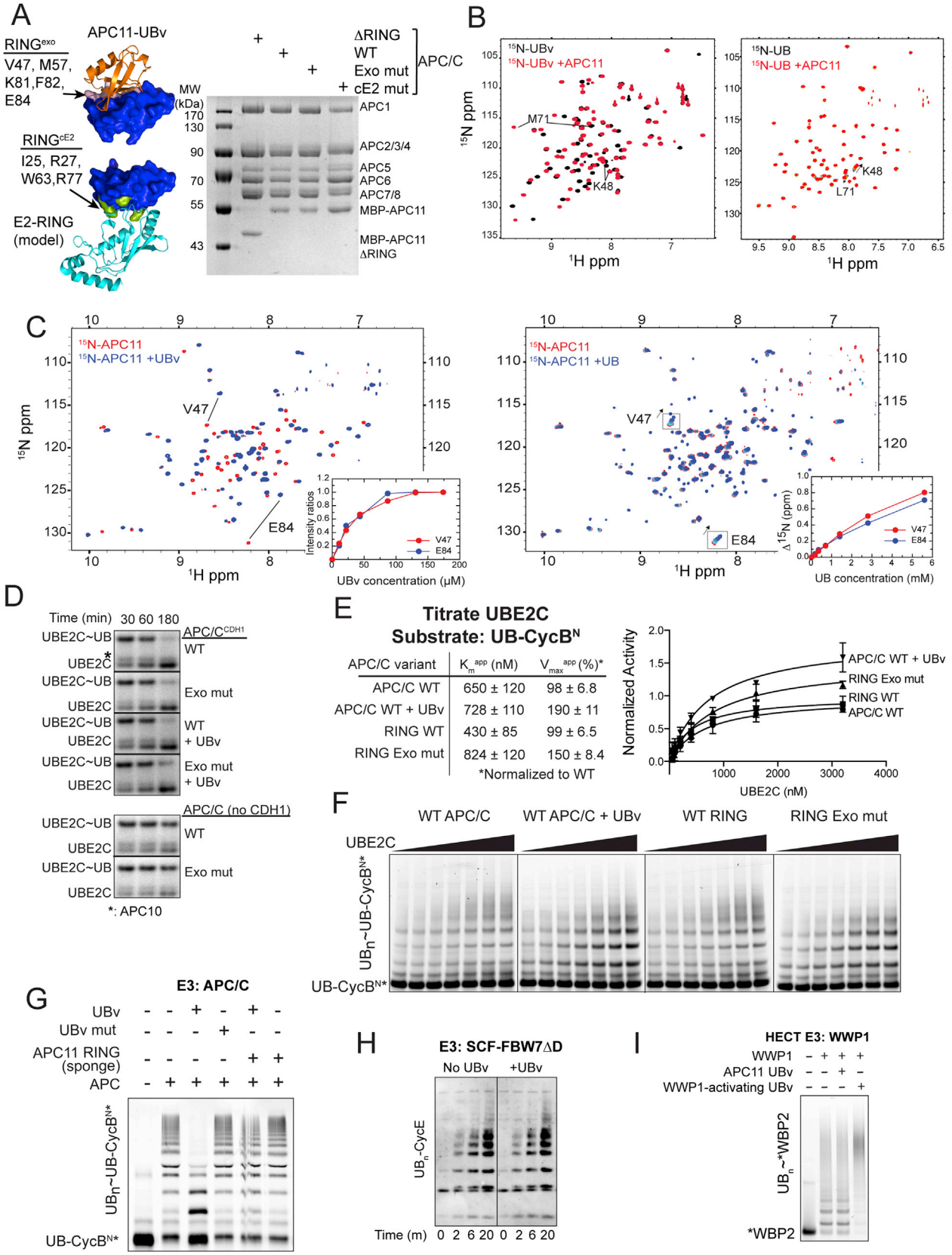

(legend on next page)

Figure S1. UB and UBv Bind the APC11 RING Exosite, Related to Figure 1

(A) Structural view of APC11 RING cE2 and exosite surfaces and representative Coomassie-stained SDS-PAGE gel of purified recombinant APC/C complexes harboring APC11 RING mutations. Left, from top to bottom, crystal structure of APC11 RING (blue)–UBv (orange) complex, showing UBv binds the previously defined exosite surface (key residues previously defined by mutagenesis and NMR in (Brown et al., 2014) shown in pink). Model of an APC11 RING–E2 complex, based on closest APC11 RING homolog (Scott et al., 2014), with canonical E2-binding site residues mutationally shown to activate UBE2C in green (Brown et al., 2014). Right, Coomassie-stained gel of recombinant APC/C complexes. RING mutant experiments use MBP-fused APC11, which allows confirming stoichiometric incorporation into APC/C by SDS-PAGE. ΔRING is APC11 (1-17), WT is full-length APC11, Exo mut contains M57A and F82A mutations, and cE2 mut contains an R27A mutation.

(B and C) NMR spectra used for CSP analyses in Figure 2C, which showed that UBv and UB bind similar APC11 RING surfaces and vice-versa, but that the UBv interaction is higher affinity.

(B) Left, overlaid [^{15}N, ^{1}H] TROSY spectra of ^{15}N-labeled UBv alone (100 μM, black) or with APC11 RING (1:2, red). Right, overlaid [^{15}N, ^{1}H] TROSY spectra of ^{15}N-labeled UB alone (100 μM, black) or with titration of 0.075, 0.15, 0.3, 0.6, and 1.2 mM APC11 RING in green, cyan, purple, orange, and red, respectively. The results for titrating the APC11 RING domain into ^{15}N-labeled UB were performed here as a control, and agree with our previously published data (Brown et al., 2014).

(C) Left, overlaid [^{15}N, ^{1}H] TROSY spectra of ^{15}N-labeled APC11 RING alone (100 μM, red) with UBv (1:2, dark blue). Right, overlaid [^{15}N, ^{1}H] TROSY spectra of ^{15}N-labeled APC11 RING alone (100 μM, red) or with titration of 0.35, 1.4, 2.8 and 5.6 mM UB in shades of light to dark blue, respectively. Tighter binding of UBv compared to UB is revealed in insets by the change in intensity or ^{15}N chemical shift of APC11 RING residues V47 and E84 when plotted as a function of concentration of either UBv, left, or UB, right, respectively. The results for titrating UB into ^{15}N-labeled APC11 RING domain were performed here as a control, and agree with our previously published data (Brown et al., 2014).

(D) Neither the APC11 RING^{exo} mutation nor adding UBv strongly affects APC/C^{CDH1}-activated hydrolysis of a UBE2C∼UB intermediate. To consider potential effects of the UB-binding exosite on intrinsic RING–E2 catalysis by APC/C, the RING exosite mutant or adding UBv were tested for APC/C^{CDH1}-dependent hydrolysis of an oxyester-linked UBE2C∼UB complex, which assays for canonical RING-dependent activation in the absence of a substrate a function of time using Coomassie-stained SDS-PAGE gels. Control experiments confirmed CDH1-dependence of APC/C's intrinsic RING–E2 catalytic activity.

(E) Enzyme kinetic analyses titrating UBE2C in substrate ubiquitination assays with APC/C^{CDH1}. Kinetic parameters, left, and curve fits, right, from titrating UBE2C to test the role of RING exosite on the catalytic efficiency in assays with fixed concentrations of APC/C^{CDH1} variants and UB-CycB^{N*}. SEM, $n \geq 3$.

(F) Representative SDS-PAGE gels for data used to determine the kinetic parameters in E. Ubiquitination of fluorescent UB-CycB^{N*} was quantified, normalized, and fitted to the Michaelis-Menten equation.

(G) UBv–APC11 RING interaction is required for UBv to inhibit APC/C^{CDH1}–UBE2S-mediated UB chain elongation. Adding UBv (200 μM) inhibits APC/C^{CDH1}–UBE2S-catalyzed UB chain elongation, whereas there is no effect of adding the hydrophobic patch (I42D F44D L68D) mutant UBv that does not bind APC11. UBv-mediated inhibition is relieved by adding excess free APC11 RING domain (200 μM), which can act like a "sponge" and sequester UBv.

(H) APC11-specific UBv does not substantially impact ubiquitination by a closely related RING E3. SCF E3s contain the RING subunit RBX1, which is APC11's closest relative. Anti-biotin western blot shows SCF$^{FBW7\Delta D}$ -dependent ubiquitination of a biotinylated phosphopeptide derived from cyclin E, using E2s UBCH5B and CDC34 that mediate priming and UB chain elongation for this SCF.

(I) APC11-specific UBv does not substantially impact ubiquitination by the HECT E3, WWP1, which has its own specific UBv activating polyubiquitination via a distinctive UB-binding exosite. WWP1-dependent ubiquitination of fluorescent *WBP2 was monitored by SDS-PAGE and fluorescent scanning. Whereas the APC11-specific UBv has no effect, the WWP1-activating UBv stimulates ubiquitination (Zhang et al., 2016).

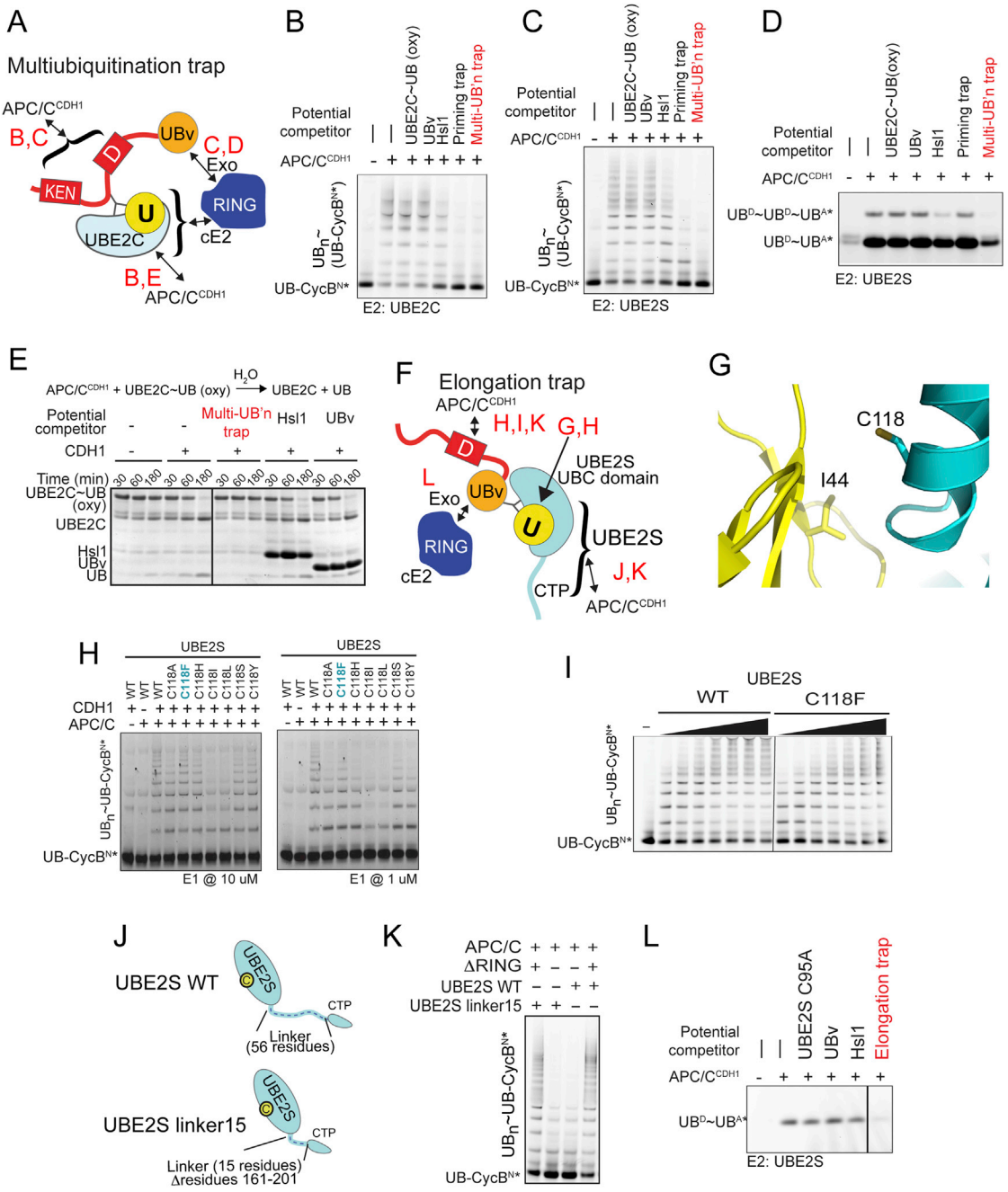

Figure S2. Generating and Validating 3-Way Crosslinked Complexes for "Trapping" APC/C^{CDH1}–E2 Architectures Representing Multiubiquitination and UB Chain Elongation, Related to Figure 2

(A) Schematic of the 3-way crosslinked complex used to trap APC/C^{CDH1}–UBE2C in architecture representing multiubiquitination. Panels investigating the complex blocking multiubiquitination (B), substrate binding to APC/C^{CDH1} (C), UBE2C binding to APC/C^{CDH1} (B, E), and UB binding to the RING exosite (C, D) are indicated. The priming trap contains the same elements except UBv, and was described previously (Brown et al., 2015).

(B) Multiubiquitination trap blocks APC/C^{CDH1}–UBE2C-mediated multiubiquitination of UB-CycB^{N*}. Representative fluorescent scan of ubiquitination assays testing whether the multiubiquitination trap properly binds APC/C^{CDH1}. If the multiubiquitination trap binds both the substrate binding site via Hsl1 and the APC2-APC11 cullin-RING catalytic core via UBE2CxUB, then the cross-linked multiubiquitination trap should inhibit APC/C^{CDH1}-UBE2C-catalyzed substrate ubiquitination at a lower concentration than Hsl1 on it own, as is observed for the trap and its constituent components at a concentration of 270 nM.

(C) Multiubiquitination trap blocks APC/C^{CDH1}-UBE2S-mediated UB chain elongation of UB-CycB^{N*}. Representative fluorescent scan of ubiquitination assays testing whether the multiubiquitination trap properly binds APC/C^{CDH1}. If the multiubiquitination trap binds both the substrate binding site via Hsl1 and the APC11 RING exosite via the UBv, then the cross-linked multiubiquitination trap should inhibit APC/C-UBE2S-mediated UB chain elongation at a lower concentration than Hsl1 or UBv on their own, as is observed for the trap and its constituent components at a concentration of 270 nM.

(legend continued on next page)

(D) Multiubiquitination trap blocks APC/C^{CDH1}-UBE2S-mediated di-UB synthesis. Effects of adding multiubiquitination trap to assays monitoring APC/C^{CDH1}–UBE2S-mediated di-UB synthesis using an unlabeled donor UB (UB^{D}) with a fluorescent acceptor (UB^{A*}, C-terminal modification prevents its use as a donor). The inhibition of free UB chain synthesis by the multiubiquitination trap (with UBv) but not the priming trap (without UBv) suggests the UBv is bound to the native UB binding exosite on the APC11 RING domain that is essential for APC/C^{CDH1}–UBE2S-catalyzed formation of UB chains. The trap and its constituent components were screened at a concentration of 270 nM.

(E) Multiubiquitination trap blocks a substrate-independent APC/C^{CDH1} activation of UBE2C∼UB. Multiubiquitination trap prevents APC/C^{CDH1}-mediated hydrolysis of UBE2C∼UB (oxy) into UBE2C and UB over time, detected with Coomassie-stained SDS-PAGE gels. This result indicates that the UBE2C component of the multiubiquitination trap properly binds to the APC2-APC11 cullin-RING catalytic core.

(F) Schematic of the elongation trap representing UBE2S (cyan) as if building a K11-linked UB chain on a substrate (Hsl1 D-box, red)-linked UBv (orange) anchoring the RING. Panels identifying a suitable mutant version of UBE2S that allows 3-way crosslinking through mutation of non-active site Cys118 (G-I), and reducing the flexible linker between UBE2S's UBC domain and APC/C-binding tip of the CTP (J-L) are indicated.

(G) Model of UBE2S∼UB^{D} in activated closed conformation showing Cys118 interacting with donor UB. The model is based on the crystal structure (PDB ID 5BNB) representing a UBE2S∼UB intermediate (Lorenz et al., 2016). UBE2S (cyan) C118 is predicted to bind the essential I44 in the donor UB (yellow), requiring a suitable alternative to generate a single active site Cys only version of UBE2S.

(H) Identification of suitable residue replacement for C118 in UBE2S to generate a single-Cys (active site only) version for crosslinking. A single-cysteine version of UBE2S was needed to ensure specific three-way crosslinking. Therefore, to generate a version of UBE2S with only a Cys at the active site, it was necessary to replace C118 in the donor UB binding site. Multiple UBE2S variants were purified and tested for their activity in APC/C^{CDH1}-UBE2S-mediated substrate ubiquitination to determine the best alternative amino acid substitution to be used in the elongation trap. Representative fluorescent scans demonstrated that a phenylalanine substitution at position C118 restored activity to near wild-type UBE2S-mediated ubiquitination levels. The E1-dependent variation of substrate ubiquitination (left, 10 μM, right, 1 μM) suggests that mutating C118 resulted in an E2∼UB conjugation defect.

(I) Validation of UBE2S C118F as suitable version for structural studies. Representative fluorescent scan of UB-$CycB^{N*}$ ubiquitination by APC/C^{CDH1}-UBE2S. A titration of either wild-type UBE2S or the C118F variant, at relatively high E1 concentration (10 μM), reveals that the UBE2S C118F variant maintains substrate ubiquitination near wild-type levels.

(J) Schematic of the domain structure of wild-type and the linker15 variant of UBE2S. The UBC domain (residues 1-156) and the C-terminal peptide (residues 213-222) are separated by 56 linker residues. In the UBE2S linker 15 variant, 41 residues (residues 161-201) were deleted from the linker.

(K) Representative fluorescent scan of APC/C^{CDH1}-UBE2S-mediated ubiquitination of UB-$CycB^{N*}$ demonstrates comparable RING-dependent activities of both wild-type and linker 15 variant of UBE2S.

(L) Avid binding of the elongation trap harboring UBv-fused substrate and a single catalytic Cys only/linker 15 UBE2S potently inhibits APC/C^{CDH1}-UBE2S-mediated di-UB* synthesis. Similar to (D), representative fluorescent scan of ubiquitination assays testing whether the elongation trap properly binds APC/C^{CDH1}. If the elongation trap binds both the substrate binding site via Hsl1 and the APC11 RING exosite via UBv, then the cross-linked elongation trap should inhibit APC/C^{CDH1}-UBE2S-mediated di-Ub synthesis at a lower concentration than UBv on its own, as is observed for the trap and its constituent components at a concentration of 100 nM.

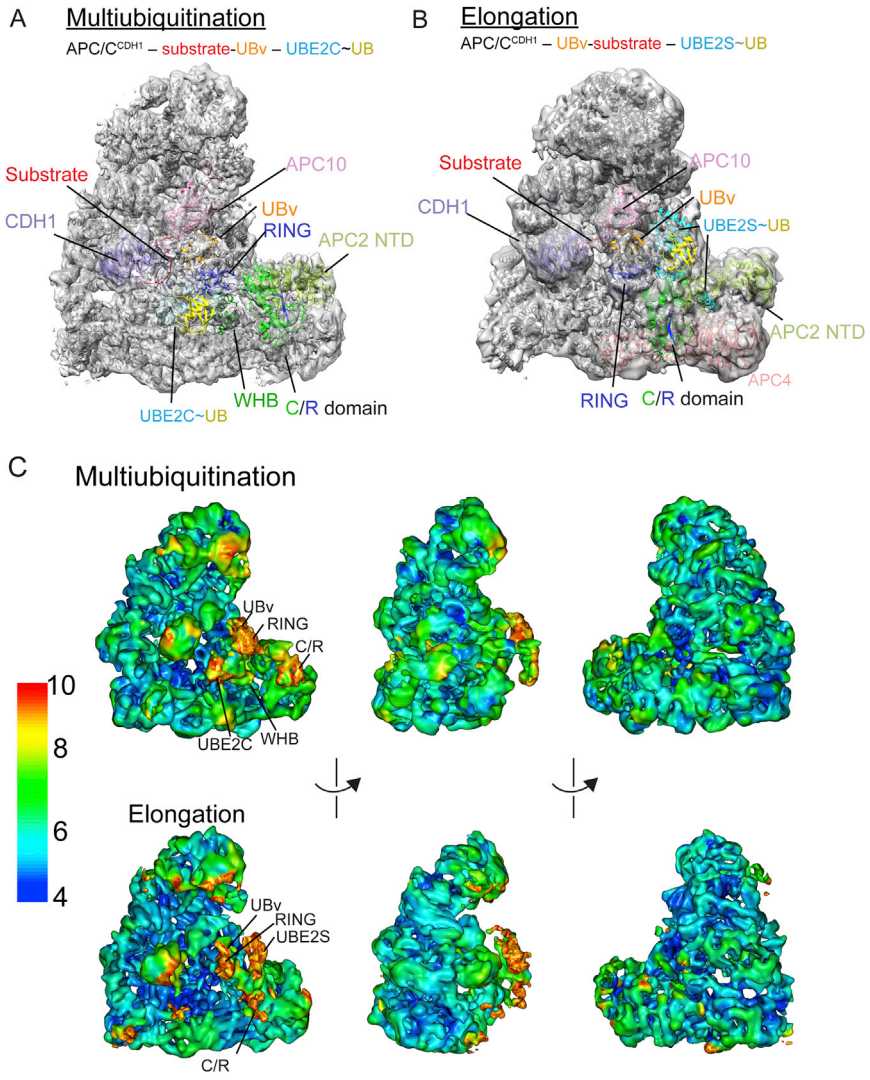

Figure S3. Molecular Models Based on Cryo-EM Reconstructions of APC/C^{CDH1} Complexes with UBE2C and UBE2S Representing Multiubiquitination and UB Chain Elongation, Respectively, Related to Figure 3

(A) Cryo-EM reconstruction of APC/C^{CDH1}–UBv-substrate-x-UBE2C-x-UB complex, i.e., representing processive multiubiquitination, whereby substrate-linked UB (represented by UBv) binding to APC11 RING exosite stimulates UB ligation to another site on the substrate. After fitting structures of APC/C and CDH1-substrate, APC2–APC11 C/R domain, the APC11 RING (navy)-UBv (orange) complex and APC2^{WHB} (dark green)-UBE2C (light cyan) complex structures were fit into the EM map using Chimera (Brown et al., 2015; Chang et al., 2015) and Figure 2B. A donor UB (yellow) was based on superimposing the UBE2C–APC11 RING assembly with homologous RING-E2~UB structures (Dou et al., 2012; Plechanovová et al., 2012) is compatible with the catalytic architecture although the donor UB is not visible in the map. Positioning of UBE2C~UB for substrate ubiquitination is achieved via UBE2C~UB recruitment by the WHB domain of APC2 and activation by the RING domain of APC11. Furthermore, the ubiquitinated substrate, represented by the substrate-UBv fusion, simultaneously binds APC/C substrate receptors, CDH1 and APC10, along with the RING exosite to mediate processive affinity amplification.

(B) Cryo-EM reconstruction of APC/C^{CDH1}–substrate-UBv-x-UBE2S-x-UB, i.e., representing UB chain elongation whereby APC/C^{CDH1}–UBE2S links UB to a Lys11 on a substrate-linked UB (represented by UBv). After fitting structures of APC/C and CDH1–substrate, the APC2–APC11 C/R domain, the APC11 RING (navy)-UBv (orange) complex, and UBE2S (light cyan) structures were fit into the EM map using Chimera (Brown et al., 2015; Chang et al., 2015; Lorenz et al., 2016; Pettersen et al., 2004) and Figure 2B. APC/C uses a distinct mechanism to recruit and position UBE2S for UB chain elongation. The EM map is compatible with clash-free modeling a UBE2S~UB complex (Lorenz et al., 2016), although the donor UB (yellow) is not visible in the map even at low contour. Unlike UBE2C, UBE2S is anchored by its CTP binding a groove between APC2 and APC4, while UBE2S's catalytic UBC domain is uniquely placed by APC2 in proximity to the APC11-recruited UB, represented by the APC11–UBv structure. Therefore, the APC/C catalytic core uses a noncanonical mechanism to recruit UBE2S, and to position both UBE2S and the acceptor UB to catalyze formation of K11-linked polyUB chains.

(C) Visualization of structural dynamics of APC/C^{CDH1} complexes with E2s. Cryo-EM maps representing the multiubiquitination and UB chain elongation are rainbow colored according to local resolution from 10 Å resolution in red to 4 Å resolution in blue.

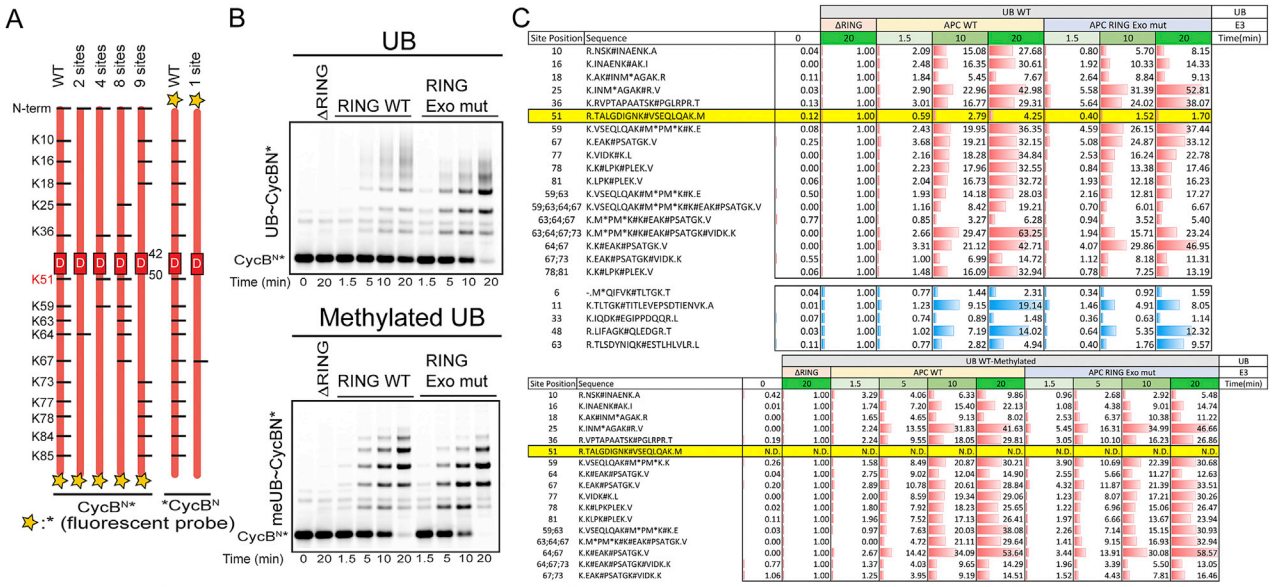

C

		UB WT							UB
		ΔRING	APC WT			APC RING Exo mut			E3
Site Position	Sequence	0	20	1.5	10	20	1.5	10	20	Time(min)
10	R.NSK#INAENK.A	0.04	1.00	2.09	15.08	27.68	0.80	5.70	8.15	
16	K.INAENK#AK.I	0.00	1.00	2.48	16.35	30.61	1.92	10.33	14.33	
18	K.AK#INM*AGAK.R	0.11	1.00	1.84	5.45	7.67	2.64	8.84	9.13	
25	K.INM*AGAK#R.V	0.03	1.00	2.90	22.96	42.98	5.58	31.39	52.81	
36	K.RVPTAPAATSK#PGLRPR.T	0.13	1.00	3.01	16.77	29.31	5.64	24.02	38.07	
51	R.TALGDIGNK#VSEQLQAK.M	0.12	1.00	0.59	2.79	4.25	0.40	1.52	1.70	
59	K.VSEQLQAK#M*PM*K#K.E	0.08	1.00	2.43	19.95	36.35	4.59	26.15	37.44	
67	K.EAK#PSATGK.V	0.25	1.00	3.68	19.21	32.15	5.08	24.87	33.12	
77	K.VIDK#K.L	0.00	1.00	2.16	18.28	34.84	2.53	16.24	22.78	
78	K.K#LPK#PLEK.V	0.00	1.00	2.23	17.96	32.55	0.84	13.38	17.46	
81	K.LPK#PLEK.V	0.06	1.00	2.04	16.73	32.72	1.93	12.18	16.23	
59;63	K.VSEQLQAK#M*PM*K#K.E	0.50	1.00	1.93	14.18	28.03	2.16	12.81	17.27	
59;63;64;67	K.VSEQLQAK#M*PM*K#K#EAK#PSATGK.V	0.00	1.00	1.16	8.42	19.21	0.70	6.01	6.67	
63;64;67	K.M*PM*K#K#EAK#PSATGK.V	0.77	1.00	0.85	3.27	6.28	0.94	3.52	5.40	
63;64;67;73	K.M*PM*K#K#EAK#PSATGK#VIDK.K	0.00	1.00	2.66	29.47	63.25	1.94	15.71	23.24	
64;67	K.K#EAK#PSATGK.V	0.00	1.00	3.31	21.12	42.71	4.07	29.86	46.95	
67;73	K.EAK#PSATGK#VIDK.K	0.55	1.00	1.00	6.99	14.72	1.12	8.18	11.31	
78;81	K.K#LPK#PLEK.V	0.06	1.00	1.48	16.09	32.94	0.78	7.25	13.19	
6	-.M*QIFVK#TLTGK.T	0.04	1.00	0.77	1.44	2.31	0.34	0.92	1.59	
11	K.TLTGK#TITLEVEPSDTIENVK.A	0.01	1.00	1.23	9.15	19.14	1.46	4.91	8.05	
33	K.IQDK#EGIPPDQQR.L	0.07	1.00	0.74	0.89	1.48	0.36	0.63	1.14	
48	R.LIFAGK#QLEDGR.T	0.03	1.00	1.02	7.19	14.02	0.64	5.35	12.32	
63	R.TLSDYNIQK#ESTLHLVLR.L	0.11	1.00	0.77	2.82	4.94	0.40	1.76	9.57	

		UB WT-Methylated									UB
		ΔRING	APC WT				APC RING Exo mut				E3
Site Position	Sequence	0	20	1.5	5	10	20	1.5	5	10	20	Time(min)
10	R.NSK#INAENK.A	0.42	1.00	3.29	4.06	6.33	9.86	0.96	2.68	2.92	5.48	
16	K.INAENK#AK.I	0.01	1.00	1.74	7.20	15.40	22.13	1.08	4.38	9.01	14.74	
18	K.AK#INM*AGAK.R	0.00	1.00	1.65	4.65	9.13	8.02	2.53	6.37	10.38	11.22	
25	K.INM*AGAK#R.V	0.00	1.00	2.24	13.55	31.83	41.63	5.45	16.31	34.99	46.66	
36	R.VPTAPAATSK#PGLRPR.T	0.19	1.00	2.24	9.55	18.05	29.81	3.05	10.10	16.23	26.86	
51	R.TALGDIGNK#VSEQLQAK.M	N.D.	N.D.	N.D.	N.D.	N.D.	N.D.	N.D.	N.D.	N.D.	N.D.	
59	K.VSEQLQAK#M*PM*K.K	0.26	1.00	1.58	8.49	20.87	30.21	3.90	10.69	22.39	30.68	
64	K.K#EAK#PSATGK.V	0.04	1.00	2.75	9.02	12.04	14.90	2.55	5.66	11.27	12.63	
67	K.EAK#PSATGK.V	0.20	1.00	2.89	10.78	20.61	28.84	4.32	11.87	21.39	33.51	
77	K.VIDK#K.L	0.00	1.00	2.00	8.59	19.34	29.06	1.23	8.07	17.21	30.26	
78	K.K#LPKPLEK.V	0.02	1.00	1.80	7.92	18.23	25.65	1.22	6.96	15.06	26.47	
81	K.KLPK#PLEK.V	0.11	1.00	1.96	7.52	17.13	26.41	1.97	6.66	13.67	23.94	
59;63	K.VSEQLQAK#M*PM*K#K.E	0.03	1.00	0.97	7.63	20.03	38.08	2.26	7.14	15.15	30.93	
63;64;67	K.M*PM*K#K#EAK#PSATGK.V	0.00	1.00	0.00	4.72	21.11	29.64	1.41	9.15	16.93	32.94	
64;67	K.K#EAK#PSATGK.V	0.00	1.00	2.67	14.42	34.09	53.64	3.44	13.91	30.08	58.57	
64;67;73	K.K#EAK#PSATGK#VIDK.K	0.77	1.00	1.37	4.03	9.65	14.29	1.96	3.39	5.50	13.05	
67;73	K.EAK#PSATGK#VIDK.K	1.06	1.00	1.25	3.95	9.19	14.51	1.52	4.43	7.81	16.46	

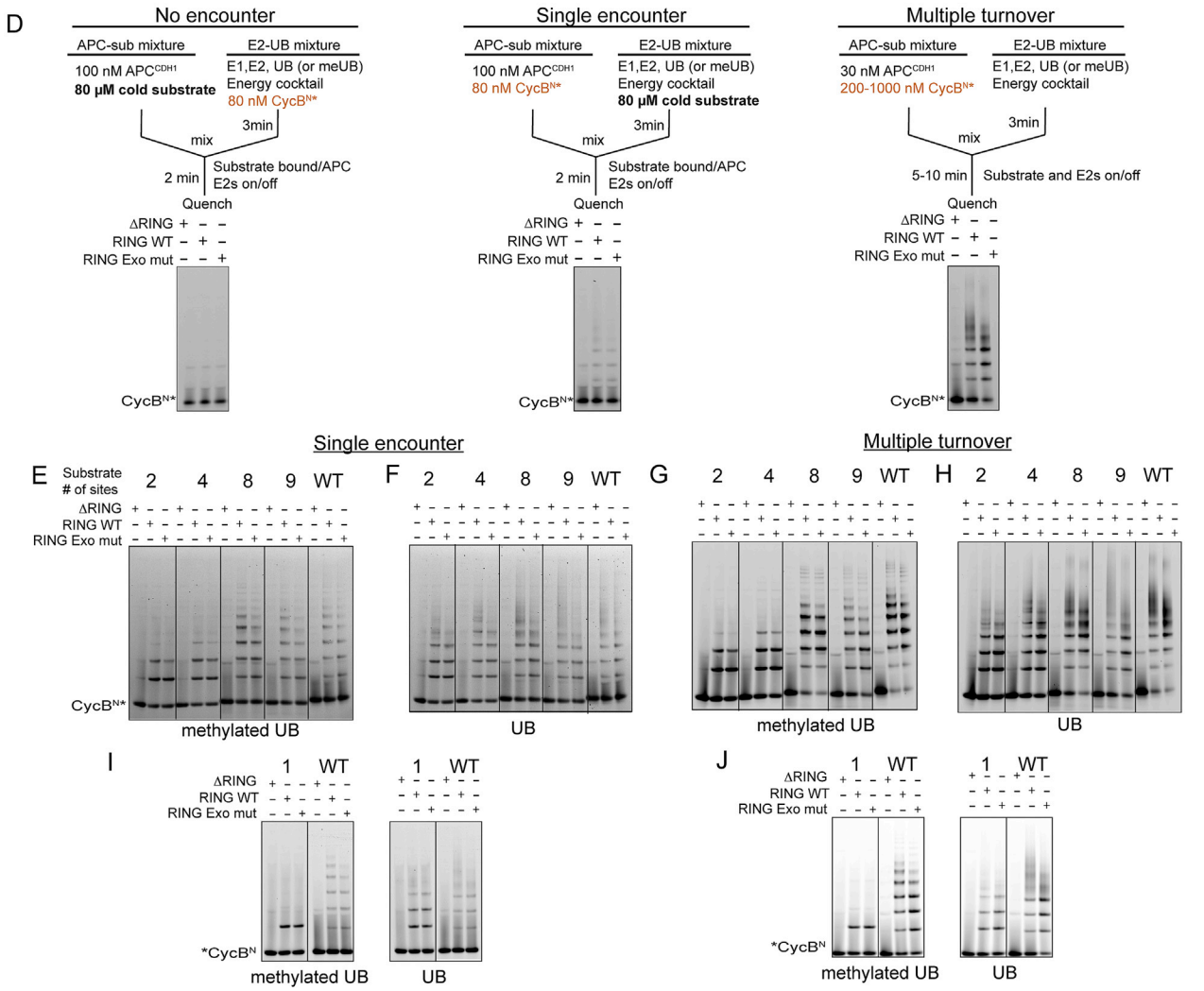

(legend on next page)

Figure S4. Ubiquitination Assays and Mass Spectrometry Revealing How Substrate-Linked UB Binding to the APC/C RING Exosite Contributes to APC/C^{CDH1}-UBE2C-Mediated Multiubiquitination, Related to Figure 4

(A) Schematic of the version of CycB^{N*} (residues 1-88) and versions with fewer ubiquitination sites. CycB^{N*} has 16 potential ubiquitination sites, from the N terminus and 15 lysines, indicated with a black lines. The D-box degron (residues 42-50) responsible for substrate recruitment is represented as a red rectangle, labeled D. All sites except K51 could access UBE2C in the multiubiquitination architecture (Figures 3C and S3A). The locations of 1, 2, 4, 8, and 9 potential ubiquitination sites retained in mutants used in panels E-H are indicated. In the mutants, all other lysines were mutated to arginines, and/or the N terminus blocked by sortase-mediated linkage of an N-terminally acetylated peptide.

(B) Representative fluorescence scans of time-courses following APC/C^{CDH1}-UBE2C-mediated substrate multiubiquitination with either WT UB or meUB reveal that mutating the APC/C RING exosite affects both substrate turnover and extent of ubiquitination. Substrate (CycB^{N*}) multiubiquitination was examined in experiments similar to Figure 4E, but side-by-side with methylated UB and for use in mass spectrometry, suggests that RING exosite mutation also effects processivity of multi-monoubiquitination of a substrate.

(C) Semiquantitative mass spectrometry analysis of reactions shown in B, showing peptides containing one or more ubiquitinated lysines. The quantifications of the peptides were normalized by the APC/C ΔRING control reaction. Consistent with the structure representing multiubiquitination (Figures 3C and S3A), the peptide corresponding to ubiquitinated Lys51 is minimally detected in reactions with wild-type UB (top) and is not detected (N.D.) in reactions with methylated UB (below).

(D) Experimental schemes for testing role of APC11 RING exosite in processive multi-monoubiquitination (meUB) and multiubiquitination (WT UB) of CycB^{N*} and lysine mutant substrates, and representative fluorescence scans of control reactions. Two independent mixtures, ''APC/C-sub'' and ''E2-UB'' represented in the schematics (top), were made as follows. For the single encounter assays (middle), APC/C^{CDH1} and CycB^{N*} are in the APC/C-sub mixture while the E2-UB mixture contains the contents for charging the E2 with UB and 1000x excess of cold substrate (Hsl1). Therefore, the CycB^{N*} substrate only encounters E2∼UB during its initial binding to APC/C, as after dissociation during the reactions ''cold'' unlabeled substrate binds APC/C^{CDH1} and potently inhibits further ubiquitination of labeled substrate. The no encounter reaction (left) demonstrates that excess cold substrate outcompetes CycB^{N*} when the two types of substrates are switched in the two independent mixtures. The multiple turnover reaction (right) is performed similarly to the single encounter except without cold competitor.

(E–J) Representative fluorescent scans of APC/C^{CDH1}–UBE2C-mediated processive multiubiquitination reactions with wild-type CycB^{N*} and versions with different numbers and locations of potential ubiquitination sites. Representative single encounter (E–F and I) and multiple turnover (G–H and J) experiments highlight the function of APC/C^{CDH1}'s RING exosite. The number of sites refers to the number of primary amines available for ubiquitination by UBE2C (A). In examples where the extent of multiubiquitination is restricted, e.g., methylated UB on a substrate with only 1 primary amine (site), the APC/C RING^{exo} mutant has a minimal effect in processive multiubiquitination. However, when a substrate contains more lysines and wild-type UB offers additional amines for modification, decreases in the extent of processive multiubiquitination (E–J) and increases in substrate turnover (G–H and J) are observed.

A

Interactions for UB chain elongation or subcomplexes	Mutated in APC/C^{CDH1} or subcomplexes indicated in figure
APC2/APC4 groove – UBE2S CTP	1. APC2 D350K-D353K 2. UBE2S L222A 3. APC4 DIDDE747-751KDKKK 4. APC4 D33K
APC2 Si helices – UBE2S UBC domain	5. Negative control: H555D, F556D 6. APC2 R568A, R569A 7. APC2 I539D 8. APC2 V542A, E543A 9. UBE2S I154A
APC2 NTD / NTD pivot	10. APC2 I501D, I502D
APC11 – Acceptor UB	11. MBP-APC11 ΔRING 12. MBP-APC11 WT 13. MBP-APC11 Exo mut

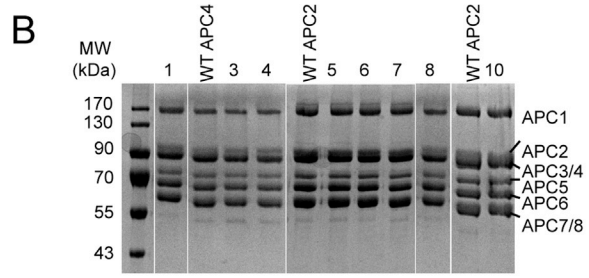

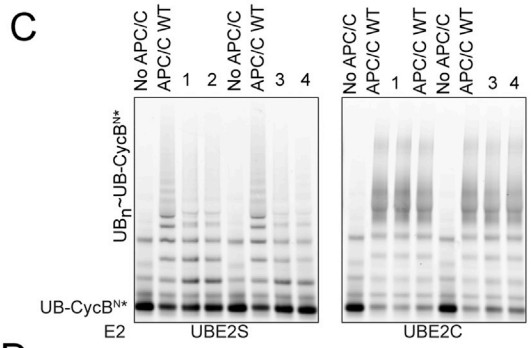

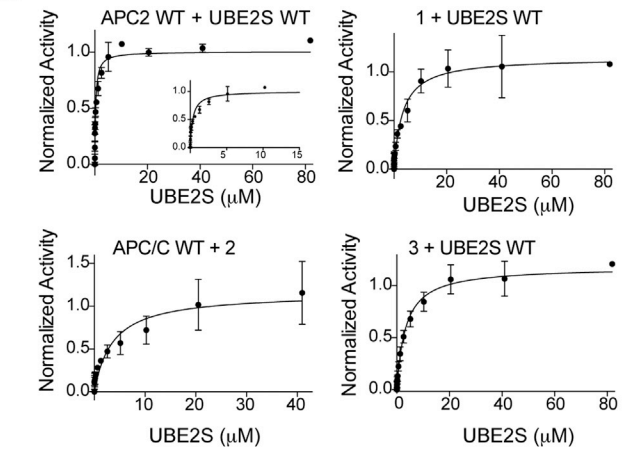

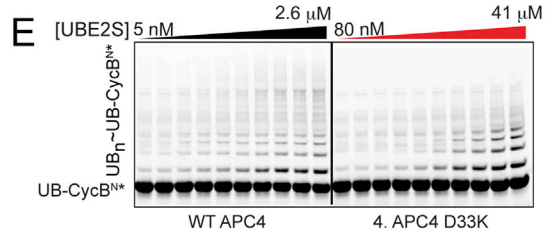

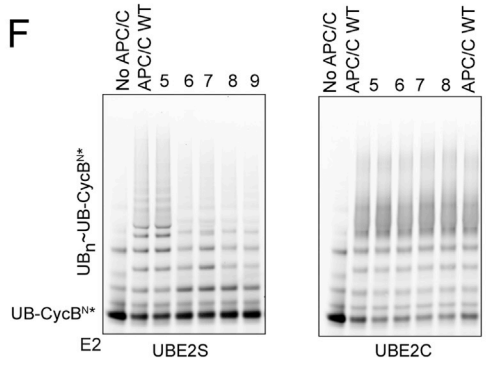

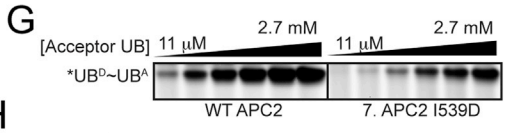

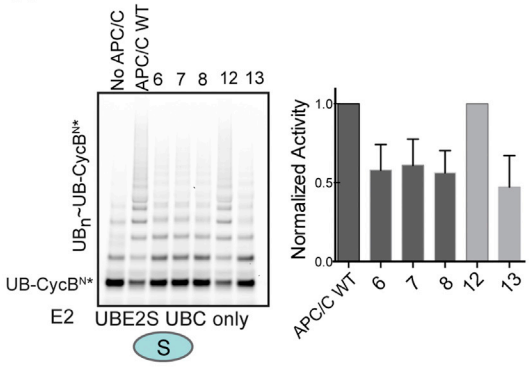

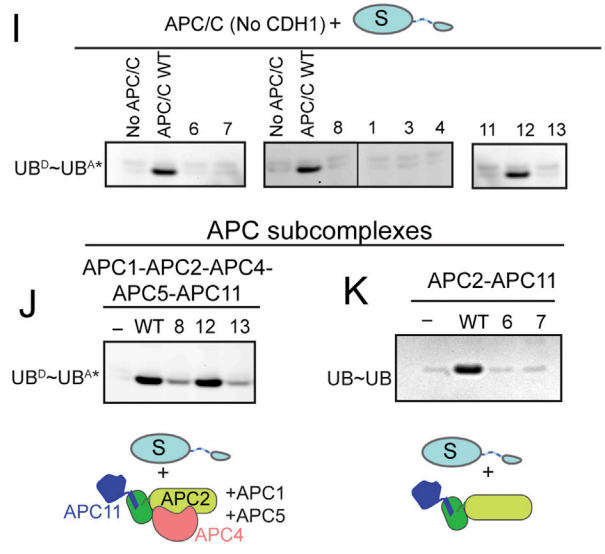

(legend on next page)

Figure S5. Reagents and Data Testing the Distinctive Architecture Based on the Cryo-EM Reconstruction Representing APC/C^{CDH1}–UBE2S-Catalyzed UB Chain Elongation, Related to Figure 5

(A) Table of APC2, APC4, APC11, or UBE2S mutants used in assays testing UB chain elongation by APC/C^{CDH1} and UBE2S. Residues directing interactions between APC/C and UBE2S or that could distinguish the catalytic architecture for UB chain elongation were identified based on cryo-EM data. The list is organized according to four structural classes of interaction: APC2/APC4 groove recruitment of UBE2S CTP, APC2 Si-helices positioning UBE2S UBC domain, the "hinge" or pivot between APC2's NTD and CTD that differs slightly between the catalytic architectures for multiubiquitination and UB chain elongation, and APC11 RING–UB interactions that are assayed in Figure S5.

(B) Coomassie-stained SDS-PAGE gel of purified WT and mutant recombinant APC/C complexes, with mutants numbered according to the list in (A).

(C) Qualitative assays monitoring UB chain elongation of UB-CycB^{N*} to test roles of residues in the APC2/APC4 groove structurally observed to recruit UBE2S's CTP. Control experiments with UBE2C were performed side-by-side to confirm proper APC/C assembly and that defects are specific to UB chain elongation by UBE2S. The indicated APC/C mutants, delineated in (A), in APC/C's APC2/APC4 groove binding UBE2S's CTP are selectively deficient in APC/C^{CDH1}-UBE2S-mediated UB chain elongation.

(D) Fitting of kinetic data assaying mutants in APC/C^{CDH1}'s APC2/APC4 groove and UBE2S's CTP. Titrations of UBE2S (wild-type and CTP L222A mutant) in assays with fixed concentrations of APC/C^{CDH1} (wild-type and indicated variants) and UB-Securin*. The kinetic parameters from the curve fits are shown. Error bars: SEM, $n \geq 3$.

(E) Representative SDS-PAGE gels for data used to determine kinetic parameters upon titrating UBE2S (wild-type and indicated variants) in assays measuring UB chain elongation for fluorescent UB-Securin* with APC/C^{CDH1} (wild-type and indicated variant).

(F) Qualitative assays monitoring UB chain elongation of UB-CycB^{N*} to test roles of residues in APC2 helices structurally observed to position UBE2S's UBC domain. Control experiments with UBE2C were performed side-by-side to confirm proper APC/C assembly and that defects are specific to UB chain elongation activity with UBE2S. Mutants in the structurally observed interacting residues in APC/C and UBE2S variants are selectively deficient in APC/C^{CDH1}-UBE2S-mediated UB-chain elongation.

(G) Representative SDS-PAGE gels for data used to determine kinetic parameters in titrating acceptor UB (UB^{A}) in assays measuring UB chain formation as monitored by di-UB synthesis with fluorescent donor UB (*UB^{D}) with UBE2S (wild-type and helix D I154A mutant) and APC/C^{CDH1} (wild-type and indicated variants).

(H–K), Qualitative assays testing importance of the structurally observed APC2 Si-A- and B-helix interactions with UBE2S's catalytic UBC domain and APC2/APC4 groove recruitment of UBE2S's CTP in minimal subcomplexes.

(H) Representative qualitative assays, left, and bar graph, right, testing wild-type and indicated variants of APC/C^{CDH1} for ubiquitination of UB-CycB^{N*} with 120 μM UBE2S's isolated UBC domain lacking the CTP. The high concentration of the isolated UBE2S UBC domain required to achieve activity in the absence of CTP-recruitment cause high background APC/C-independent background activity. Nonetheless, even at this high UBE2S concentration, point mutations in the Si-A- and B-helices impair APC/C^{CDH1}-dependent UB chain elongation.

(I–K) Mutations in the APC2 SiA- and B-helices structurally observed to position UBE2S's UBC domain and in the RING exosite disrupt UBE2S-dependent diubiquitin synthesis by progressively more minimal subcomplexes: APC/C alone without coactivator (I), APC1–APC2–APC4–APC5–APC11 (J), and APC2–MBP-APC11 (K). The fluorescent scanning (I-J) or Coomassie-staining (K) of SDS-PAGE gels monitored UBE2S-dependent diubiquitin synthesis.

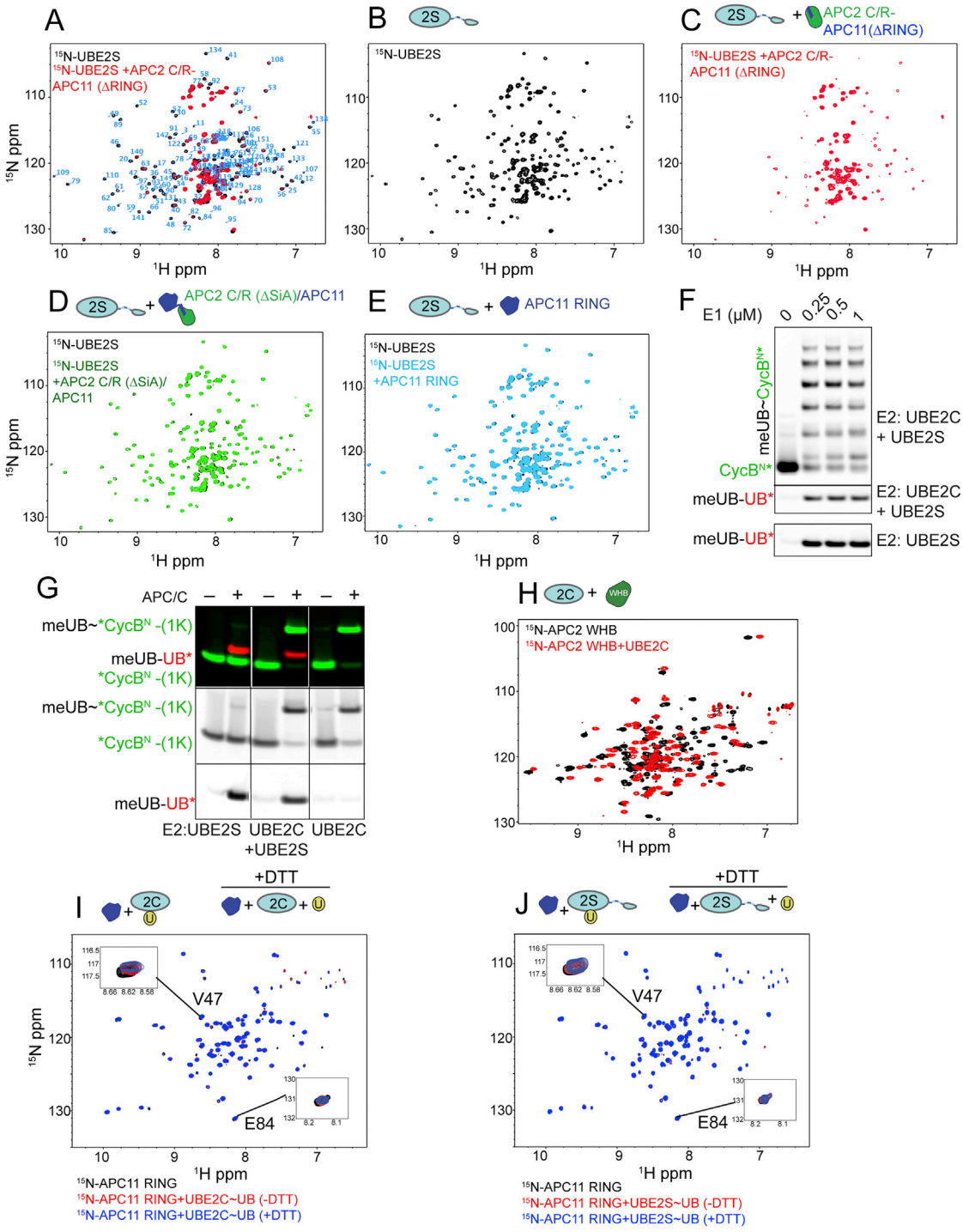

Figure S6. Interrogation of the Dual RING E3 Architectures by NMR and Ubiquitination Assays, Related to Figure 6

(A–E) NMR experiments testing roles of APC2 SiA-helix and APC11 RING domain in binding to UBE2S.

(A) Overlaid 2D [^{15}N, ^{1}H] TROSY spectra for ^{15}N-labeled UBE2S alone (50 μM, black) or with APC2–APC11$^{\Delta RING}$ C/R+WHB (APC2 residues 446-822 and APC11 residues 1-17, 1:1.5, red). Resonance assignments for the UBC domain from UBE2S are shown in blue.

(B) 2D [^{15}N, ^{1}H] TROSY spectrum of ^{15}N-labeled UBE2S alone (50 μM, black) from (A).

(C) 2D [^{15}N, ^{1}H] TROSY spectrum of ^{15}N-labeled UBE2S mixed with unlabeled APC2-APC11$^{\Delta RING}$ C/R (1:1.5, red) from (A) showing extreme line-broadening for resonances from UBE2S core domain, indicating interaction with APC2–APC11 C/R domain is RING-independent.

(D) Overlaid 2D [^{15}N, ^{1}H] TROSY spectra for ^{15}N-labeled UBE2S alone (50 μM, black) or mixed with APC2-APC11 C/R domain with APC2's Si-A-helix deleted (1:1.5, green), suggesting that the line-broadening observed in (A) and (C) depends on APC2's Si-A-helix.

(legend continued on next page)

(E) Overlaid 2D [^{15}N, ^{1}H] TROSY spectra for ^{15}N-labeled UBE2S alone (50 μM, black) or mixed with APC11 RING (1:10, light blue) showing no indication of interaction.

(F) Control experiment for the dual color fluorescent assays (Figure 6F-G) simultaneously monitoring UBE2C-catalyzed meUB transfer to CycB^{N*} and UBE2S-catalyzed di-UB synthesis. Titrating E1 enzyme suggests that UBE2C-dependent inhibition of UBE2S does not involve competition for E1, as inhibition is observed even with 1 μM E1.

(G) Representative fluorescent scan for data used in Figure 6G. This reveals that the ubiquitination of a single lysine on *CycB^{N}-(1K) by APC/C^{CDH1}-UBE2C inhibits di-UB formation catalyzed by APC/C^{CDH1}-UBE2S.

(H) Control experiment confirming UBE2C-binding to APC2's WHB domain. Overlaid 2D [^{15}N, ^{1}H] TROSY spectra for ^{15}N-labeled APC2^{WHB} alone (100 μM, black), or mixed with UBE2C (1:2, red) shows large chemical shift perturbation, indicative of interaction. This is an independent repeat of an experiment described in (Brown et al., 2015) performed here as a control.

(I) Overlaid 2D [^{15}N, ^{1}H] TROSY spectra for ^{15}N-labeled APC11 RING domain alone (100 μM, black), or with disulfide-linked UBE2C∼UB mimic (red, 1:4) or DTT-induced separation into UBE2C and UB (blue, 1:4). UBE2C does not induce substantial chemical shift perturbation of RING domain.

(J) Overlaid 2D [^{15}N, ^{1}H] TROSY spectra for ^{15}N-labeled APC11 RING domain alone (100 μM, black), or with disulfide-linked UBE2S∼UB mimic (red, 1:4) or DTT-induced separation into UBE2S and UB (blue, 1:4). UBE2S does not induce substantial chemical shift perturbation of RING domain.

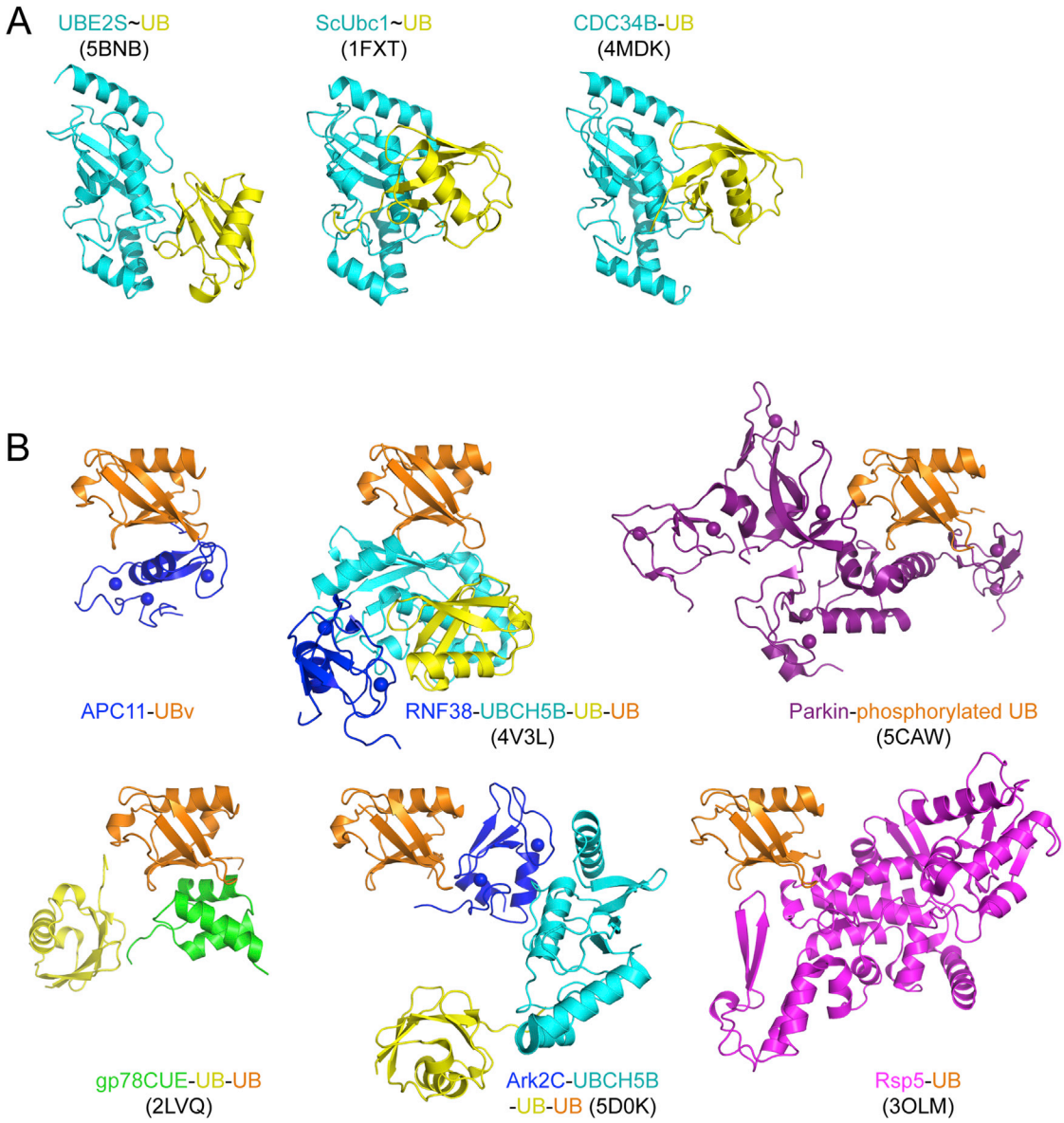

Figure S7. Structural Implications for Other E2 and E3 Ligase Enzymes, Related to Figure 7

(A) Similar to UBE2S (cyan, left), the UB chain elongating E2s yeast Ubc1 (cyan, middle) and human CDC34 (cyan, right) adopt activated "closed" conformations in complexes with a donor UB mimic (yellow) in the absence of E3s, and they harbor distinctive C-terminal peptides that bind their cognate E3s yeast APC/C and SCF, respectively (not shown) (Girard et al., 2015; Hamilton et al., 2001; Kleiger et al., 2009; Saha et al., 2011).

(B) An emerging theme in ubiquitination is that UB-binding exosites participate in allosteric activation and processive ubiquitination in some RING E3–E2 or HECT E3 ligases (Bagola et al., 2013; Brzovic et al., 2006; Buetow et al., 2015; Metzger et al., 2014; Ordureau et al., 2015; Wauer et al., 2015; Wright et al., 2016). In addition to UB (shown by UBv as a proxy in orange) binding to the APC11 RING domain (Table S1), UB has been shown to bind the so-called "backside" of an E2 to allosterically modulate RING-dependent activation (Brzovic et al., 2006). One example is the complex representing a backside-bound UB (orange)–UBCH5 (cyan) ~UB (yellow)–RING (top middle) (Buetow et al., 2015). PhosphoUB (orange) binds the RBR E3 Parkin (purple) to mediate allosteric activation (Kazlauskaite et al., 2015; Kumar et al., 2015; Ordureau et al., 2015; Pickrell and Youle, 2015; Sauve et al., 2015; Wauer et al., 2015) (top right). UB (orange) binding to exosites in non-catalytic domains such as in gp78 (green), the RING domain from Arkadia, and to NEDD4-family HECT E3s as shown for Rsp5 (bottom left, middle, right respectively) has been implicated in roles in catalysis and processivity (Bagola et al., 2013; Kathman et al., 2015; Kim et al., 2011a; Maspero et al., 2011; Wright et al., 2016; Zhang et al., 2016).

Cell, Volume *165*

Supplemental Information

Dual RING E3 Architectures Regulate Multiubiquitination and Ubiquitin Chain Elongation by APC/C

Nicholas G. Brown, Ryan VanderLinden, Edmond R. Watson, Florian Weissmann, Alban Ordureau, Kuen-Phon Wu, Wei Zhang, Shanshan Yu, Peter Y. Mercredi, Joseph S. Harrison, Iain F. Davidson, Renping Qiao, Ying Lu, Prakash Dube, Michael R. Brunner, Christy R.R. Grace, Darcie J. Miller, David Haselbach, Marc A. Jarvis, Masaya Yamaguchi, David Yanishevski, Georg Petzold, Sachdev S. Sidhu, Brian Kuhlman, Marc W. Kirschner, J. Wade Harper, Jan-Michael Peters, Holger Stark, and Brenda A. Schulman

Supplemental Experimental Procedures

Protein purification

For ubiquitination assays, human APC/C, CDH1, UBA1, wild type and mutant versions of APC2–APC11, APC11 RING domain (residues 17-84), UBE2C, UBE2S, $CycB^{N}$ (residues 1-95), UB-$CycB^{N}$ (UB-fused to N-terminus of $CycB^{N}$), UB-Securin, and Hsl1 (residues 768-842) were expressed largely as described (Brown et al., 2015; Brown et al., 2014; Jarvis et al., 2016), with some minor differences. APC/C was expressed from a baculovirus expression construct system allowing relatively facile incorporation of mutants (Weissmann et al., 2016). The proteins used in the $SCF^{FBW7\Delta D}$- and WWP1-dependent ubiquitination assays were expressed and purified as previously described (Scott et al., 2014; Zhang et al., 2016).

For all experiments other than EM, APC/C, mutants and the APC1–APC2–APC4–APC5–APC11 subcomplex were purified with a 3-step scheme: 1) affinity purification with Strep-Tactin Sepharose (IBA Life Sciences) and elution with desthiobiotin (Sigma-Aldrich), 2) anion exchange with gradient NaCl elution, and 3) size exclusion chromatography (SEC) in a final buffer of 20 mM HEPES pH 8.0, 200 mM NaCl, 1 mM DTT. Because some APC11 mutants are difficult to observe by SDS-PAGE during protein purification owing to small size (e.g. APC11 ΔRING has only 17 residues), all experiments examining APC11 mutants used MBP fusions, including the wild type counterpart. This allowed confirming stoichiometric inclusion of MBP-APC11 using Coomassie-stained SDS-PAGE gels. Based on a previous alanine scanning study of APC11 RING domain in the context of APC/C^{CDH1} (Brown et al., 2014), the RING exo mutant harbors M57A and F82A mutations and the RING cE2 mutant harbors an R27A mutation. APC2–APC11 subcomplexes #s 2, #3, and #4 in **Fig. 5H** were obtained by coexpressing APC11 and full-length APC2, APC2 residues 446-822 (C/R + WHB domains but referred to in main text as C/R owing to WHB being dispensable for UB chain elongation by UBE2S (Brown et al., 2014)), or APC2 residues 549-822 (C/R + WHB domains with the SiA-helix deleted) as previously described (Brown et al., 2014; Jarvis et al., 2016).

CDH1 was expressed with a HRV13 3C protease cleavable N-terminal 3x MYC-tag using a baculovirus expression system, and purified by nickel affinity chromatography (Sigma-Aldrich). After HRV13 3C-mediated proteolytic cleavage, the 3X MYC-His_6 tag was removed by purifying CDH1 by cation exchange chromatography and SEC in a final buffer of 20 mM HEPES pH 7.0, 300 mM Ammonium Sulfate, 1 mM DTT, 2.5% Glycerol.

Wild type and mutant versions of UBE2C were expressed in BL21(DE3) Codon Plus (RIL) cells. For assaying ubiquitination and hydrolysis of oxyester-linked UBE2C~UB, wild type and C114S (active site mutant) versions were purified by nickel affinity chromatography based on a flush C-terminal His_6 tag. Wild type UBE2C was purified by SEC in 20 mM HEPES pH 8.0, 200 mM NaCl, 1 mM DTT. The UBE2C~UB oxyester-linked complex used to assay hydrolysis was generated as previously described (Brown et al., 2015). In short, we mixed UBE2C C114S, UBA1, $MgCl_2$, ATP, and UB at concentrations of 560 μM, 2 μM, 5 mM, 5 mM, and 3 mM, respectively, at 30°C overnight. The oxyester-linked UBE2C~UB complex was separated from other reaction components by SEC. For cross-linking, UBE2C harboring a single Cys only at the active site (C102A) was expressed and purified via either a C-terminal flush Strep tag or a C-terminal HRV13 3C protease-cleavable Flag-Strep tag. After the initial purification using Strep-Tactin Sepharose, the protein was then used in the cross-linking reactions described below. The UBE2C-UBE2S CTP chimera had residues 157-222 from UBE2S fused at the C-terminus of UBE2C, as described (Chang et al., 2015), allowing purification by cation exchange chromatography from a cell lysate and subsequent polishing by SEC.

Unless otherwise specified, WT and mutant versions of UBE2S were expressed with an N-terminal multipurpose composite tag in BL21(DE3) Codon Plus (RIL) cells from a modified pRSF duet vector. The tag consisted of an N-terminal His_6 tag, followed by a TEV protease cleavage site, a FLAG tag, and an HRV13 3C protease site. UBE2S and variants were purified by nickel affinity chromatography, subsequently treated with HRV13 3C protease, and purified by cation exchange. For broad mutagenesis screens of UBE2S, such as suite of substitutions for C118 used to identify suitable replacements in a single catalytic Cys only version of UBE2S **(Fig. S2H)**, or the linker deletion series **(Fig. 5I)**, wild type and mutant versions of UBE2S were purified by cation exchange prior to assaying APC/C-dependent ubiquitination activity. The series of UBE2S constructs removing subsets of the 56 linker residues between the UBC domain (residues 1-156) and the CTP sequence (residues 213-222) named Linker 51, Linker 46, Linker 36, Linker 26, Linker 15, Linker 6, and Linker -6 (this deletion includes part of the CTP) correspond

to deletion of residues 182-186, 178-187, 168-187, 161-190, 161-201, 157-206, 157-218, respectively **(Fig. 5I)**. The UBE2S Linker -6 variant could not be purified by cation exchange due to the deletion of 13 strongly basic residues and was instead purified nickel affinity chromatography followed by SEC. Wild type and mutant variants of UBE2S used for kinetic assays, and those selected from broad mutagenesis screening for follow-up studies, were subjected to a third purification step, SEC in a final buffer of 20 mM HEPES pH 8.0, 200 mM NaCl, 1 mM DTT. Two different versions of UBE2S were used for EM studies. For our initial attempts to trap a complex representing UBE2S in action, UBE2S catalytic Cys only (C118A) was expressed with a His_6-MBP-TEV protease site-fused to the N-terminus, and purified by nickel affinity chromatography, treated with TEV protease, further purified by cation exchange chromatography, used in cross-linking reactions described below, an analyzed by negative stain EM. The version of UBE2S used in the cryo EM reconstruction contained only a single Cys at the active site, with C118F based on optimization shown in **Fig. S2H**.

For assays comparing WT UBv, UBv mutant (I42D F44D L68D), and UB, these were expressed in BL21(DE3) Codon Plus (RIL) cells from a modified pRSF duet vector with a TEV protease-cleavable N-terminal His_6-tag. The proteins were purified by nickel affinity chromatography, subjected to TEV-mediated proteolytic cleavage to liberate the tag and purified by SEC in a final buffer of 20 mM HEPES pH 8.0, 200 mM NaCl.

UB was expressed in BL21(DE3) Codon Plus (RIL) cells as previously described (Brown et al., 2014). UB used as a donor in substrate ubiquitination assays and as an acceptor in **Figures 5F and S5G** was purified as described previously (Pickart and Raasi, 2005). Methylated UB was used as a donor in **Figures 1C, 2E, 6F-G,S4B, S4E, S4G, S4I-J, and S6F-G** was reductively methylated as previously described (White and Rayment, 1993). The fluorescent donor UB (*UB) for experiments in **Figures 5F and S5G** and the fluorescent acceptor UB (UB*) for experiments in **Figures 5H, 6F-G, S2D, S2L, S5I-K and S6F-G** were expressed as TEV-cleavable N-terminal GST fusions, purified by glutathione-affinity chromatography, treated with TEV to liberate the GST tag, and polished by SEC. The fluorescent donor and acceptor UBs contain a single cysteine at either position -1 or at 77 (G75S G76S C77), respectively, for fluorescein-5-maleimide or Cyanine5 maleimide labeling as previously described (Brown et al., 2014).

The substrates in ubiquitination assays - $CycB^N$, UB-$CycB^N$, and UB-Securin - were purified as previously described (Jarvis et al., 2016; Yamaguchi et al., 2015). Briefly, the substrates were expressed as N-terminal GST-TEV and C-terminal Cys-His_6 fusions in BL21(DE3) Codon Plus (RIL) cells. The substrates were then purified by glutathione-affinity chromatography, treated with TEV protease to liberate GST, and further purified by nickel-affinity chromatography. The substrates were then labeled with fluorescein-5-maleimide (denoted by an asterisk) as previously described (Brown et al., 2014). Free label was removed by desalting and SEC. For CycB mutants with fewer ubiquitination sites, Lys-to-Arg substitutions were made **(Figs. 1C, 6G, and S4D-J)**. These substrates were expressed with an additional modified N-terminal Strep-tag sequence, GGGSAWSHPQFEGGS, following the TEV proteolysis site (ENLYFQG) and contain only residues 1-88 of CycB. To remove degradation products that are more prevalent when multiple arginines replace existing lysines, an additional purification with Strep-Tactin Sepharose was used instead of SEC after the labeling reaction. For the single ubiquitination site mutant **(Figs. 1C and S4I-J),** the N-terminus of $CycB^N$ was blocked using a sortase-mediated reaction as follows. After TEV-mediate cleavage, 10 µM $CycB^N$ was subjected to 150 nM Sortase and 40 µM Fluorescent-LPETGG peptide in a buffer of 20 mM HEPES pH 8, 50 mM NaCl, and 10 mM $CaCl_2$. After a 2 hour incubation at 4°C, the reaction was quenched with 20 mM EGTA and then purified by Strep-Tactin Sepharose and SEC.

APC11 RING (residues 17-84) and RBX1 RING (residues 36-108) domains were expressed with a TEV-cleavable, N-terminal GST-tag in BL21(DE3) Codon Plus (RIL) cells from a modified pGEX4T1 vector. GST-tagged RING domains purified by glutathione affinity chromatography and SEC and were used for phage display selection and Bio-Layer Interferometry (BLI) experiments.

The APC11-UBv complex for crystallization was purified after coexpression of TEV-cleavable GST-tagged APC11 RING (residues 17-84) and TEV-cleavable His_6-tagged UBv in BL21(DE3) Codon Plus (RIL) cells from modified pGEX4T1 and pRSF duet vectors, respectively. The complex was purified by glutathione affinity chromatography, followed TEV-mediated proteolysis. Subsequent purification steps included dialysis, removal of GST with Glutathione Sepharose, and SEC. The final SEC buffer was 50 mM TRIS pH 7.6, 200 mM NaCl, 1 mM DTT.

For cryo EM, the "substrate" used in the Multiubiquitination trap, $Hsl1^P$(K788C)-UBv was expressed in BL21(DE3) Codon Plus (RIL) cells from a modified pGEX4T1 vector containing a TEV

protease site. After purification by glutathione affinity chromatography, the GST-fusion was treated with TEV protease during overnight dialysis, and free GST was then removed by glutathione affinity chromatography and SEC. The "substrate" used in the UB chain Elongation trap, a UBv (K11C)-Hsl1 D-box fusion, was expressed in BL21(DE3) Codon Plus (RIL) cells from a modified pRSF duet vector with an N-terminal TEV-cleavable His_6-tag. In an initial attempt to visualize UB chain elongation, using negative stain EM and APC/C purified from HeLa cells as described below, the "substrate" His_6-UB(K6R, K11C, K27R, K29R, K33R, K48R, K63R)-Hsl1 (residues 768-842) was expressed in BL21(DE3) Codon Plus (RIL) cells and purified by nickel affinity chromatography prior to crosslinking.

Proxies for "Donor UB" were Flag-UB (1-74, G75C), except the initial attempt to visualize UB chain elongation without a UBv acceptor used Flag-HRV13 3C protease site-UB (1-74, G75C),and were expressed as N-terminal GST fusions. Following glutathione affinity purification and TEV-treatment during overnight dialysis to remove glutathione, the GST-tag was removed by Glutathione Sepharose (GE Life Sciences) chromatography. These proteins were then used in the cross-linking reactions described below. Flag-UB (1-75, G76C) used in disulfide-linked proxies for E2~UB intermediates was purified similarly.

UBv selection

The phage-displayed UBv library used in this study was re-amplified from Library 2 as previously described (Ernst et al., 2013). Protein immobilization and subsequent phage selections were done according to established protocols (Tonikian et al., 2007). Briefly, purified GST-APC11 RING fusion was coated on 96-well MaxiSorp plates (Thermo Scientific 12565135) by adding 100 µL of 1 µM proteins and incubating overnight at 4ºC. Afterwards, five rounds of selections using the phage displayed UBv library were performed against immobilized proteins. A total of 96 phage clones obtained from the fourth and the fifth round of binding selections (48 from each round) were subjected to clonal ELISA to identify individual phages with improved binding properties against 53BP1. Afterwards, UBv sequences were derived through phagemid DNA sequencing (Tonikian et al., 2007). For phage ELISA, proteins in study were immobilized on 384-well MaxiSorp plates (Thermo Scientific 12665347) by adding 30 µL of 1 µM proteins for overnight incubation at 4ºC before adding overnight amplified phages (1:3 dilution in PBS+1%BSA+0.05%Tween). Binding of phage was detected using anti-M13-HRP antibody (GE Healthcare 27942101). The ELISA and sequencing identified a single APC11 RING-binding UBv, with sequence differences from UB shown in **Fig. 2A**.

X-ray Crystallography

The APC11 RING–UBv complex was mixed with reservoir solution at a 1:1 volume:volume ratio for crystallization by the hanging-drop vapor diffusion method. The reservoir solution contained 0.2 M Ammonium acetate, 0.1 M Sodium acetate pH 4.6, 33% PEG4000. For cryoprotection during the flash-freezing in liquid nitrogen, the crystals were harvested in the reservoir solution supplemented with 24% glycerol. Diffraction data were processed with HKL2000 (Otwinowski and Minor, 1997). The structure was determined by molecular replacement using Phaser with APC11 [Protein Data Bank (PDB) ID 4R2Y] and UB (1-70) (PDB ID 1UBQ) as search models (Brown et al., 2014; Vijay-Kumar et al., 1987). Model construction and refinement was performed using COOT, Refmac5, and Phenix (Adams et al., 2010; Emsley et al., 2010; Murshudov et al., 1997). Diffraction data and refinement statistics are provided in **Supplemental Table 1**.

Generation of 3-way crosslinked complexes to trap APC/C^{CDH1}–E2–UB-linked substrate assemblies representing multiubiquitination and UB chain elongation

Ever since our initial efforts to visualize UBE2C and UBE2S bound to APC/C indicated tremendous conformational variability, we and others recognized that incorporating additional stabilizing interactions would be required (Brown et al., 2015; Chang et al., 2015). We turned toward 3-way crosslinking, with the goal of avidly capturing multisite interactions for the catalytic core, which is highly dynamic in CDH1-activated APC/C (Chang et al., 2014). Our initial attempt to visualize placement of UBE2S utilized UB with K11C and other lysines mutated to arginines. Extremely high concentrations of this version of UB can slightly inhibit UB chain elongation. Thus, the initial attempt at an "Elongation trap" contained Strep-UBE2S (C118A) as E2, HRV13 3C protease-cleavable Flag-HRV13 3C protease UB (1-74,G75C) to represent the donor UB, and His_6-UB (K6R, K11C, K27R, K29R, K33R, K48R, K63R)-Hsl1 (residues 768-842) to represent substrate (sequence:

MGSSHHHHHHSQDPGGGSMQIFVRTLTGCTITLEVEPSDTIENVRARIQDREGIPPDQQRLIFAGRQ
LEDGRTLSDYNIQRESTLHLVLRLRISGVSTNKENEGPEYPTKIEKNQFNMSYKPSENMSGLSSFPIF
EKENTLSSSYLEEQKPKRAALSDITNSFNKMN). After 3-way crosslinking, this was added to an IP of APC/C from HeLa cell lysate and recombinant CDH1, and the complex was purified as described previously for APC/C^{CDH1} complexes with EMI1 (Frye et al., 2013). The reconstruction determined by negative-stain EM for the first generation complex is shown in **Movie S2**. While this initial studies enabled localizing UBE2S's UBC domain as binding the APC2–APC11 C/R domain even in the absence of a UBv, obtaining complex suitable for cryo EM involved numerous improvements, including anchoring the mobile RING domain with the UBv.

For the samples used for structure determination by cryo EM, the three-way cross-linked complexes contain E2, a "donor UB", and a surrogate for a polyubiquitination substrate, to "trap" APC/C^{CDH1} architectures for multiubiquitination and UB chain elongation. To visualize Multiubiquitination, the trap contained UBE2C (C102A)-Strep as E2 with only a Cys at the active site, Flag-UB (1-74, G75C) to represent donor UB, and $Hsl1^{P}$(K788C)-UBv to represent substrate (sequence: GSRENELSAGLSKRKHRGSGSGSGSISGVSTNKENEGPEYPTKIECYLEEQKPKRAALSDITNSFNK
MNSGSSGSGSSGMQILVKTPRGKTITLEVEPSDTIENVKAKIQDKEGIPPDQQILFFAVKRLEDGRTL
SDYNIQKKSSLLLAMRVPGKMK).

To visualize UB chain elongation, the trap contained UBE2S Linker15 (C118F) as E2 with only a Cys at the active site, Flag-UB (1-74, G75C) to represent the donor UB, and UBv-Hsl1 D-box (K11C) to represent substrate (sequence:
GSGGSMQILVKTPRGCTITLEVEPSDTIENVKAKIQDKEGIPPDQQILFFAVKRLEDGRTLSDYNIQK
KSSLLLAMRVPGKMKSSYLEEQKPKRAALSDITNSFNKMN).

The Multiubiquitination and UB chain Elongation "traps" were three-way crosslinked using methods similar to those previously described (Kamadurai et al., 2013) except a trifunctional crosslinker containing three sulfhydryl-reactive maleimide groups, TMEA (tris(2-maleimidoethyl)amine, 33043, ThermoFisher Scientific), was used. The proteins were treated with 10 mM DTT for 30 min before they were desalted into 50 mM HEPES pH 7.0, 150 mM NaCl. First, a 5:1 TMEA:UB mixture reacted for 20 min on ice before desalting to remove unreacted TMEA. The final three way product was prepared by reacting the E2 for each trap with this UB at a 1:1 ratio for 20 min on ice and then subsequently adding the third protein that mimics the acceptor lysine at a 2-3 fold molar excess at room temperature (RT). Following a 2-hour incubation of all three proteins, the reaction was quenched with β-mercaptoethanol.

The Multiubiquitination trap was then purified using Strep-Tactin Sepharose and SEC. For use in biochemical assays, a related version of this complex was used with the Strep-tag cleaved from UBE2C by HRV13 3C protease **(Fig. S2A-E)**.

The UB chain elongation trap was purified by cation exchange chromatography and nickel affinity chromatography. The His_6-tag was removed from the complex by TEV-mediated proteolytic cleavage and subsequent SEC.

The initial attempt at a cross-linked complex to represent UB chain elongation, which used a UB rather than UBv mutant, was purified by nickel affinity chromatography and subsequent SEC.

A control complex without the UBv representing Priming, used in **Fig. S2B-D**, was described previously (Brown et al., 2015), except the C-terminal Strep-tag was liberated from UBE2C by HRV13 3C protease.

All cross-linked complexes were ultimately purified by SEC in 20 mM HEPES and 200 mM NaCl. After purification, intact mass spectrometry confirmed correct identity of the three-way cross-linked complex (Hartwell Center for Biotechnology and Bioinformatics, St. Jude Children's Research Hospital, Memphis, TN).

Purification of APC/C^{CDH1} with Multiubiquitination or Elongation traps for cryo EM

Recombinant APC/C^{CDH1} for use in the complex representing multiubiquitination was purified as described previously (Brown et al., 2015). For the complex representing UB chain elongation, APC/C was expressed with HRV13 3C protease-cleavable tags, a Twin-Strep tag at the N-terminus of APC2 and a GST-tag at the N-terminus of APC16, and the complex with CDH1 was purified as previously described (Brown et al., 2015). APC/C^{CDH1} was incubated with the Multiubiquitination or UB chain elongation trap, Anti-FLAG affinity gel (Genscript), and HRV13 3C protease for 1 hour. The resin was thoroughly washed in microspin columns, and complexes eluted by the addition of FLAG peptide.

Cryo Electron Microscopy

For cryo electron microscopic studies of APC/C complexes representing Multiubiquitination or UB chain elongation, 100 µg of purified APC/C was loaded onto a 10%–40% glycerol gradient containing 50 mM HEPES pH 8.0, 200 mM NaCl, 2 mM $MgCl_2$. For particle fixation by GraFix (Kastner et al., 2008), the gradient also contained 0.025% and 0.1% glutaraldehyde in the lighter and denser glycerol solution, respectively, creating an additional glutaraldehyde gradient from top to bottom (0.025–0.1%). Centrifugation was performed at 34,000 rpm in a SW55TI rotor (Beckman) for 15 hr at 4°C. For cryo EM the fractions containing APC/C were subjected to a buffer exchange procedure using Zeba spin columns (Pierce) to remove the sugar prior to EM grid preparation. APC/C particles were allowed to adsorb on a thin film of carbon for 5 min, transferred onto a cryo EM grid (Quantifoil 3.5/1 1 µm, Jena) and then plunged into liquid ethane under controlled environmental conditions of 4 °C and 100% humidity in a vitrification device (Vitrobot Mark IV, FEI Company, Eindhoven). Images were recorded on a Falcon II direct detector under liquid-nitrogen conditions with a Titan Krios electron microscope (FEI, Eindhoven) equipped with a XFEG electron source and a C_s corrector (CEOS, Heidelberg) using 300 kV acceleration voltage. An electron dose of ~40 electrons per $Å^2$, −0.7 to −3.5 µm defocus and a nominal magnification of 94,000× were used, resulting in a final pixel size of ~1.57 Å. The extracted particle images were corrected locally for the contrast-transfer function by classification and averaging of power spectra (Sander et al., 2003). Initial 2D sorting of images was performed based on CTF parameters. Only images showing isotropic Thon rings better than 6 Angstrom were used for further processing. Additional image sorting was performed applying several rounds of multivariate statistics, first without alignment and subsequently after image alignment to remove ice contaminations and bad particle images. The remaining good particle images were used for further processing. 3D classification in RELION 1.2 was used to obtain the particles revealing the highest UBE2S/UBE2C factor occupancy (Scheres, 2012). The best class was then used for the final refinement using the 'gold-standard procedure' in RELION 1.2. The final resolution (6.4 and 6 Å) was calculated applying a mask for the entire APC/C using the FSC 0.143 criterion.

Structure	Picked particles	Remaining particles after 2D sorting	Number of particles in best class after 3D classification in Relion	Resolution without masking (Angstrom)	Resolution with soft mask for the entire APC/C (Angstrom)
Multiubiquitination	784,672	399,597	135,578	7.4	6.4
Elongation	873,870	392,468	125,390	7.2	6.0

For the heat maps, **Fig. S3C**, a sphere of 14 voxel in diameter was run over the entire 3D volume moving it by one voxel in all directions. At each position the calculation of the local FSC values was performed. This then generates the FSC values to generate the heat map and to visualize the local resolution. Local resolution measurements are dependent on the size of the small volume used to calculate the local FSC. The size of the sphere was adjusted to 14 voxel because the mean value of all local correlations agrees with the calculated global resolution.

Docking crystal structures into cryo EM maps representing multiubiquitination and UB chain elongation

Coordinates for APC/C with the mobile catalytic core deleted (from 4UI9.PDB lacking the APC2–APC11 C/R, WHB, and RING domains, (Chang et al., 2015)) were placed as a single unit into the cryo EM maps using Chimera (Pettersen et al., 2004). For the map representing Multiubiquitination, the additional density was fit with structures of three subcomplexes, the APC2–APC11 C/R domain (4UI9.PDB, (Chang et al., 2015)), UBE2C bound to APC2's WHB domain (4YII.PDB (Brown et al., 2015)), and of the APC11 RING-UBv complex **(Fig. 2B)**. For the model representing UB chain elongation, additional density from maps from classes initially calculated to overall 9 Å resolution were segmented into three separate maps, with the density from the best map for each segment fit individually with the corresponding coordinates for the APC2–APC11 C/R domain, the crystal structure of the APC11 RING-UBv complex, and the crystal

structure of UBE2S (Brown et al., 2015; Chang et al., 2015; Lorenz et al., 2016; Pettersen et al., 2004). In the higher resolution map, density corresponding to the N-terminal portion of UBE2S distal from APC2 was lacking, and a truncated version of UBE2S corresponding to residues 46-156 was used for further calculations. The models were rigid body fitted in UCSF Chimera (Pettersen et al., 2004) and then subjected to molecular dynamics flexible fitting (MDFF). The MDFF simulation was run using the Charmm force field applying implicit solvent conditions and using secondary structure, chirality and cis-peptide restraints. First an energy minimization was calculated for 2ps. The simulation was performed for 150 ps using a ξ value of 0.3. Afterwards energy minimization of the resulting model was performed for 2 ps with a ξ of 10 (Trabuco et al., 2008). The resultant models are shown in **Movies S1 and S2**, except that the structural representation for UB chain elongation is shown with the full-length UBE2S in place of the truncated version. To visualize an acceptor Lys relative to UBE2S, the APC11–UBv portion of the map was substituted by isolated APC11 RING domain (and the closest homology model of UB (PDB ID 4RF0)) (Bailey-Elkin et al., 2014; Brown et al., 2014). There is no density in any of the maps corresponding to a donor UB, which is shown to be clash-free in **Fig. S3** for Multiubiquitination based on a prior structure of a RING–E2~UB complex (Dou et al., 2012; Plechanovova et al., 2012), and for UB chain elongation using a model of UBE2S~UB generated based on crystallographic symmetry (Lorenz et al., 2016). The structural data guided biochemical experiments in **Figs. 4-6** and **Figs. S4-S6**, which validate the models. For example, the model for UB chain elongation predicted a charge-swap rescue experiment that confirmed placement of UBE2S, and maintained geometry for UBv's residue 11 and UBE2S's active site imposed by the crosslink despite this not a restraint during molecular dynamics.

Enzyme Assays

"Single encounter" experiments **(Figs. 1C and S4D-J)** were used to examine ubiquitination occurring during a substrate's single binding event with APC/C^{CDH1}. This is monitored using a fluorescently labeled substrate and excess unlabeled Hsl1, such that APC/C^{CDH1} dissociated from the labeled substrate is rapidly sequestered. Two different sets of reaction components were independently made and then mixed to begin the reaction. The first, APC-sub, was made by mixing components such that the final concentrations in the actual reaction were 100 nM APC/C, 400 nM CDH1, and 80 nM fluorescent $CycB^{N}$ versions for 30 min. The second mix, E2-UB, consisted of components for charging E2 with UB, which in the ultimate reaction mix were at final concentrations of 50 nM E1, 5 µM E2, 5 mM $MgCl_2$, 5 mM ATP, and 80 µM (1000-fold excess) unlabeled Hsl1. UB (or meUB) was added to the E2-UB mix last such that the final concentration was 65 µM. Both sets of components were immediately allowed to warm to room temperature for 3 min and co-mixed to begin the reaction. The ubiquitination reactions were then quenched at 2 min. The "No-encounter" control assay in **Fig. S4D** swaps the labeled $CycB^{N}$* and unlabeled Hsl1 but is otherwise performed identically, and shows that unlabeled Hsl1 effectively blocks ubiquitination of labeled $CycB^{N}$*.

Qualitative assays probing the function of APC/C and E2 variants were performed with 30 nM APC/C, 1 µM CDH1, 0.2 µM UBE2C or UBE2S (unless otherwise indicated), 0.1 µM E1, 250 µM UB, 0.2 µM $CycB^{N}$* or UB-$CycB^{N}$* **(Figs. 2D, 2E, 5G, 5I, 6D, S1G, S2B, S2C, S2K, S5C, S5F)**. The assay in **Fig. 2E** was performed similarly except using meUB. **Figs. 2D and 2E** also included UBv titrations from 0.9-25 µM, over 3-fold dilution series. In **Fig. 6B**, the E2 concentrations ranged from 0.26 - 7 µM, over 3-fold dilution series. In **Fig. S2I**, the concentrations of WT and C118F mutant versions of UBE2S ranged from 20 nM to 1.2 µM over 2-fold dilution series. These reactions were quenched at 12 min. Qualitative assays in **Figs. S2H** were performed similarly, except the APC/C concentration is 14 nM and the reaction was quenched at 8 min. The assays monitoring UB transfer to an acceptor UB* **(Figs. 5H, 6F-G, S2D, S2L, S5I-K, and S6F-G)** were performed in similar conditions as assays for UB-$CycB^{N}$* ubiquitination assays, except the acceptor substrate was UB-fluorescein (G75S:G76S:C77) and the reaction was quenched at 20 min. Fluorescent labeling of the C-terminal Cys prevents the UB* from conjugating to either the E1 or E2.

Ubiquitination assays monitoring substrate depletion as a measure of Processive Affinity Amplification (PAA) **(Figs. 4E-G)** were performed as described above except concentrations of 40 nM APC/C, 5 µM UBE2C, 0.5 µM E1, 250 µM UB or meUB, and either 6 µM $CycB^{N}$* or UB-$CycB^{N}$* were used. The reaction mixtures were quenched at the time points indicated. Substrate bands were quantified and normalized to the reaction using the negative control APC/$C^{\Delta RING}$ mutant. Product bands were quantified and APC/$C^{\Delta RING}$ products were subtracted as background. Reactions that were subjected to mass spectrometry **(Fig. 4D and S4B)** analysis were performed similarly except 80 nM APC, 100 nM E1, and 20

μM $CycB^{N}$* were used and quenched at 30 min. unless otherwise indicated.

In kinetic experiments, apparent K_m (K_m^{app}) and apparent V_{max} (V_{max}^{app}) values were determined by fitting the initial velocities to the hyperbolic Michaelis-Menten, $v = V_{max}^{app}[X]/(K_m^{app}+[X])$, equation, where X is either the UBE2C, UBE2S, or ^{Acceptor}UB concentration, using GraphPad Prism 6 software. Single time points were taken under conditions that satisfy initial velocity regimes. In summary, a time course was monitored at both the minimum and maximum point of each titration to ensure a single time point could be taken where the substrate or UBE2S~UB depletion are minimal and product formation remained linear. The activity for each quantitative assay was normalized to the V_{max}^{app} of wild type UBE2C or UBE2S with APC/C^{CDH1}.

The kinetic parameters, K_m^{app} and V_{max}^{app} values, were determined for UBE2C **(Figs. S1E-F)** and UBE2S **(Figs. 5C, 5E and S5D-E)** in assays monitoring substrate polyubiquitination with APC^{CDH1} to evaluate E2–APC/C binding and the maximum rate of ubiquitination. Concentrations of 10 nM APC/C variant, 50 nM or 1 μM E1, 65 μM or 250 μM UB, and 200 nM UB-$CycB^{N}$* or 1 μM UB-Securin* were used and the reactions were quenched after 6 min. or 10 min. for UBE2C and UBE2S, respectively. In **Fig. S1E and S1F**, the UBv concentration was 50 μM. These data were normalized to the V_{max}^{app} of wild type UBE2C–APC/C^{CDH1} or UBE2S–APC/C^{CDH1}, respectively.

The K_m^{app} and V_{max}^{app} values for the acceptor UB were determined to evaluate the effects of APC2 mutants on APC/C^{CDH1}-dependent stimulation of UBE2S-mediated di-ubiquitin synthesis, **(Figs. 5F and S5G)**. The N-terminally labeled wild type UB (20 μM *UB) was first loaded onto 10 μM E1 in the presence of 5 mM $MgCl_2$ and 5 mM ATP for 10 min at RT. Formation of the E1~*UB intermediate was quenched with 25 mM EDTA and two passes over microspin desalting columns (Zeba spin column, Pierce) to remove MgATP and chelate any residual Mg^{2+} to prevent reloading of the E1. The E1~*UB was then diluted at a final concentration of 2 μM into a second independent mixture that contained unlabeled UB, BSA, 0.2 μM UBE2S and 0.1 μM APC/C^{CDH1}, and ubiquitination reactions were then carried out for 4 min at RT. The data were normalized to the V_{max}^{app} of wild type UBE2S–APC/C^{CDH1}.

A dual-color assay was used to monitor the activities of UBE2C and UBE2S simultaneously **(Figs. 6F-G and S6F-G)**. Methylated UB was used as the donor UB to prevent UBE2S targeting of $CycB^{N}$*(fluorescein-labeled)-linked UB. Instead, UBE2S could only form diubiquitin on a Cyanine5-labeled acceptor UB (1-74, G75S G76S C77). For these experiments, 0.25 μM UBA1, 50 nM of APC/C, 1 μM of UBE2S, 10 μM $CycB^{N}$* or *$CycB^{N}$-(1K), and 10 μM UB* were mixed on ice, equilibrated to room temperature and initiated by the addition of 250 μM methylated UB. After 30 min, the reaction was quenched and the products were resolved by SDS-PAGE and fluorescent scanning. Inhibition of APC/C^{CDH1}-UBE2S-mediated di-UB synthesis was tested upon addition of varying concentrations of UBE2C.

To demonstrate that the UBv is specific for APC/C, 30 μM UBv was tested for effects on two other E3s, $SCF^{FBW7\Delta D}$, which harbors APC11's closest relative (RBX1) as the catalytic subunit **(Fig. S1H)** and WWP1, which has its own distinct UB-binding exosite **(Fig. S1I)**. $SCF^{FBW7\Delta D}$ -dependent ubiquitination of a phosphopeptide derived from CycE was assayed with 75 nM NEDD8~CUL1-RBX1, 75 nM FBW7ΔD, CycE-Biotin, 1 μM UBCH5B, 500 nM CDC34, 150 nM UBA1, and 1 mg/mL BSA first mixed on ice, then equilibrated to room temperature prior to initiating the reaction by the addition of 140 μM UB. Substrate ubiquitination was monitored over the indicated time course through western blotting for biotinylated CycE with anti-Biotin (Rockland Inc. 600-401-098) and HRP-linked rabbit IgG whole antibody (GE Healthcare NA934). For the HECT-type E3 fluorescent WBP2 was the substrate. 750 nM WWP1, 250 nM *WBP2, 500 nM UBCH7, and 50 nM UBA1 were mixed on ice and equilibrated to room temperature. The reaction was initiated by the addition of 70 μM UB. As a positive control for activation by the WWP1-specific UBv that is distinct from the APC11-specific UBv, 7.5 μM UBv P2.3 (Zhang et al., 2016) was added. SDS-loading buffer was added at 30 min to quench the reaction.

Substrate-independent assay for APC/C^{CDH1} activation of UBE2C, monitoring hydrolysis of oxyester-linked analog of UBE2C~UB

To test effects of shackling the RING away from the position in the architecture for multiubiquitination, it was necessary to assay APC/C^{CDH1} activation of UBE2C without a substrate, because substrate binding is blocked by the Elongation trap. Thus, we assayed the ability of APC/C complexes to activate hydrolysis of oxyster-linked UBE2C~UB (Brown et al., 2015). It was necessary to use the isosteric oxyester mimic rather than the native UBE2C~UB intermediate due to the thioesester rapidly discharging via automodification of UBE2C in the absence of substrate. For the oxyester-linked version of

the UBE2C~UB complex, UB's C terminus is enzymatically linked to a serine substituted for the catalytic Cys114 of UBE2C. The oxyester-linked UBE2C (C114S)~UB was mixed with either wild type or variant versions of APC/C in the absence or presence of CDH1. Experiments were performed at 30°C and monitored the persistence of E2~UB and generation of the hydrolytic products UBE2C and UB over time **(Figs. 6C, S1D, and S2E)**. Reaction mixtures contained 5 μM UBE2C~UB and 1 μM wild type or variant versions of APC/C. Reaction products were separated by SDS-PAGE and visualized by staining with Coomassie blue.

Bio-Layer Interferometry (BLI)

Concentrated analyte and ligand proteins were diluted into BLI reaction buffer (20 mM HEPES pH 8.0, 200 mM NaCl, 0.1 mg/ml BSA, 0.01% Tween20). BLI experiments were performed on an Octet RED96 system (ForteBio) using anti-GST antibody biosensors for GST-tagged ligands (APC11 or RBX1 RING domains) UB, UBv, or UBv mutant analytes were titrated at 25°C. Nine dilution points of analytes covering 0.16 – 7.5 μM concentration range were applied. Sensorgram raw data was processed and extracted by Octet Analysis 9.0 software. Dissociation constants (K_D) were obtained by fitting the response wavelength shifts in the steady-state regions using single-site binding system (Eq. 1) shown below.

$$R_{eq} = R_{max}\frac{[C]}{K_D+[C]} \quad (1)$$

where R_{eq} is value of steady-state response shift in each sensorgram curve, $[C]$ is the titrant concentration, R_{max} is the maximal response in the steady-state region, K_D is the binding constant for single-site binding system. R_{max} and K_D values are unknown and Levenberg–Marquardt algorithm was used to perform iterative non-linear least squares curve fitting in Profit 6.2 (QuantumSoft) to obtain the fitted R_{max} and K_D.

Assaying APC/C substrate degradation in *Xenopus* egg extracts

Interphase *Xenopus* egg extract was prepared as described (Rudner and Murray, 2000; Yamaguchi et al., 2015). CycB Δ90 was added at 300 nM and incubated for 120 min. at RT. Buffered (20 mM HEPES pH 8.0, 200 mM NaCl) wild type UB or UBv were added at 10 μM and incubated for 10 min. 110 nM full-length CycB/CDK1 was then added. To monitor substrate degradation, samples were diluted in SDS-PAGE sample buffer at 0 - 60 min. post substrate addition and processed for SDS-PAGE and immunoblotting using antibodies raised against CycB (Thermo Scientific RB-008-P), APC3 (BD Biosciences C40920) and Smc3 (A846, (Sumara et al., 2000)).

Single-molecule assays monitoring APC/C^{CDH1} binding during substrate multiubiquitination

Monitoring the kinetics of the APC/C^{CDH1}-Securin interaction during ubiquitination was performed as previously described (Lu et al., 2015). In brief, biotinylated Securin was immobilized on a passivated slide with 0.2 mg/ml streptavidin. *In vitro* ubiquitination reactions were performed using 20 nM recombinant APC/C^{CDH1} mixed with 100 nM E1, 200 nM UBE2C, 5 mg/ml BSA, and 1.5 μM alexa647-UB in UBAB buffer (25 mM Tris pH 7.5, 50 mM NaCl, 10 mM $MgCl_2$) with an ATP regenerating system. Recombinant APC/C was monitored during the reaction using an anti-APC4 antibody (ab97658, Abcam) labeled with dylight 550-NHS (62263, Pierce). Experiments were performed at RT. A Nikon Ti TIRF microscope equipped with three laser lines of 491nM(50 mW), 561 nM(50 mW), 640 nm(125 mW), and a Hamamatsu C9100 EMCCD camera (the non-EM mode was used for a better signal-to-noise). Time-series were acquired at 5 sec/frame for 15 minutes. Exposure time: 3 seconds for the ubiquitin channel; 750 ms for the APC/C channel; 500 ms for the substrate channel.

Generation of disulfide-linked E2~UB for NMR titrations with ^{15}N-labeled APC11 RING domain

Disulfide-linked UBE2C~Flag-UB and UBE2S~Flag-UB complexes were generated using 2,2'-Dipyridyl disulfide (Sigma-Aldrich). Flag-UB (1-75, G76C) and versions of both E2s harboring only a single Cys at the active site (UBE2C-His_6 C102A, and UBE2S C118F) were treated with 10 mM DTT for at least 30 min before they were desalted into 50 mM HEPES pH 7.0, 150 mM NaCl. 2,2'-Dipyridyl disulfide was, first, added to Flag-UB (1-75, G76C) in 5-molar excess. After a 20 minute incubation on ice, the disulfide-linked UBE2C~UB and UBE2S~UB complexes were then purified by nickel affinity chromatography or cation exchange chromatography, respectively, and ultimately sized in 20 mM HEPES pH 7.0 with 100 mM NaCl.

NMR experiments

NMR experiments were measured on a Bruker 600 or 800 MHz spectrometer equipped with a ^{1}H and ^{13}C detect, TCI triple resonance cryogenic probe using standard Bruker pulse programs. ^{1}H, ^{13}C, and ^{15}N backbone resonances were assigned using standard triple resonance experiments, such as HNCA, HNCACB, CBCA(CO)NH, HNCO and HN(CA)CO. All of the 3D experiments were collected with 8 or 16 transients at 298 K. All the ^{1}H chemical shifts were referenced with respect to DSS measured in the same buffer, while the ^{13}C and ^{15}N chemical shifts were referenced indirectly with respect to the DSS shift. All of the spectra were processed using topspin software and analyzed using the computer-aided resonance software, CARA (Keller, 2004).

Assignments of ubiquitin resonances were obtained using BMRB database 17437 and APC11 assignments were done by our group earlier (Brown et al., 2014). Assignment of UBv was carried out at 298 K using uniformly labeled ^{13}C, ^{15}N-labeled sample in the apo state and in complex with APC11 (1:2) at 500 μM concentration, independently, since the resonances of the complexes exhibited slow exchange. The NMR experiments were performed in a 20 mM sodium phosphate buffer (pH 7.0) with 100 mM NaCl, 10 mM DTT and 0.1% sodium azide in 90% H_2O and 10% D_2O. Titration experiments were carried out with either ^{15}N-labeled or ^{13}C, ^{15}N-labeled APC11 or UBv at 100 μM concentration in the same buffer. Titration experiments testing different APC/C subcomplexes were carried out with ^{15}N-labeled UBE2S at 50 μM. Resonance assignments for UBv and UBE2S will be published elsewhere. The chemical shift perturbations (CSPs) were calculated using CSP (ppm) = $\sqrt{\Delta\delta_{HN}^2 + 0.2\Delta\delta_N^2}$, which included the difference in the proton and nitrogen chemical shifts between the free and bound resonance.

UB-AQUA/PRM Proteomics

For UB-AQUA/PRM, *in vitro* UB reaction samples were quenched with 20 mM EDTA at the indicated time and flash frozen. Aliquots of samples were subject to TCA precipitation. Samples were digested first with Lys-C [in 100 mM tetraethylammonium bromide, 0.1% Rapigest (Waters Corporation), 10% (vol/vol) acetonitrile (ACN)] for 3 hours at 37°C, followed by the addition of trypsin and further digested overnight. Digests were acidified with an equal volume of 5% (vol/vol) formic acid (FA) to a pH of ~2 for 30 min, dried down, and resuspended in 1% (vol/vol) FA.

UB-AQUA/PRM was performed largely as described previously but with several modifications (Ordureau et al., 2015; Ordureau et al., 2014; Phu et al., 2011). A collection of 16 heavy-labeled reference peptides (Ordureau et al., 2014), each containing a single $^{13}C/^{15}N$-labeled amino acid, was produced at Cell Signaling Technologies and quantified by amino acid analysis. UB-AQUA peptides from working stocks [in 5% (vol/vol) FA] were diluted into the digested sample [in 1% (vol/vol) FA] to be analyzed to an optimal final concentration predetermined for individual peptide. Samples and AQUA peptides were oxidized with 0.05% hydrogen peroxide for 30 min, subjected to C18 StageTip and resuspended in 1% (vol/vol) FA. Experiments were performed in triplicate and MS data collected sequentially by LC/MS on a Q Exactive mass spectrometer (Thermo Fisher Scientific) coupled with a Famos Autosampler (LC Packings) and an Accela600 LC pump (Thermo Fisher Scientific). Peptides were separated on a 100-μm i.d. microcapillary column packed with ~0.5 cm of Magic C4 resin (5 μm, 100 Å; Michrom Bioresources) followed by ~20 cm of Accucore C18 resin (2.6 μm, 150 Å; Thermo Fisher Scientific). Peptides were separated using a 45-min gradient of 3–25% ACN in 0.125% FA with a flow rate of ~300 $nL \cdot min^{-1}$. The scan sequence began with an Orbitrap full MS^1 spectrum with the following parameters: resolution of 70,000, scan range of 200–1,000 Thomson (Th), AGC target of 1×10^6, maximum injection time of 250 ms, and profile spectrum data type. This scan was followed by 12 targeted MS^2 scans selected from a scheduled inclusion list with a 5-min retention time window. Each targeted MS^2 scan consisted of high-energy collision dissociation (HCD) with the following parameters: resolution of 35,000, AGC of 1×10^6, maximum injection time of 200 ms, isolation window of 1 Th, normalized collision energy (NCE) of 25, and profile spectrum data type. Raw files were searched, and precursor and fragment ions were quantified using Skyline version 3.1 (MacLean et al., 2010). The UB-AQUA peptides used for quantitation were previously listed by Ordureau et al.(Ordureau et al., 2014). Data generated from Skyline were exported into an Excel spreadsheet and Prism for further analysis as previously described (Ordureau et al., 2014). Total UB was determined as the average of the total UB calculated for each individual locus, unless specified otherwise.

Tandem Mass Tag (TMT) Proteomic analysis

For TMT analysis of *in vitro* ubiquitylation reactions, samples were quenched with 20 mM EDTA

at the indicated time and flash frozen. Aliquots of samples were reduced (10 mM TCEP) and alkylated (20 mM chloroacetamide) prior to TCA precipitation. Samples were digested first with Lys-C [in 200 mM EPPS (pH 8.0), 0.1% Rapigest (Waters Corporation), 10% (vol/vol) ACN] for 3-4 hours at 37°C, followed by the addition of trypsin and further digested overnight. Digests were acidified with an equal volume of 5% (vol/vol) FA to a pH of ~2 for 30 min, dried down, resuspended in 1% (vol/vol) FA, and subjected to C18 StageTip (packed with Empore C18; 3M Corporation) desalting. Eluted peptides were resuspended in 100 µl [200 mM EPPS pH 8.0] and labeled using 10-plex tandem mass tag (TMT) reagents (Thermo Fisher Scientific, Rockford, IL). TMT reagents (0.8 mg) were dissolved in 42 µl dry ACN and 5 µl was added to samples. After 1hr (RT), the reaction was quenched by adding 6 µl of 5% hydroxylamine. Labeled peptides were combined, acidified with final 2% FA (pH ~2), dried down, resuspended in 1% (vol/vol) FA 2.5% (vol/vol) ACN, and subjected to C18 StageTip (packed with Empore C18; 3M Corporation) desalting. Mass spectrometry data were collected using an Orbitrap Fusion mass spectrometer (Thermo Fisher Scientific, San Jose, CA) coupled to a Proxeon EASY-nLC II liquid chromatography (LC) pump (Thermo Fisher Scientific). Peptides were fractionated on a 100 µm inner diameter microcapillary column packed with ~0.5 cm of Magic C4 resin (5 µm, 100 Å, Michrom Bioresources) followed by ~35 cm of GP- 18 resin (1.8 µm, 200 Å, Sepax, Newark, DE). Peptides were separated using a 100 min gradient of 4 to 25% ACN in 0.125% FA at a flow rate of ~425 nL/min. The scan sequence began with an MS^1 spectrum (Orbitrap analysis; resolution 120,000; mass range 400−1400 m/z; AGC target 2×10^5; maximum injection time 100 ms, monoisotopic peak). In addition, unassigned, singly and doubly charged species were excluded from MS^2 analysis and dynamic exclusion (1 min) was set to 5 after 30 sec. A list of targeted mass (m/z (7 ppm mass tolerance), z, 6 min schedule window) for all possible single di-GLY sites in CycB sequence as well as previously observed multiply di-GLY modified CycB peptides found in a test-run were defined and data dependent analysis was performed if no target species were found. By default precursors for MS^2 analysis were selected using the Top10 most abundant peptides. MS2 analysis consisted of high energy collision-induced dissociation (quadrupole ion trap analysis; AGC 4×10^4; CID normalized collision energy (NCE) 35; maximum injection time 50 ms; isolation window 0.7; with injection of all available parallelizable time). We performed multinotch MS3 (McAlister et al., 2012; Ting et al., 2011) with synchronous-precursor-selection (SPS) where precursor ions (n=10) were collected (Orbitrap analysis; resolution 60,000; mass range 100−1000 m/z; HCD normalized collision energy 55; AGC target 5×10^4; maximum injection time 250 ms; with injection of all available parallelizable time).

Sequest-based identification using first a Human UNIPROT database (containing common contaminants) followed by a target decoy-based linear discriminant analysis (FDR 1%) was used for peptide and protein identification as described (Huttlin et al., 2010). A custom database that included all the identified proteins (excluding CycB) during the first search, plus the CycB[1-95]-His_6 sequence was then generated and used for a novel search. Parameters used for database searching include: 50 p.p.m. Precursor mass tolerance; 0.9 product ion mass tolerance; tryptic digestion with up to three missed cleavages; Carboxyamidomethylation of Cys was set as a fixed modification, while oxidation of Met and di-Gly modification of Lys were set as variable modifications. Localization of di-Gly sites used a modified version of the A-score algorithm (Beausoleil et al., 2006) as described (Kim et al., 2011b). A-scores of 13 were considered localized. For quantification, a 0.003 m/z window centered on the theoretical m/z value of each ten reporter ions and the closest signal intensity from the theoretical m/z value was recorded. Reporter ion intensities were adjusted based on the overlap of isotopic envelopes of all reporter ions (manufacturer specifications). Total signal to noise values for all peptides were summed for each TMT channel (with the exception of CycB, UB and common contaminant proteins present in samples), and all values were adjusted to account for variance in sample handling. For each peptide use for protein quantification, a total minimum signal to noise value of 150 and isolation specificity of 0.7 was required (McAlister et al., 2012; Ting et al., 2011). For diGly peptides use for quantification, a total minimum signal to noise value of 100 and isolation specificity of 0.5 was required.

Supplemental Table

Table S1, related to Figure 2. Crystallographic data and refinement statistics for APC11 RING–UBv complex.

Data Collection	
Beamline	NECAT 24-ID-E
Wavelength (Å)	0.97918
Space Group	C121
Cell Dimensions	
a, b, c (Å)	131.1, 35.2, 72.8
α, β, γ (˚)	90, 120, 90
Resolution (Å) (highest shell)	36.3−2.0 (2.07−2.00)
Number of measured reflections	64,390
Number of unique refections	19,650
Overall R_{sym} (%)	10.4 (57.2)
Overall I/σI	10.2 (2.0)
Completeness (%)	99.7 (99.7)
Multiplicity	3.3 (3.3)
Wilson B-factor	25.49
Refinement	
Resolution range (Å)	36.3−2.0
No. of reflections (σ≥0)	19,400
R_{work}/ R_{free} (%)	18.52/21.95
Number of non-solvent atoms	2,163
Number of metal ligands	6
Number of solvent	116
RMSD bond lengths (Å)	0.007
RMSD bond angles (°)	0.947
Isotropic B-factor Min/Maxi	12.2/67.8
Isotropic B-factor Mean	28.1
Molprobity statistics	
All-atom Clashscore	2.37
Ramachandran Plot	
Residues in preferred regions (%)	98.53
Residues in allowed regions (%)	1.47
Residues in disallowed regions (%)	0.0
Rotamer outliers (%)	0.0
C-beta outliers	0

Supplemental References

Adams, P.D., Afonine, P.V., Bunkoczi, G., Chen, V.B., Davis, I.W., Echols, N., Headd, J.J., Hung, L.W., Kapral, G.J., Grosse-Kunstleve, R.W.*, et al.* (2010). PHENIX: a comprehensive Python-based system for macromolecular structure solution. Acta crystallographica *66*, 213-221.

Bagola, K., von Delbruck, M., Dittmar, G., Scheffner, M., Ziv, I., Glickman, M.H., Ciechanover, A., and Sommer, T. (2013). Ubiquitin binding by a CUE domain regulates ubiquitin chain formation by ERAD E3 ligases. Molecular cell *50*, 528-539.

Bailey-Elkin, B.A., van Kasteren, P.B., Snijder, E.J., Kikkert, M., and Mark, B.L. (2014). Viral OTU deubiquitinases: a structural and functional comparison. PLoS Pathog *10*, e1003894.

Beausoleil, S.A., Villen, J., Gerber, S.A., Rush, J., and Gygi, S.P. (2006). A probability-based approach for high-throughput protein phosphorylation analysis and site localization. Nat Biotechnol *24*, 1285-1292.

Brown, N.G., VanderLinden, R., Watson, E.R., Qiao, R., Grace, C.R., Yamaguchi, M., Weissmann, F., Frye, J.J., Dube, P., Ei Cho, S.*, et al.* (2015). RING E3 mechanism for ubiquitin ligation to a disordered substrate visualized for human anaphase-promoting complex. Proceedings of the National Academy of Sciences of the United States of America *112*, 5272-5279.

Brown, N.G., Watson, E.R., Weissmann, F., Jarvis, M.A., VanderLinden, R., Grace, C.R., Frye, J.J., Qiao, R., Dube, P., Petzold, G.*, et al.* (2014). Mechanism of polyubiquitination by human anaphase-promoting complex: RING repurposing for ubiquitin chain assembly. Molecular cell *56*, 246-260.

Brzovic, P.S., Lissounov, A., Christensen, D.E., Hoyt, D.W., and Klevit, R.E. (2006). A UbcH5/ubiquitin noncovalent complex is required for processive BRCA1-directed ubiquitination. Molecular cell *21*, 873-880.

Buetow, L., Gabrielsen, M., Anthony, N.G., Dou, H., Patel, A., Aitkenhead, H., Sibbet, G.J., Smith, B.O., and Huang, D.T. (2015). Activation of a primed RING E3-E2-ubiquitin complex by non-covalent ubiquitin. Molecular cell *58*, 297-310.

Chang, L., Zhang, Z., Yang, J., McLaughlin, S.H., and Barford, D. (2014). Molecular architecture and mechanism of the anaphase-promoting complex. Nature *513*, 388-393.

Chang, L., Zhang, Z., Yang, J., McLaughlin, S.H., and Barford, D. (2015). Atomic structure of the APC/C and its mechanism of protein ubiquitination. Nature *522*, 450-454.

Dou, H., Buetow, L., Sibbet, G.J., Cameron, K., and Huang, D.T. (2012). BIRC7-E2 ubiquitin conjugate structure reveals the mechanism of ubiquitin transfer by a RING dimer. Nature structural & molecular biology *19*, 876-883.

Emsley, P., Lohkamp, B., Scott, W.G., and Cowtan, K. (2010). Features and development of Coot. Acta crystallographica *66*, 486-501.

Ernst, A., Avvakumov, G., Tong, J., Fan, Y., Zhao, Y., Alberts, P., Persaud, A., Walker, J.R., Neculai, A.M., Neculai, D.*, et al.* (2013). A strategy for modulation of enzymes in the ubiquitin system. Science *339*, 590-595.

Frye, J.J., Brown, N.G., Petzold, G., Watson, E.R., Grace, C.R., Nourse, A., Jarvis, M.A., Kriwacki, R.W., Peters, J.M., Stark, H.*, et al.* (2013). Electron microscopy structure of human APC/C(CDH1)-EMI1 reveals multimodal mechanism of E3 ligase shutdown. Nature structural & molecular biology *20*, 827-835.

Girard, J.R., Tenthorey, J.L., and Morgan, D.O. (2015). An E2 accessory domain increases affinity for the anaphase-promoting complex and ensures E2 competition. The Journal of biological chemistry *290*, 24614-24625.

Hamilton, K.S., Ellison, M.J., Barber, K.R., Williams, R.S., Huzil, J.T., McKenna, S., Ptak, C., Glover, M., and Shaw, G.S. (2001). Structure of a conjugating enzyme-ubiquitin thiolester intermediate reveals a novel role for the ubiquitin tail. Structure *9*, 897-904.

Huttlin, E.L., Jedrychowski, M.P., Elias, J.E., Goswami, T., Rad, R., Beausoleil, S.A., Villen, J., Haas, W., Sowa, M.E., and Gygi, S.P. (2010). A tissue-specific atlas of mouse protein phosphorylation and expression. Cell *143*, 1174-1189.

Jarvis, M.A., Brown, N.G., Watson, E.R., VanderLinden, R., Schulman, B.A., and Peters, J.M. (2016). Measuring APC/C-Dependent Ubiquitylation In Vitro. Methods Mol Biol *1342*, 287-303.

Kamadurai, H.B., Qiu, Y., Deng, A., Harrison, J.S., Macdonald, C., Actis, M., Rodgrigues, P., Miller, D.J., Souphron, J., Lewis, S.M.*, et al.* (2013). Mechanism of ubiquitin ligation and lysine prioritization by a HECT E3. eLIFE *2*, e00828.

Kastner, B., Fischer, N., Golas, M.M., Sander, B., Dube, P., Boehringer, D., Hartmuth, K., Deckert, J., Hauer, F., Wolf, E.*, et al.* (2008). GraFix: sample preparation for single-particle electron cryomicroscopy. Nat Methods *5*, 53-55.

Kathman, S.G., Span, I., Smith, A.T., Xu, Z., Zhan, J., Rosenzweig, A.C., and Statsyuk, A.V. (2015). A Small Molecule That Switches a Ubiquitin Ligase From a Processive to a Distributive Enzymatic Mechanism. Journal of the American Chemical Society *137*, 12442-12445.

Kazlauskaite, A., Martinez-Torres, R.J., Wilkie, S., Kumar, A., Peltier, J., Gonzalez, A., Johnson, C., Zhang, J., Hope, A.G., Peggie, M.*, et al.* (2015). Binding to serine 65-phosphorylated ubiquitin primes Parkin for optimal PINK1-dependent phosphorylation and activation. EMBO reports *16*, 939-954.

Keller, R.L.J. (2004). Computer Aided Resonance Assignment Tutorial. http://cara.nmr-software.org/downloads/3-85600-112-3.pdf.

Kim, H.C., Steffen, A.M., Oldham, M.L., Chen, J., and Huibregtse, J.M. (2011a). Structure and function of a HECT domain ubiquitin-binding site. EMBO reports *12*, 334-341.

Kim, W., Bennett, E.J., Huttlin, E.L., Guo, A., Li, J., Possemato, A., Sowa, M.E., Rad, R., Rush, J., Comb, M.J.*, et al.* (2011b). Systematic and quantitative assessment of the ubiquitin-modified proteome. Molecular cell *44*, 325-340.

Kleiger, G., Saha, A., Lewis, S., Kuhlman, B., and Deshaies, R.J. (2009). Rapid E2-E3 assembly and disassembly enable processive ubiquitylation of cullin-RING ubiquitin ligase substrates. Cell *139*, 957-968.

Kumar, A., Aguirre, J.D., Condos, T.E., Martinez-Torres, R.J., Chaugule, V.K., Toth, R., Sundaramoorthy, R., Mercier, P., Knebel, A., Spratt, D.E.*, et al.* (2015). Disruption of the autoinhibited state primes the E3 ligase parkin for activation and catalysis. The EMBO journal *34*, 2506-2521.

Lorenz, S., Bhattacharyya, M., Feiler, C., Rape, M., and Kuriyan, J. (2016). Crystal Structure of a Ube2S-Ubiquitin Conjugate. PLoS ONE *11*, e0147550.

Lu, Y., Wang, W., and Kirschner, M.W. (2015). Specificity of the anaphase-promoting complex: a single-molecule study. Science *348*, 1248737.

MacLean, B., Tomazela, D.M., Shulman, N., Chambers, M., Finney, G.L., Frewen, B., Kern, R., Tabb, D.L., Liebler, D.C., and MacCoss, M.J. (2010). Skyline: an open source document editor for creating and analyzing targeted proteomics experiments. Bioinformatics *26*, 966-968.

Maspero, E., Mari, S., Valentini, E., Musacchio, A., Fish, A., Pasqualato, S., and Polo, S. (2011). Structure of the HECT:ubiquitin complex and its role in ubiquitin chain elongation. EMBO reports *12*, 342-349.

McAlister, G.C., Huttlin, E.L., Haas, W., Ting, L., Jedrychowski, M.P., Rogers, J.C., Kuhn, K., Pike, I., Grothe, R.A., Blethrow, J.D.*, et al.* (2012). Increasing the multiplexing capacity of TMTs using reporter ion isotopologues with isobaric masses. Analytical chemistry *84*, 7469-7478.

Metzger, M.B., Pruneda, J.N., Klevit, R.E., and Weissman, A.M. (2014). RING-type E3 ligases: Master manipulators of E2 ubiquitin-conjugating enzymes and ubiquitination. Biochimica et biophysica acta *1843*, 47-60.

Murshudov, G.N., Vagin, A.A., and Dodson, E.J. (1997). Refinement of Macromolecular Structures by the Maximum-Likelihood Method. Acta crystallographica *D53*, 240-255.

Ordureau, A., Heo, J.M., Duda, D.M., Paulo, J.A., Olszewski, J.L., Yanishevski, D., Rinehart, J., Schulman, B.A., and Harper, J.W. (2015). Defining roles of PARKIN and ubiquitin phosphorylation by PINK1 in mitochondrial quality control using a ubiquitin replacement strategy. Proceedings of the National Academy of Sciences of the United States of America *112*, 6637-6642.

Ordureau, A., Sarraf, S.A., Duda, D.M., Heo, J.M., Jedrychowski, M.P., Sviderskiy, V.O., Olszewski, J.L., Koerber, J.T., Xie, T., Beausoleil, S.A.*, et al.* (2014). Quantitative proteomics reveal a feedforward mechanism for mitochondrial PARKIN translocation and ubiquitin chain synthesis. Molecular cell *56*, 360-375.

Otwinowski, Z., and Minor, W. (1997). Processing of X-ray Diffraction Data Collected in Oscillation Mode. Methods in Enzymology, Macromolecular Crystallography, part A *276*, 307-326.

Pettersen, E.F., Goddard, T.D., Huang, C.C., Couch, G.S., Greenblatt, D.M., Meng, E.C., and Ferrin, T.E. (2004). UCSF Chimera--a visualization system for exploratory research and analysis. J Comput Chem *25*, 1605-1612.

Phu, L., Izrael-Tomasevic, A., Matsumoto, M.L., Bustos, D., Dynek, J.N., Fedorova, A.V., Bakalarski, C.E., Arnott, D., Deshayes, K., Dixit, V.M.*, et al.* (2011). Improved quantitative mass spectrometry methods for characterizing complex ubiquitin signals. Mol Cell Proteomics *10*, M110 003756.

Pickart, C.M., and Raasi, S. (2005). Controlled synthesis of polyubiquitin chains. Methods in enzymology *399*, 21-36.

Pickrell, A.M., and Youle, R.J. (2015). The roles of PINK1, parkin, and mitochondrial fidelity in Parkinson's disease. Neuron *85*, 257-273.

Plechanovova, A., Jaffray, E.G., Tatham, M.H., Naismith, J.H., and Hay, R.T. (2012). Structure of a RING E3 ligase and ubiquitin-loaded E2 primed for catalysis. Nature *489*, 115-120.

Rudner, A.D., and Murray, A.W. (2000). Phosphorylation by Cdc28 activates the Cdc20-dependent activity of the anaphase-promoting complex. The Journal of cell biology *149*, 1377-1390.

Saha, A., Lewis, S., Kleiger, G., Kuhlman, B., and Deshaies, R.J. (2011). Essential role for ubiquitin-ubiquitin-conjugating enzyme interaction in ubiquitin discharge from Cdc34 to substrate. Molecular cell *42*, 75-83.

Sander, B., Golas, M.M., and Stark, H. (2003). Automatic CTF correction for single particles based upon multivariate statistical analysis of individual power spectra. Journal of structural biology *142*, 392-401.

Sauve, V., Lilov, A., Seirafi, M., Vranas, M., Rasool, S., Kozlov, G., Sprules, T., Wang, J., Trempe, J.F., and Gehring, K. (2015). A Ubl/ubiquitin switch in the activation of Parkin. The EMBO journal *34*, 2492-2505.

Scheres, S.H. (2012). RELION: implementation of a Bayesian approach to cryo-EM structure determination. Journal of structural biology *180*, 519-530.

Scott, D.C., Sviderskiy, V.O., Monda, J.K., Lydeard, J.R., Cho, S.E., Harper, J.W., and Schulman, B.A. (2014). Structure of a RING E3 Trapped in Action Reveals Ligation Mechanism for the Ubiquitin-like Protein NEDD8. Cell *157*, 1671-1684.

Sumara, I., Vorlaufer, E., Gieffers, C., Peters, B.H., and Peters, J.M. (2000). Characterization of vertebrate cohesin complexes and their regulation in prophase. The Journal of cell biology *151*, 749-762.

Ting, L., Rad, R., Gygi, S.P., and Haas, W. (2011). MS3 eliminates ratio distortion in isobaric multiplexed quantitative proteomics. Nat Methods *8*, 937-940.

Tonikian, R., Zhang, Y., Boone, C., and Sidhu, S.S. (2007). Identifying specificity profiles for peptide recognition modules from phage-displayed peptide libraries. Nat Protoc *2*, 1368-1386.

Trabuco, L.G., Villa, E., Mitra, K., Frank, J., and Schulten, K. (2008). Flexible fitting of atomic structures into electron microscopy maps using molecular dynamics. Structure *16*, 673-683.

Vijay-Kumar, S., Bugg, C.E., and Cook, W.J. (1987). Structure of ubiquitin refined at 1.8 A resolution. Journal of molecular biology *194*, 531-544.

Wauer, T., Simicek, M., Schubert, A., and Komander, D. (2015). Mechanism of phospho-ubiquitin-induced PARKIN activation. Nature *524*, 370-374.

Weissmann, F., Petzold, G., VanderLinden, R., Huis in 't Veld, P.J., Brown, N.G., Lampert, F., Westermann, S., Stark, H., Schulman, B.A., and Peters, J.M. (2016). biGBac - rapid gene assembly for expression of large multi-subunit protein complex. Proceedings of the National Academy of Sciences of the United States of America.

White, H.D., and Rayment, I. (1993). Kinetic characterization of reductively methylated myosin subfragment 1. Biochemistry *32*, 9859-9865.

Wright, J.D., Mace, P.D., and Day, C.L. (2016). Secondary ubiquitin-RING docking enhances Arkadia and Ark2C E3 ligase activity. Nature structural & molecular biology *23*, 45-52.

Yamaguchi, M., Yu, S., Qiao, R., Weissmann, F., Miller, D.J., VanderLinden, R., Brown, N.G., Frye, J.J., Peters, J.M., and Schulman, B.A. (2015). Structure of an APC3-APC16 complex: insights into assembly of the anaphase-promoting complex/cyclosome. Journal of molecular biology *427*, 1748-1764.

Zhang, W., Wu, K.P., Sartori, M.A., Kamadurai, H.B., Ordureau, A., Jiang, C., Mercredi, P.Y., Murchie, R., Hu, J., Persaud, A.*, et al.* (2016). System-Wide Modulation of HECT E3 Ligases with Selective Ubiquitin Variant Probes. Molecular cell *62*, 121-136.